ABSTRACT

Title of Document: THE INFLUENCE OF IRON AND MANGANESE OXIDES ON THE PRODUCTION OF MARINE SEDIMENTARY CERIUM ANOMALIES

Kathleen S. Marshall, MS., 2011

Directed By: Assistant Professor Johan Schijf, Marine Estuarine Environmental Sciences

Cerium is the only metal in the yttrium and rare earth element (YREE) series that can be oxidized under natural conditions, resulting in anomalous Ce distributions relative to those of the other YREE. Marine sedimentary cerium anomaly records have thus been used to signify relative shifts in bottom water oxygenation. However, Ce anomalies form via several pathways often not considered in paleo-oceanographic interpretations. To determine the relative influence of two important marine particulate components, Fe and Mn, on Ce oxidation, YREE sorption was investigated under anaerobic conditions in 0.5 M NaCl solutions over a range of pH (4-8) on hydrous ferric, manganese(IV) and ferromanganese oxides. Non-electrostatic surface complexation models were developed that describe non-oxidative sorption mechanisms on each surface. Cerium oxidation occurred on all sorbents containing Mn, indicating that sedimentary Ce records cannot be directly related to past marine oxygen conditions, even in the presence of relatively little manganese.

THE INFLUENCE OF IRON AND MANGANESE OXIDES ON THE PRODUCTION OF MARINE SEDIMENTARY CERIUM ANOMALIES

By

Kathleen S. Marshall

Thesis submitted to the Faculty of the Graduate School of the
University of Maryland, College Park, in partial fulfillment
of the requirements for the degree of
Master of Science
2011

Advisory Committee:
Assistant Professor Johan Schijf, Chair
Professor H. Rodger Harvey
Associate Professor Jeffrey C. Cornwell

Acknowledgements

First of all, many thanks to Dr. Johan Schijf, my adviser, for guidance and support through my first foray into environmental chemistry. You have introduced me to this new research field as a patient teacher and I certainly could not have accomplished all this without your help. Thanks to my other committee members, Drs. Jeffrey C. Cornwell and H. Rodger Harvey, for always reminding me to consider the bigger picture of my project and for your support over the past few years. To my lab buddies, Alison Zoll and Emily Christenson, thanks for being there when I needed lab help or someone to listen and discuss my research ideas. Many thanks to the Heyes Lab, especially Dr. Andrew Heyes and Elizabeth Jenny, for help working out the kinks in the anaerobic glove bag; you both made it much easier and more enjoyable. Thanks to Dr. Peter Zavalij at College Park for X-ray diffraction analyses. Acknowledgment is also made to the donors of the American Chemical Society Petroleum Research Fund, the CBL Graduate Education Committee and the UMD Jacob K. Goldhaber Award for financial support of this research.

Finally, I must give many thanks to my amazing support group. To my family, your love and encouragement has been a source of comfort and strength that has allowed me to accomplish so much. To the BFL gang (past and present), thanks for creating a great work environment that encourages important research as well as strong friendships. Thanks to all my Maryland friends for the memories as well as helping me grow both professionally and personally.

Table of Contents

List of Tables

Table 3.6. Best-fit R values for regressions of log ${}_iK_{FeMn}$ *vs.* pH using the composite non-electrostatic surface complexation model (Equation (3.3)) where R indicates the relative influence of hydrous Fe and Mn oxides during metal sorption on mixed oxides such that larger values reflect greater effect of Fe oxides than Mn oxides. Uncertainties are one standard error of the mean.

List of Figures

Figure 2.6. Comparison of model predictions of sorption with literature data (De Carlo et al., 1998; Ohta and Kawabe, 2001; Davranche et al., 2005, 2008) converted to my definition of ${}_iK_{Mn}$ (Equation (2.3)). The model predictions (solid line) were calculated at matching pH values using Equation ((2.10)) and the best fit parameters from Table 2.3. Cerium sorption was not modeled since it occurs via oxidative processes (section 2.4.4). The predicted values were adjusted vertically along the arrows to give the best overlap with literature values and are shown as dashed lines. The model predictions at pH 5.59, 6.8 and 6 (dotted lines) were not adjusted.

Figure 2.7. Linear regression of cerium (circles) and praseodymium (triangles) sorption at pH < 5.5 (closed points) and pH > 5.5 (open points) where the slope indicates the average number of protons released for each metal sorbed over the pH range. The proton exchange associated with Ce sorption increases by 0.81 above pH 5.5, while that of Pr sorption increases only 0.17 units above pH 5.5.

Figure 2.8. Cerium anomalies over experimental pH ranges from the current data (left panel) calculated as $\log(K_{Ce}/K_{Ce^*})$ and Ohta and Kawabe (2001) (right panel) calculated as $\log K_{Ce}-\log K_{Ce^*}$. Experimental conditions were similar in both studies (0.5 M NaCl, 25°C), except Ohta and Kawabe did not purge their solutions with inert gas. Distribution coefficients, K_d, are calculated as mole fractions by Ohta and Kawabe (2001) unlike in the current investigation (Equation (2.3)). In both datasets, Ce anomalies indicate Ce oxidation over the entire investigated pH range (values greater than 1) with a steady increase in oxidation above pH 5.5.

Figure 3.1. Linear regression of La (top) and Lu (bottom) distribution coefficients ($\log {}_iK_s$) *vs.* pH for sorption on hydrous ferric oxide (HFO, open circles), hydrous manganese oxide (HMO, closed circles) in the left panel and on 3:1 FeMn mixed oxide (open diamonds), 1:1 FeMn mixed oxides (gray diamonds) and 1:9 FeMn mixed oxide (closed diamonds) in the right panel. The resulting slopes (Table 3.5) indicate the average number of protons released per YREE cation sorbed over the experimental pH range (0.5 M NaCl, 25°C) increased with increasing Fe content of the sorbent (excluding 1:1 FeMn oxides, which had the highest proton exchange). Distribution coefficients obtained at pH > 7.60 (shown as an 'x') were excluded from linear regression since these points consistently deviated from linearity. The two highest pH points in the HFO dataset as well as the highest pH points in the HMO and 3:1 FeMn oxide datasets consequently did not affect the regressions.

Figure 3.2. Linear regression of Ce distribution coefficients on hydrous manganese oxide (HMO, circles) and 1:9 FeMn oxides (diamonds) at pH < 5.5 (closed symbols) and pH > 5.5 (open symbols). The change in slope near pH 5.5 of 0.70 units on 1:9 mixed oxides is similar to the shift found previously of 0.81 units on HMO (Chapter 2).

Figure 3.3. Distribution coefficients ($\log {}_iK_s$) of all YREE at intermediate pH (~ 6.4) on hydrous Fe, Mn and FeMn oxides. Coefficients have been vertically adjusted to have equal Yb values in order to emphasize relative YREE behaviors between the sorbents.

Figure 3.4. Cerium anomalies formed on pure (left panel) (Schijf and Marshall, 2011; Chapter 2) and mixed oxide (right panel) sorbents over the experimental pH range. Positive Ce anomalies, log(Ce/Ce*) > 0, indicate enhanced Ce sorption due to Ce oxidation whereas Ce is not oxidized when anomalies are near zero. For reference, the regression lines of the HMO data were added to the right side panel.

Figure 3.5. Fractionation of Y from Ho, as determined by the ratio of their distribution coefficients, on each of the pure oxides (Schijf and Marshall, 2011; Chapter 2) over the experimental pH range. Values from mixed oxide datasets are intermediate to those shown here.

Figure 3.6. Model regressions (Equation (3.3)) of La (top panels) and Lu (bottom panels) sorption on 3:1 and 1:9 mixed oxide sorbents over the experimental pH ranges. The relative effect of Fe and Mn on metal interaction with a given sorbent is determined by the resulting R values (Table 3.6) such that higher numbers indicate greater contribution from Fe. Dashed lines indicate the 95% confidence interval and uncertainties are one standard error of the mean.

Figure 3.7. Best fit values of R (Equation (3.3)) for all YREE, except Ce, on 3:1 and 1:9 FeMn oxides. Higher values of R reflect greater contribution from Fe sites while lower R values indicate a greater contribution from Mn sites to sorption. Uncertainties are one standard error of the mean.

Figure 3.8. The ability of the model (Equation (3.3)) to predict samarium sorption on each modeled mixed oxide over the investigated pH range. The average ratio of predicted to measured distribution coefficients is near unity for all YREE (mean = 0.997 and 0.995 for 3:1 and 1:9 FeMn oxides, respectively), but model skill varies with pH and sorbent.

Figure 3.9. Comparison of measured (closed circles) and predicted (open circles) patterns of YREE sorption on each of the mixed oxides at three values of pH. Predicted patterns were calculated using Equation (3.3) with appropriate c constants and R values (Table 3.6). The model accurately reproduces relative and absolute sorption behavior of strictly trivalent YREE on 1:9 FeMn oxides (right panel) and relative behavior on 3:1 FeMn oxides (left panel). Cerium distribution coefficients are predicted from only Ce(III) sorption which is much lower than measured values on all FeMn oxides.

Figure 3.10. Comparison of model predictions of sorption with literature data at pH 6.4 (Kawabe et al., 1999) converted to my definition of ${}_{i}K_{FeMn}$ (Equation (3.2)). The composite model prediction (solid line) was calculated at pH 6.4 using Equation (3.3) with R as the fraction of Fe in the experiment (~ 0.17) and without c. The hydrous Mn model prediction (dashed line) was calculated at pH 6.4 using Equation (2.10) and best-fit parameters (Table 2.3). The predicted values were adjusted upward along the arrows to give the best overlap with literature values. Sorption behavior is described better by the composite than hydrous Mn model, especially for HREE.

Chapter 1: Introduction

1.1. Yttrium and the rare earth elements

Yttrium and the rare earth elements (YREE) always coexist in the environment because of their similar origin and chemistry. Specific YREE properties (Table 1.1) make this group of elements well suited as probes of many physical and chemical processes associated with trace metals in natural systems. All YREE have the same oxidation state (+III) and thus relatively high ionic charge at the low temperatures common near Earth's surface, making them very particle reactive. The removal of dissolved metals, such as YREE, from solution through their interaction with a particle surface is known as sorption. Dissolved metals are attracted to surfaces by electrostatic forces and complexation with surface ligands, but sorption occurs in competition with metal complexation by dissolved ligands that stabilize metals in solution. Sorption reactions become more favorable with increasing charge and decreasing ionic radius of dissolved species (Turner et al., 1981; Sverjensky, 2006). The inner 4f electron shell of rare earth elements is sequentially filled resulting in a gradual decrease in ionic radii from lanthanum to lutetium, known as the lanthanide contraction, leading to a gradual decrease in polarizability such that REE reactivity increases with atomic number. Although the ionic radius of yttrium is similar to that of Ho, the behavior of Y is not consistent with Ho but instead yttrium may act as a light REE (LREE) or heavy REE (HREE) under different conditions (Byrne and Lee, 1993; Zhang et al., 1994). Since YREE have the same charge under natural conditions, their reactivity is mostly determined by their ionic radii so that their distribution and sorption occur in a somewhat predictable manner. Therefore, YREE

have been used to investigate many geochemical processes including ocean circulation patterns, groundwater discharge, ore formation and planetary evolution (Herd et al., 2002; Charette and Sholkovitz, 2006; Roberts et al., 2010; Valley et al., 2010).

Table 1.1. Basic physical properties of YREE including atomic number (Z), atomic weight, trivalent ionic radius with 6-coordination (Shannon, 1976) and outer electron configuration. The inner electron configuration of yttrium is $1s^2\ 2s^2\ 2p^6\ 3s^2\ 3p^6\ 3d^{10}\ 4s^2\ 4p^6$. The inner electron configuration of all REE is $1s^2\ 2s^2\ 2p^6\ 3s^2\ 3p^6\ 3d^{10}\ 4s^2\ 4p^6\ 4d^{10}$.

Element	Symbol	Z	Atomic Weight ($g \cdot mol^{-1}$)	Ionic Radius (Å)	Outer electron configuration	
					atom	+3 ion
yttrium	Y	39	88.91	0.900	$4d^1\ 5s^2$	$4s^2\ 4p^6$
lanthanum	La	57	138.91	1.032	$5s^2\ 5p^6\ 5d^1\ 6s^2$	$5s^2\ 5p^6$
cerium	Ce	58	140.12	1.01	$4f^1\ 5s^2\ 5p^6\ 5d^1\ 6s^2$	$4f^1\ 5s^2\ 5p^6$
praseodymium	Pr	59	140.91	0.99	$4f^2\ 5s^2\ 5p^6\ 5d^1\ 6s^2$	$4f^2\ 5s^2\ 5p^6$
neodymium	Nd	60	144.24	0.983	$4f^3\ 5s^2\ 5p^6\ 5d^1\ 6s^2$	$4f^3\ 5s^2\ 5p^6$
promethium[a]	Pm	61	145.00	0.970	$4f^4\ 5s^2\ 5p^6\ 5d^1\ 6s^2$	$4f^4\ 5s^2\ 5p^6$
samarium	Sm	62	150.36	0.958	$4f^5\ 5s^2\ 5p^6\ 5d^1\ 6s^2$	$4f^5\ 5s^2\ 5p^6$
europium	Eu	63	151.96	0.947	$4f^6\ 5s^2\ 5p^6\ 5d^1\ 6s^2$	$4f^6\ 5s^2\ 5p^6$
gadolinium	Gd	64	157.25	0.938	$4f^7\ 5s^2\ 5p^6\ 5d^1\ 6s^2$	$4f^7\ 5s^2\ 5p^6$
terbium	Tb	65	158.93	0.923	$4f^8\ 5s^2\ 5p^6\ 5d^1\ 6s^2$	$4f^8\ 5s^2\ 5p^6$
dysprosium	Dy	66	162.50	0.912	$4f^9\ 5s^2\ 5p^6\ 5d^1\ 6s^2$	$4f^9 5s^2\ 5p^6$
holmium	Ho	67	164.93	0.901	$4f^{10}\ 5s^2\ 5p^6\ 5d^1\ 6s^2$	$4f^{10}\ 5s^2\ 5p^6$
erbium	Er	68	167.27	0.890	$4f^{11}\ 5s^2\ 5p^6\ 5d^1\ 6s^2$	$4f^{11}\ 5s^2\ 5p^6$
thulium	Tm	69	168.93	0.880	$4f^{12}\ 5s^2\ 5p^6\ 5d^1\ 6s^2$	$4f^{12}\ 5s^2\ 5p^6$
ytterbium	Yb	70	173.04	0.868	$4f^{13}\ 5s^2\ 5p^6\ 5d^1\ 6s^2$	$4f^{13}\ 5s^2\ 5p^6$
lutetium	Lu	71	174.97	0.861	$4f^{14}\ 5s^2\ 5p^6\ 5d^1\ 6s^2$	$4f^{14}\ 5s^2\ 5p^6$

[a] Does not occur naturally

Marine YREE distribution patterns are largely determined by their estuarine signature delivered to the oceans which is generally LREE enriched (Sholkovitz, 1988) but further fractionation of YREE occurs in the oceans. As such, YREE distributions in pelagic systems vary with depth, ocean basin and concentration of organic and inorganic particulates. As marine particles sink through the water column, YREE sorb on their surfaces influencing surface water YREE distributions. In all oceans, except the well mixed Arctic Ocean (Westerlund and Öhman, 1992), vertical profiles of dissolved YREE

concentrations are low in the upper water column and increase with depth. High concentrations of particulate matter in surface waters encourage sorption of YREE which are transported down the water column and then released upon degradation of their sorbents in bottom waters. Global ocean circulation occurs on a much longer time scale of approximately 1,000 years and also influences YREE distributions between particulate and dissolved phases. As a water mass ages, new particulates are introduced to the water column leading to YREE sorption from an increasingly fractionated pool of dissolved YREE such that their depth profiles become more exaggerated between basins along the global ocean circulation path. This magnification of YREE depth profiles creates surface waters with progressively lower YREE concentrations and bottom waters with gradually increasing YREE concentrations as a water mass traverses the globe. Since older deeper waters contain higher dissolved YREE concentrations, YREE concentrations are highest in the bottom water of the Pacific Ocean. The heightened stability of dissolved HREE, due to their more extensive solution complexation, results in a greater relative removal of LREE from the water column than of HREE. Bottom water concentrations of dissolved YREE are thus highest in the basins containing the oldest waters and HREE enriched relative to their source signatures.

1.2.Cerium anomaly and its use as a paleo-redox proxy

Cerium is the only YREE that can be oxidized to a higher (+IV) oxidation state in natural waters which increases its reactivity and sorption to create anomalous Ce distributions relative to the strictly trivalent YREE. Oxidation of Ce after sorption on particulates lowers surface bound Ce(III) concentrations thus encouraging heightened Ce removal from solution compared to the remaining YREE. Cerium oxidation leads to

increased scavenging, resulting in an enhanced transport of particulate Ce to the sediments. Sedimentary cerium records are unique compared to those of other redox-sensitive metals because the neighboring elements of Ce, other rare earth metals, sorb on particulates in a predictable manner. A comparison of Ce abundance with that of other YREE therefore allows redox influences on Ce distributions to be distinguished from all other solution effects. By assuming that Ce oxidation is solely controlled by and reflects the surrounding dissolved O_2 content at the time of its sorption, paleoclimatologists have used the relative shifts in the degree of excess Ce in sediment cores to infer variations in marine bottom water oxygenation. Cerium abundances and proposed O_2 alterations can be mapped through Earth's history since sediments are formed by distinct strata consisting of the newest layer at the sediment-water interface and layers of increasing age with depth. Within sediments, greater Ce enrichment relative to the other YREE is thus interpreted to indicate more oxidizing conditions while lower Ce enrichment to signify less oxidizing conditions in past marine bottom waters (Figure 1.1). Presumed shifts in the oxygen content of bottom waters have then been used to describe changes in ocean circulation resulting from continental movements that opened marine basins, major glacial cycles and sea-level fluctuations.

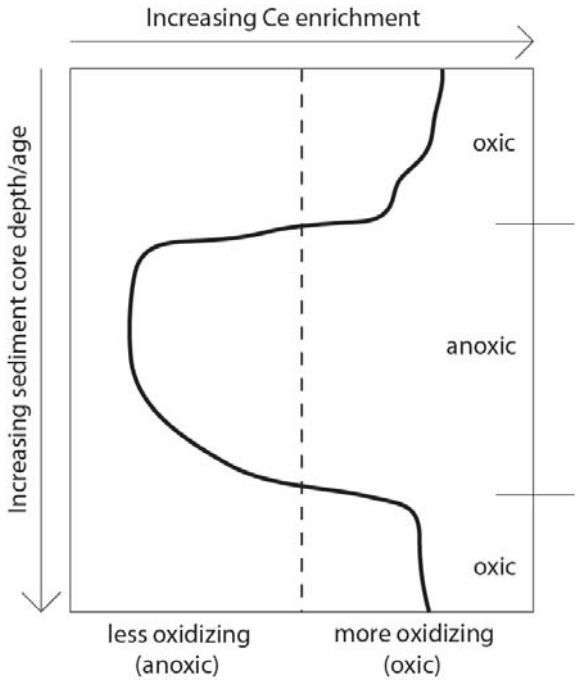

Figure 1.1. A generalized sediment core with varying degrees of cerium enrichment. From the bottom to the top of the sediment core, Ce enrichment decreases across a threshold (dashed line) to reach a minimum and then gradually increases across the same threshold. This has been interpreted by some to indicate that marine bottom waters transitioned from oxic to anoxic and then back to oxic conditions above this sediment as it was forming on the seafloor.

Most interpretations of deviations in sedimentary Ce concentrations do not account for Ce oxidation by solution components other than O_2. Yet it is well established that Ce distributions may be influenced by additional biotic and abiotic factors. The inorganic cycling of YREE, including Ce, has been linked to the cycling of Mn (De Baar et al., 1988; Masuzawa and Koyama, 1989; Schijf et al., 1991; Sholkovitz et al., 1994) and Fe oxides (German et al., 1991; Sholkovitz et al., 1992; Haley et al., 2004), but Mn oxides are known oxidants of Ce (De Carlo et al., 1998; Ohta and Kawabe, 2001; Takahashi et al., 2002) while the oxidative capacity of Fe oxides is debated (De Carlo et al., 1998; Bau, 1999; Ohta and Kawabe, 2001). Manganese oxides can thus increase sedimentary Ce enrichment independent of ambient O_2 but it is unlikely that Fe oxides have this same ability since several investigations found no evidence of Ce oxidation

associated with Fe oxides (Koeppenkastrop and De Carlo, 1992; De Carlo et al., 1998; Ohta and Kawabe, 2001; Quinn et al., 2006a, b, 2007; Schijf and Marshall, 2011). Active microbial oxidation of Ce below the photic zone in surface waters occurs faster than abiotic Ce oxidation by O_2 and may involve siderophores, ligands produced to enhance Fe uptake, that have been found in association with Ce(IV) (Yoshida et al., 2004). Bacterial oxidation of Ce appears to be more influential than inorganic Ce oxidation in surface waters based on oxidation rates of Ce and Mn in marine surface waters from the Sargasso Sea and Vineyard Sound, Massachusetts as well as the seasonality of Ce oxidation in Chesapeake Bay (Moffett, 1990, 1994). Moffett suggested that the correlation of Ce and Mn oxidation resulted from their similar redox chemistry rather than oxidation of Ce by Mn oxides. However, others have suggested that microbes merely facilitate Ce oxidation by accumulating Ce before it is transferred to, and oxidized by, bacterially produced Mn oxides (Ohnuki et al., 2008) or that Mn oxides first oxidize Ce before its complexation with organic ligands (Tanaka et al., 2010). It appears that humic substances are not capable of oxidizing Ce and may prevent Ce oxidation when present in concert with Mn oxides (Davranche et al., 2005; Pourret et al., 2008). The uncertainty in the relative impact of organic matter and Mn oxides on Ce oxidation may be explained by differences in sampling locations or experimental solution compositions. Some of these discrepancies may be answered with a more thorough understanding of Ce oxidative pathways and Ce cycling in the oceans.

1.2.1. Generalized Ce oxidation reaction and the calculation of Ce anomalies

Cerium oxidation is irreversible and thus kinetically controlled whereas sorption of all other YREE occurs by reversible equilibrium processes. Although the mechanism and

electron acceptor for cerium oxidation vary with changing conditions, the process may be generally described by the reaction

$$Ce^{3+} + 2H_2O \rightarrow CeO_2 + 4H^+ + e^- \quad (1.1)$$

that is promoted at elevated pH and pε. Electron potential, or pε, is a measure of a solution's likelihood to transfer electrons. At high potentials, electrons are depleted and there is a tendency to oxidize solutes whereby a system can oxidize any other system with lower pε, assuming excess oxidant concentrations. The potential of Ce oxidation is low enough that it can be oxidized by dissolved O_2 as well as stronger oxidants, like Mn oxides (Takahashi et al., 2007). The redox potential of Ce is situated in the middle of the marine electron acceptor sequence, near the couples of Fe(II)/Fe(III) and Mn(II)/Mn(IV), making Ce sensitive to changing redox conditions in natural environments.

Preferential sorption of Ce, due to its oxidation, has been determined in field and laboratory samples as the deviation of Ce abundances from values that would be expected if only Ce(III) was present. Before interpretations are made in field samples, YREE concentrations are typically normalized to a geological reference such as the North American Shale Composite (NASC) or Post-Archean Average Australian Shale (PAAS) to remove the saw-tooth abundance pattern resulting from the increased natural occurrence of elements with even atomic numbers. In this thesis, the Ce anomaly was calculated from measured solid-solution distribution coefficients (cf. Equation (1.9)), as

$$Ce/Ce^* = \frac{Ce}{1/2(La+Pr)} \quad (1.2)$$

where Ce^* represents the expected cerium sorption without oxidation based upon the sorption of lanthanum and praseodymium (De Baar et al., 1985). Before the development

of Inductively Coupled Plasma instruments (ICP-AES, ICP-MS), neodymium was used in place of Pr such that cerium anomalies were reported as (De Baar et al., 1988):

$$Ce/Ce^{*}=\frac{Ce}{1/3\left(2La+Nd\right)} \tag{1.3}$$

Relative Ce depletion gives Ce/Ce* values less than one and negative log(Ce/Ce*) values (a negative Ce anomaly) while relative Ce enrichment gives Ce/Ce* values greater than one and positive log(Ce/Ce*) values (a positive Ce anomaly). Logarithmic Ce anomalies are reported in this thesis (Chapters 2 and 3) but non-logarithmic values are often reported in field studies, including all anomalies listed in this chapter. Concerns for the influence of La anomalies in these calculations spurred some to quantify Ce anomalies with Ce/Nd ratios (e.g., Schijf et al., 1991) or to compare Ce and Pr anomalies, where Pr/Pr* = 2Pr/(Ce+Nd) (e.g., Webb and Kamber, 2000). Cerium and Pr anomalies are inversely related when there is no La anomaly indicating a true Ce anomaly while a La anomaly creates a false Ce anomaly when a Ce anomaly exists without a Pr anomaly (Bau and Dulski, 1996). The most appropriate calculation depends on the YREE behavior within a specific sample as well as the analytical tools available.

1.2.2. Interpretation of sedimentary Ce anomalies

Cerium anomalies are typically interpreted in terms of their coexistence with other geological records in sediment cores to ensure that accurate interpretations of Ce fractionation are made. Since major shifts in marine oxygenation inferred from Ce anomalies are often used to explain mass extinction events, Ce anomalies are frequently investigated with co-occurring fossils. Wright and others pioneered this research by identifying cerium anomalies within conodont and other apatite fossils that coincided

with major extinction events (e.g., Wright et al., 1987). Others have expanded this work to include sedimentary $\delta^{13}C$ records since more negative $\delta^{13}C$ values can indicate biological respiration and organic matter degradation under anoxic conditions while in oxic waters photosynthesis can produce less negative $\delta^{13}C$ values. Wang et al. (1993) used the correlation of sea level change and fossil $\delta^{13}C$ records with shifts in Ce anomaly values to suggest that the Ce anomalies indicated a short oxic period during glaciation, leading to upwelling of toxic sedimentary materials resulting in extinctions. Kakuwa and Matsumoto (2006) also used a covariance between $\delta^{13}C$ and Ce anomaly values along with an understanding of modern-day YREE cycling in the Black Sea to make similar interpretations, but neglected to measure shifts in Mn oxides with depth which may have significantly influenced sedimentary Ce anomalies. Nevertheless, the oxidative capacity of Mn oxides has been considered by a few authors. For example, Kato et al. (2002) interpreted the concomitant loss of high Mn oxide concentrations and negative Ce anomalies at the Permian-Triassic boundary of sediments to indicate dissolution of Mn oxides containing high Ce concentrations under anoxic Mn-reducing conditions. The relative shifts in Ce/Ce* and concentrations of Mn and Fe were thus assumed to suggest long-term global anoxia for ~10 My resulting in the most extensive extinction event in recent history. Yet, the mechanisms of Ce oxidation are still unknown, so it cannot be unequivocally stated that correlation of Ce anomalies with other paleo-proxies provides direct confirmation of bottom water oxygen content (Holser, 1997).

In response to the gap in knowledge of Ce anomalies, requirements for appropriate conditions under which they can be used as a paleo-redox proxy were defined; stating that the oxidation state of Ce must respond to ambient redox conditions, must remain as

an unaltered record of instantaneous redox conditions at the time of deposition and must be predictably influenced by sorption (German and Elderfield, 1990). These authors also suggested that in light of the modern day variability in Ce anomalies (0.1-0.6) under oxic conditions in the NW Indian Ocean, Ce anomalies in paleo-sediments may be over-interpreted. Moreover, there is considerable evidence that the correlations between Ce anomalies and extinction events often do not represent cause and effect relationships. MacLeod and Irving (1996) were unable to directly relate the covariance of Ce anomalies, organic carbon content and bioturbation rates with assumed O_2 shifts. Interpretations of sedimentary Ce anomaly depth profiles may even contradict those of other redox parameters, such as % organic carbon and U/Th ratios (Pattan et al., 2005). To remove some of these interferences, it has been proposed that Ce anomalies be determined within individual sediment components and coupled with other indicators of paleo-redox states. However, biogenic phosphates and granular phosphorites can be overprinted during diagenesis making them poor records of Ce anomalies (Shields and Webb, 2004; Bright et al., 2009) and suggesting that previous interpretations by the Wright group may be inaccurate. If Ce is oxidized by solution components other than dissolved O_2 (e.g., Mn oxides), Ce anomalies within individual sediment components may not agree with other redox parameters since the oxidation state of Ce will not relate to past shifts in oxygenation.

1.2.3. Cerium oxidation in modern-day seawater

In the modern oceans, dissolved cerium concentrations continually decrease with water column depth and water mass age while concentrations of the other YREE are low in surface waters but increase with water depth and age. The increased removal of Ce

through its oxidation creates Ce anomalies that vary with water mass depth and age. Since Ce oxidation is kinetically controlled (Moffett, 1990; Koeppenkastrop and De Carlo, 1993) its distribution is influenced by particle size and particle residence time in the water column (Fowler et al., 1992). Marine surface water cerium anomalies can range from 0.18 to 0.75, largely reflecting an estuarine YREE signature, while Ce anomalies below 1000 m vary from 0.07 to 0.15 (Byrne and Sholkovitz, 1996) indicating enhanced Ce removal from solution with increasing age. The depth dependent oxidation of Ce in the Sargasso Sea is slow in the mixed zone but faster in the lower euphotic zone where light-inhibition of Ce oxidation is diminished such that the rate of Ce oxidation is insignificant at 20 m, 0.3% per day at 60 m and 0.7% per day at 200 m (Moffett 1990). These gradients can be explained by photo-inhibition of microbial Ce oxidation in surface waters followed by active microbial oxidation of cerium to more reactive Ce(IV) below the photic zone. Cerium anomalies are also more pronounced with increasing age of a water mass illustrating that Ce oxidation occurs over time scales less than that of global ocean circulation as reflected in basinal differences (German et al., 1995). As water ages while moving from the Atlantic to Pacific deep waters, cerium becomes more depleted and the dissolved anomaly changes from 0.16±0.05 to 0.08±0.03 (Bertram and Elderfield, 1993). Consequently, shifts in sedimentary Ce anomalies should only be considered within basins or in relation to the history of a water mass and with caution in regard to microbial influences.

At oxic-anoxic interfaces, Ce anomalies can also be intensified with little contribution from dissolved O_2. Most oceans are oxic throughout the water column but may have anoxic sediments, whereas in deep trenches or stratified seas restricted flows

create anoxic waters (e.g., Cariaco Trench, Black Sea). In a redoxcline, the suboxic zone between oxic and anoxic layers, the available electron acceptors are altered and consequently affect nutrient and trace metal cycling. Cycling of the trivalent YREE is controlled by that of their particulate carriers such that YREE are pumped across the redox boundary to deeper waters with their sorbents and then released into solution once the carriers are reductively dissolved under the surrounding anoxic conditions (De Baar et al., 1988). YREE diffuse upward to more oxic waters and after doing so are quickly sorbed on Mn oxides, which are undergoing redox cycling, and returned to anoxic waters. Trivalent Ce is transported by the same mechanism as other YREE but can additionally be oxidized and subsequently concentrated in deep anoxic waters. The redox cycling of Mn and Ce at oxic-anoxic transitions appear to be largely microbially controlled (van Cappellen et al., 1998) yet Ce oxidation by particulate carriers (e.g., Mn oxides) is also possible. These processes lead to enrichments of YREE in anoxic waters and a dramatic removal of Ce from solution directly above the redox interface. The faster turnover of Ce than the other YREE yields positive particulate Ce anomalies in oxic zones and slightly positive to no anomalies in solid phases of anoxic waters, as expected, but these anomalies are more pronounced than anticipated when only considering O_2-driven Ce oxidation and coincide with Mn distributions. Cerium deposited after cycling through a redoxcline thus introduces exaggerated Ce anomalies that may after several years increase sedimentary Ce concentrations above levels expected under anoxic conditions.

1.3. Cerium sorption on iron and manganese oxides

Sorption of all YREE, including Ce, occurs through proton exchange with the surface hydroxyl groups of metal oxides. Hydrous metal oxides are fairly simple sorbent

surfaces since they contain only hydroxyl groups and have no long range or crystalline structure. Surface hydroxyl groups are positively charged at low pH and become progressively deprotonated with increasing pH such that at a given condition the surface will be overall neutrally charged, known as the pH point of zero charge (pH_{pzc}). This value is determined by the acidity of a surface and thus provides insight into the possible surface reactions. Surface acidity of a hydroxylated surface, S, is described by the deprotonation reactions

$$S-OH_2^+ \rightleftharpoons S-OH + H^+ \tag{1.4}$$

$$S-OH \rightleftharpoons S-O^- + H^+ \tag{1.5}$$

and corresponding constants

$$K_{a1} = \frac{[S-OH][H^+]}{[S-OH_2^+]} \tag{1.6}$$

$$K_{a2} = \frac{[S-O^-][H^+]}{[S-OH]} \tag{1.7}$$

These K values are often written on a logarithmic scale, $pK_a = -\log K_a$, where lower pK_a values indicate higher surface acidity and $pH_{pzc} = ½(pK_{a1} + pK_{a2})$. The distribution of a sorbate between the solid and liquid phases can be described by the simplified reaction between a sorbent surface, S, and dissolved metal, M:

$$S + M \rightleftharpoons S-M \tag{1.8}$$

with an equilibrium constant K_s:

$$K_s = \frac{[S-M]}{[M][S]} \tag{1.9}$$

Higher values of K_s represent greater sorption and thus increased removal of dissolved metal from solution. Since sorption occurs on surface hydroxyl groups of metal oxides

via proton exchange, it is strongly pH dependent whereby most surfaces contain negative charges and thus promote cation sorption under natural conditions. For example, marine pH values are often near 8.

Iron oxides are first formed as amorphous hydrous ferric oxides (HFO) whose surface characteristics, including proton-exchange equilibria and pH-dependent surface charge, have been extensively studied (Dzombak and Morel, 1990; Pretorius and Linder, 1998). Manganese oxides can exist in two oxidized states (+III or +IV) and various degrees of crystallinity and crystal structures, but a common marine form consists of stacked layers of Mn(IV) known as birnessite and is structurally similar to hydrous manganese oxides (HMO) (Murray, 1974). Hydrous Mn oxides generally have a greater surface acidity, lower pH_{pzc}, and thus contain more negatively charged surface groups than hydrous Fe oxides, making Mn oxides a strong sorbent for YREE over a larger range of pH. Surfaces containing a mixture of Fe and Mn oxides are less well-defined and considered to consist of independent Fe and Mn oxide components that are highly reactive scavengers of many elements.

Cerium oxidation is kinetically controlled and thus occurs via more complicated mechanisms than the proton exchange sorption pathways of the other YREE. Iron oxides have only been shown to produce Ce anomalies at low pH by one investigator (Bau, 1999). This finding contradicts the proposed Ce oxidation reaction (Reaction (1.1)) and is most likely caused by sample contamination of additional Ce at low pH rather than Ce oxidation. It is therefore unlikely that Fe oxides can produce Ce anomalies that do not directly relate to ambient O_2 conditions. However, cerium anomalies on Mn oxides increase with pH, as expected from Reaction (1.1) (Ohta and Kawabe, 2001). In the

presence of Mn oxides, Ce removal from solution can occur by surface complexation as well as oxidative scavenging that is coupled to Mn reduction and enhanced by dissolved anions (De Carlo et al., 1998). Iron and Mn oxides often coexist in surface coatings and mixed particulates that have a high affinity for YREE. Minerals containing mixtures of Fe and Mn oxides can be formed in the water column as hydrogenetic oxides, during sedimentary diagenesis as diagenetic nodules, or from hydrothermal vent plumes as hydrothermal concretions. Each category of FeMn oxides contains different Ce enrichments due to their varying growth rates and YREE source signatures, but all oxidized Ce is primarily associated with Mn components (Ohta et al., 1999; Takahashi et al., 2007). Therefore, Mn oxides and mixed particulates containing Fe and Mn oxides may have a strong influence on Ce oxidation irrespective of the surrounding O_2 content yielding misleading Ce anomalies. A more detailed understanding of YREE interactions and Ce oxidation on Fe and Mn oxides is required to better interpret the sedimentary Ce abundances found in complex natural systems.

1.4. Research objectives and approaches

Despite the considerable knowledge of Fe and Mn oxide surface properties and marine YREE cycling, questions remain as to the specific interactions between these components. What is the relative affinity of Fe and Mn oxides for YREE? What are the possible oxidants of Ce in ferromanganese oxides? Are sedimentary records with Fe and Mn likely to contain Ce anomalies indicative of bottom water O_2 content? To address these issues, I have performed end-member sorption analyses of YREE interactions with pure Fe and Mn oxides as well as mixed particulates of varying Fe and Mn concentrations under anaerobic conditions at an ionic strength similar to marine

conditions over a range of pH. I used mixed oxides to mimic freshly formed ferromanganese oxides and FeMn surface coatings. To gain a better mechanistic understanding of the sorption processes, I used non-electrostatic surface complexation models since these models provide information similar to that from electrostatic models but unlike electrostatic models do not require extensive sorbent characterization. Once the pathways to YREE sorption are known we can begin to develop a framework from which inferences on the fate and transport of other metals, in the absence of organics, can be made. For example, by understanding the influences of iron and manganese oxides on the formation of cerium anomalies we can propose their likely behavior with other redox active elements such as arsenic, chromium and uranium. This work will thus provide insights into the surface reactivity of Fe and Mn oxides at seawater ionic strength as well as the applicability of Ce anomalies as paleo-redox indicators.

Yttrium and rare earth element sorption on hydrous ferric oxides has been previously published and is attached as an appendix to this thesis. Chapter 2 addresses YREE sorption on hydrous manganese oxides while sorption on hydrous ferromanganese oxides is described in Chapter 3. The goals of this project were:

(1) Develop a non-electrostatic surface complexation model to describe YREE sorption on each of the investigated surfaces as a function of pH. This not only provides mechanistic information on the nature of YREE surface complexes but also the surface properties of sorbents at an ionic strength similar to marine conditions.

(2) Determine the relative influence of Fe and Mn oxides on YREE sorption at an ionic strength similar to marine conditions. This is addressed in Chapter 3 by comparison of the pure end-member and mixed-oxide data.

(3) Shed light on the debate of the oxidative capacity of Fe and Mn oxides. Comparisons of Ce sorption on each of the oxide types will provide data to help determine the appropriate conditions under which Ce anomalies may be used as paleo-redox indicators.

Chapter 2: Anaerobic Ce oxidation during YREE sorption on hydrous manganese oxides in 0.5 M NaCl solutions

2.1. Abstract

Distribution coefficients, ${}_iK_{Mn}$, were calculated for the equilibrium partitioning of yttrium and the rare earth elements (YREE) between 0.5 M NaCl solutions and synthetic hydrous manganese oxides (HMO) during batch sorption experiments over the pH range 3.71-7.83 under N_2 atmosphere (T=25°C). A non-electrostatic surface complexation model was derived with composite conditional stability constants (A_n), representing specific YREE sorption reactions exchanging *n* protons, and two surface speciation parameters (${}_sK_1$ and ${}_sK_2$) to describe the (de)protonation of HMO surface hydroxyl groups. The model accurately describes trivalent YREE distributions found in the current experiments and in the literature, but not those of cerium which are kinetically controlled.

Sorption occurs through surficial proton exchange with an average of 0.5 H^+ released per YREE cation sorbed over the experimental pH range, except for cerium which undergoes preferential sorption. Enhanced Ce sorption occurs over the entire pH range indicating that Ce oxidation by HMO is favorable under these conditions. The sudden increase in Ce sorption at pH ≥ 5.5 suggests a change in Ce speciation on the HMO surface, affecting the mechanism of Ce oxidation and consequently its reaction stoichiometry. Hydrous Mn oxides are known to oxidize other dissolved metals by similar pathways. Since cerium is oxidized by hydrous manganese oxides under anaerobic conditions, profiles of sedimentary Ce anomalies are unlikely to provide a reliable record of marine bottom water oxygen content.

2.2. Introduction

Marine sediments are an important sink for many trace metals and may contain relevant geological records of past oceanic events that have influenced metal speciation. For example, the oceans have experienced many shifts in dissolved O_2 concentrations over Earth's history due to the evolution of marine oxidative respiration and subsequently to processes like continental drift, glacial cycles and sea level fluctuations that have been considered a cause of mass extinctions. Trace metal distributions were likely also influenced by these shifts in dissolved O_2 such that their concentration over time in a sediment core may reflect past changes in the O_2 content of the surrounding bottom waters. However, identifying the specific cause of such records is difficult since natural sediments are complex mixtures of minerals and organics which affect trace metal mobility (see Section 1.2 for a discussion of Ce oxidants). Interpretations of sedimentary metal abundances are thus inherently dependent upon the characterization of sediment components and their collective influence. There are two approaches to unraveling the behavior of trace metal associations with composite surfaces. One is to use well characterized but complex natural material, which provides realistic conditions but may be difficult to explain mechanistically. The other assumes the effect of a substrate is controlled by the sum of its individual contributions such that interactions with end-members are additive and can be combined to estimate the impact of bulk sediments on trace metal distributions. I have used the latter method of simpler systems as building blocks for natural sediments since it may provide more mechanistic insight than the former.

Manganese oxides are ubiquitous in sediments and are strong natural oxidants of redox-sensitive elements of environmental concern such as arsenic, chromium, selenium, iodine and uranium thus influencing their fate and transport (Murray and Dillard, 1979; Fendorf and Zasoski, 1992; Koppi et al., 1996; Scott and Morgan, 1996; Fox et al., 2009; Lafferty et al., 2010). The presence of even minute quantities of Mn oxides on a surface may significantly affect the reactivity of a substrate and consequently the sorption of trace metals. Marine cycling of Mn oxides is largely microbially controlled since abiotic Mn oxidation reactions are kinetically much slower. Manganese oxidizing microbes produce hydrous manganese oxides (van Cappellen et al., 1998; Tebo et al., 2005) likely via a siderophore similar to desferrioxamine B that is known to oxidize Mn(II) (Duckworth and Sposito, 2005). To complete the microbial loop, oxidized Mn species are reduced by other bacteria during organic matter degradation (Kostka et al., 1995). Although Mn oxides are important oxidants under many conditions, they become one of the main electron acceptors in suboxic zones and as such may define redox boundaries between oxic and anoxic conditions. While cycling in suboxic zones, particulate Mn binds dissolved phosphate to create typical "phosphate dipoles" whereby dissolved phosphate concentrations are lowest directly above a suboxic zone and highest directly below (Yakushev et al., 2009). Although Mn oxides play an important role in organic matter degradation as well as nutrient and trace metal cycling, the surface properties of Mn oxides have not been studied as extensively as those of other sediment components, such as Fe oxides.

The goal of this work is to provide new insights into the surface properties of hydrous manganese oxides (HMO) and their impact on Ce anomalies as well as other

redox processes. There is limited literature on sorption mechanisms associated with HMO (as opposed to, for instance, hydrous ferric oxides) since it is difficult to characterize poorly crystalline Mn oxides and slight changes in oxide synthesis can produce different structures with varying reactivities (Villalobos et al., 2003; Tonkin et al., 2004). Non-electrostatic surface complexation models are well suited to explain sorption mechanisms, especially on HMO, because they require the least amount of sorbent characterization while providing a great deal of mechanistic information. I have developed a non-electrostatic surface complexation model from first principles to describe YREE sorption on HMO as a function of pH. The utility of YREE lies in their chemical coherence such that their relative behaviors provide a wealth of knowledge on sorption mechanisms. Since YREE form a coherent group with systematic behaviors, Ce anomalies can be used to isolate redox influences from all other solution speciation effects. Understanding YREE fractionation will thus provide insights into the sorption mechanisms of these and other metals on Mn oxides. This work has implications not only for paleo-redox interpretations of Ce anomalies but also the fate and reactivity of other redox sensitive compounds in the presence of Mn oxides.

2.3. Materials and methods

All solutions were prepared in a class-100 laminar flow hood with Milli-Q water (18.2 MΩ·cm) from a Millipore Direct-Q 3UV purification system. Solids of $NaMnO_4$ (97+% purity), $MnCl_2$ (99.99+% purity), oxalic acid (99.0% reagent grade), KI (99+% ACS reagent) and NaCl (Reagent-Plus) as well as solutions of certified $Na_2S_2O_3$ (0.1011 N) and 1% starch indicator were purchased from Sigma-Aldrich. Solutions of concentrated HNO_3 and H_2SO_4 (TraceMetal grade) and 1 M NaOH were obtained from

Fisher while certified HCl (1.0011 M) was purchased from Brinkmann (Westbury, NY). Stock solutions of 100 $\mu g \cdot L^{-1}$ Co, 100 $\mu g \cdot L^{-1}$ Mn and a mixed stock solution containing 83.3 $mg \cdot L^{-1}$ Ce and 8.33 $mg \cdot L^{-1}$ of all other YREE were made from 1000 $mg \cdot L^{-1}$ single-element standards purchased from SPEX/CertiPrep (Metuchen, NJ). These cobalt and manganese stock solutions were used to make a Mn calibration line for ICP-MS analysis. An YREE calibration line was similarly created from a premixed standard with 10 $mg \cdot L^{-1}$ of each YREE (plus Sc and Th). All plastic equipment was acid cleaned and thoroughly rinsed with Milli-Q water before use. Small Teflon parts were cleaned in sub-boiling 8 M HNO_3 for at least 24 h while 1 L Teflon bottles and non-Teflon parts were cleaned in cold 4 M HCl for at least 1 week.

2.3.1. Sorbent synthesis

Hydrous manganese oxides (HMO) were synthesized externally by oxidizing $MnCl_2$ with $NaMnO_4$ under basic conditions by the following reaction from Murray (1974)

$$3MnCl_2 + 2NaMnO_4 + 4NaOH \rightarrow 5MnO_2(s) + 6NaCl + 2H_2O \qquad (2.1)$$

and then thoroughly rinsed with Milli-Q water to remove excess reactants. A 1 L $MnCl_2$ solution was mixed with a floating Teflon stir bar to prevent particle grinding and bubbled with N_2 gas for 1 h to remove CO_2 and O_2 before the dropwise addition of an alkaline $NaMnO_4$ solution. This mixture was stirred under anaerobic conditions for 3 h to ensure reaction completion although a black precipitate began forming immediately upon $NaMnO_4$ addition. Milli-Q rinsed particles were stored until use in suspension at 2°C in a polypropylene centrifuge tube covered with aluminum foil to prevent aging and photo-

reduction. All sorption experiments were performed within 7 months of HMO production, except X-ray diffraction analysis which occurred 1 year after synthesis.

2.3.2. Manganese oxidation state determination

The oxidation state of manganese oxides ranges from +III to +IV and dictates structural characteristics that may influence YREE sorption. Therefore I determined the oxidation state of HMO by iodometric titration under anaerobic conditions with a method modified from Kalhorn and Emerson (1984). In an anaerobic chamber, manganese oxides were reductively dissolved by the sequential addition of 85 mL degassed Milli-Q water, 5 mL 50% H_2SO_4 and 10 mL alkaline 2M KI with stirring. Upon dissolution, 1 mL of starch indicator was added and the solution was titrated with a known volume of standardized $Na_2S_2O_3$ using a Gilmont microburette. The O:Mn ratio was calculated for each titration as

$$x = 1 + 0.5 \times \frac{[Na_2S_2O_3]}{[Mn]} \quad (2.2)$$

where brackets indicate moles and the manganese oxidation state is 2x. The method was first standardized by titrating known amounts of crystalline MnO_2 and Mn_2O_3 solids (99.99% purity, Sigma-Aldrich) before replicate analyses (n = 6) of HMO particles were performed over a range of masses (22-98 mg wet weight). Subsamples (100 µL) of each titration were collected directly before the addition of starch, diluted at least 10,000-fold with 1% HNO_3 to reduce matrix effects, spiked with 5 $\mu g \cdot L^{-1}$ Co as an internal standard and analyzed for Mn content by ICP-MS, as described below, using an external calibration line (0, 0.5, 1, 2 and 5 $\mu g \cdot L^{-1}$).

2.3.3. X-ray diffraction characterization

X-ray powder diffraction was performed on the Mn oxides to determine their degree of crystallinity. A hydrous manganese oxide subsample was air-dried in a laminar flow hood for 5 days before analysis. The sample was irradiated with CuKα wavelengths using a Bruker D8 Advance powder diffractometer at room temperature in the X-ray Crystallography Center of the University of Maryland-College Park. Inorganic and mineral subfiles of the ICDD powder diffraction database were searched to identify specific Mn minerals in the diffraction spectrum.

2.3.4. YREE sorption experiments

Sorption experiments were performed similarly to previous YREE titrations with hydrous ferric oxides as the sorbent (Schijf and Marshall, 2011). Briefly, two 1-L Teflon bottles containing 0.5 M NaCl solutions were temperature controlled (25.0 ± 0.1°C) by a recirculating water bath (LAUDA-Brinkmann RE-106). One solution was set to pH 3 with HCl to standardize all pH measurements which were performed using an Orion glass combination electrode (no. 810200) connected to a PerpHecT 350 millivolt meter. The remaining 1-L bottle contained the experimental solution of 0.5 M NaCl, 500 $\mu g \cdot L^{-1}$ Ce, 50 $\mu g \cdot L^{-1}$ of all other YREE and approximately 100 mg HMO (wet weight) that was stirred with a floating magnetic Teflon stir bar to prevent particle grinding. Cerium concentrations were 10-fold higher to compensate for its enhanced sorption relative to the other YREE. Hydrous manganese oxides were pre-equilibrated in 0.5 M NaCl at least overnight before each experiment. Prior to their transfer to the experimental YREE solution, excess solution was removed from the particles by centrifugation. Three samples of the centrifuged manganese oxide stock were also weighed and dried in a

laminar flow hood to determine their water content in each batch experiment. Throughout the titration, carbonate complexation and aerobic Ce oxidation were prevented by bubbling the experimental solution with ultra-high purity N_2 gas which was first passed through an in-line trap (Supelco) to remove any traces of CO_2.

At the start of each experiment, YREE were added from a stock solution, the pH was raised to approximately 3.7 by addition of 1 M NaOH with a Gilmont microburette and wet HMO particles were then added. The experimental pH was raised before HMO addition to prevent manganese dissolution and subsequent Mn^{2+} adsorption which occurs near pH 3.5 (Murray, 1974). Filtered samples of the solution were collected, as described below, at least 15 minutes after each of these adjustments. The sample collected just before HMO addition was used to determine the initial dissolved YREE concentration, $[M]_{init}$. For the remainder of the titration, lasting 3-5 days, the experimental pH was slowly raised with 1 M NaOH. After 6-24 h of equilibration time, stirring was briefly stopped to allow the particles to settle before two 5 mL aliquots were removed from the experimental solution and then sequentially filtered through a 13 mm HDPE filter cartridge with a 0.22 μm PVDF membrane (Fisher). The first aliquot served as a rinse to prevent YREE loss caused by sorption on the filter membrane and was discarded. The second filtrate was collected in a 15 mL polypropylene centrifuge tube and acidified with 10 μL of concentrated HNO_3. Samples were diluted with 1% HNO_3 to reduce NaCl matrix effects, then spiked with an internal standard solution (2 $\mu g \cdot L^{-1}$ each of In, Cs and Re) in preparation for ICP-MS analysis, as described below, against a matrix-matched (5 mM NaCl) external calibration line (0, 0.5, 1, 2 and 5 $\mu g \cdot L^{-1}$).

2.3.5. ICP-MS analyses

Dissolved concentrations of Mn and YREE, in titration and sorption samples respectively, were measured on an Agilent 7500cx ICP-MS equipped with a High Matrix Introduction accessory. For all analyses the instrument was tuned for maximum signal as well as minimum interference from doubly charged and metal oxide ions. Standards, blanks and samples were injected in triplicate through a MicroMist concentric nebulizer (0.4 mL/min) and a Scott-type double-pass spray chamber, Peltier-cooled to 2°C. A 1% HNO_3 rinse was performed before and after each analyte solution. Each batch of samples was analyzed at least twice in random order with a precision of approximately 1-2% and often less than 1%.

Distribution coefficients were calculated from dissolved YREE concentrations, $[M]_{diss}$, as

$$ {}_{i}K_{Mn} = \frac{[M]_{init} - [M]_{diss}}{[M]_{diss} \times [Mn]_{T}} \tag{2.3} $$

where $[M]_{init}$ is the initial YREE concentration and $[Mn]_T$ is the total Mn concentration added to the experimental solution, calculated from the weight of HMO corrected for water content and its stoichiometry as determined from the iodometric titrations.

The effect of colloidal HMO on YREE sorption was investigated by ultracentrifugation of an additional (15 mL) 0.22 μm filtered sample at pH ~ 6.5 since colloid-bound YREE would erroneously increase $[M]_{diss}$ (Schijf and Zoll, 2011). The filtrate was sequentially passed through two 50 mL Millipore Amicon ultrafiltration tubes (30kDa and 3kDa MWCO, respectively) using a Hettich EBA 21 centrifuge. Retentates were collected by centrifugation of 10 mL of 1% HNO_3 through each Amicon tube.

2.4. Non-electrostatic surface complexation model

Based on the results of iodometric redox titrations (Table 2.1) and X-ray powder diffraction, synthetic HMO used in these sorption experiments contained only Mn(IV) oxides as $MnO_{2.01\pm0.05}$ that were mostly amorphous which is in agreement with previous investigations (Murray, 1974; Villalobos et al., 2003). Therefore the sorbent surface is described in its most hydrated state, $S \equiv Mn(OH)_4^0$ where the triple bond symbol simply indicates that Mn is tightly bound to the oxide surface, S. Based on the extensive surface complexation modeling of amphoteric metal oxides, I derived a model for YREE sorption on hydrous manganese oxides as done previously with hydrous ferric oxides (Schijf and Marshall, 2011). The surface groups considered were $S \equiv Mn(OH)_3^+$ at low pH, $S \equiv Mn(OH)_4^0$ at intermediate pH and $S \equiv Mn(OH)_5^-$ at high pH with the final equation written in terms of $S \equiv Mn(OH)_4^0$. Conversion between these species can be described by (de)protonation reactions

$$S \equiv Mn(OH)_4^0 + H^+ \rightleftharpoons S \equiv Mn(OH)_3^+ + H_2O$$

$$S \equiv Mn(OH)_4^0 + H_2O \rightleftharpoons S \equiv Mn(OH)_5^- + H^+$$

with equilibrium constants:

$${}_sK_1 = \frac{[S \equiv Mn(OH)_3^+]}{[S \equiv Mn(OH)_4][H^+]} \quad (2.4)$$

$${}_sK_2 = \frac{[S \equiv Mn(OH)_5^-][H^+]}{[S \equiv Mn(OH)_4]} \quad (2.5)$$

The total concentration of surface sorption sites, $[S\equiv Mn]_T$, is then calculated as:

$$\begin{aligned}[S \equiv Mn]_T &= [S \equiv Mn(OH)_3^+] + [S \equiv Mn(OH)_4^0] + [S \equiv Mn(OH)_5^-] \\ &= [S \equiv Mn(OH)_4^0]({}_sK_1[H^+] + 1 + {}_sK_2[H^+]^{-1})\end{aligned} \quad (2.6)$$

Only YREE surface complexes with charges of 2+ to 0 are considered here, in agreement with previous investigations (Quinn et al., 2006a; Schijf and Marshall, 2011). Consequently, YREE sorption can be defined by proton exchange reactions between the dissolved metal, M^{3+}, and each form of the HMO surface, as those releasing no protons:

$$S \equiv Mn(OH)_5^- + M^{3+} \rightleftharpoons S \equiv Mn(OH)_5M^{2+}$$

one proton:

$$S \equiv Mn(OH)_4^0 + M^{3+} \rightleftharpoons S \equiv Mn(OH)_3OM^{2+} + H^+$$
$$S \equiv Mn(OH)_5^- + M^{3+} \rightleftharpoons S \equiv Mn(OH)_4OM^{+} + H^+$$

two protons:

$$S \equiv Mn(OH)_3^+ + M^{3+} \rightleftharpoons S \equiv Mn(OH)O_2M^{2+} + 2H^+$$
$$S \equiv Mn(OH)_4^0 + M^{3+} \rightleftharpoons S \equiv Mn(OH)_2O_2M^{+} + 2H^+$$
$$S \equiv Mn(OH)_5^- + M^{3+} \rightleftharpoons S \equiv Mn(OH)_3O_2M^{0} + 2H^+$$

and three protons:

$$S \equiv Mn(OH)_3^+ + M^{3+} \rightleftharpoons S \equiv MnO_3M^{+} + 3H^+$$
$$S \equiv Mn(OH)_4^0 + M^{3+} \rightleftharpoons S \equiv Mn(OH)O_3M^{0} + 3H^+$$

These sorption reactions can be expressed by stability constants

$$\begin{aligned}
{}_3\beta_n &= \frac{[S \equiv Mn(OH)_{3-n}O_nM^{(4-n)+}][H^+]^n}{[S \equiv Mn(OH)_3^+][M^{3+}]} = \frac{[S \equiv Mn(OH)_{3-n}O_nM^{(4-n)+}][H^+]^{n-1}}{{}_sK_1[S \equiv Mn(OH)_4^0][M^{3+}]} \\
{}_4\beta_n &= \frac{[S \equiv Mn(OH)_{4-n}O_nM^{(3-n)+}][H^+]^n}{[S \equiv Mn(OH)_4^0][M^{3+}]} \\
{}_5\beta_n &= \frac{[S \equiv Mn(OH)_{5-n}O_nM^{(2-n)+}][H^+]^n}{[S \equiv Mn(OH)_5^-][M^{3+}]} = \frac{[S \equiv Mn(OH)_{5-n}O_nM^{(2-n)+}][H^+]^{n+1}}{{}_sK_2[S \equiv Mn(OH)_4^0][M^{3+}]}
\end{aligned} \tag{2.7}$$

where ${}_3\beta_n$, ${}_4\beta_n$ and ${}_5\beta_n$ indicate those sorption reactions releasing *n* protons from positively charged, neutral and negatively charged surface groups respectively. The total

sorbed metal concentration, $[MS_i]_T$, can now be calculated with composite complexation constants of the form A_n where *n* now indicates the number of protons exchanged relative to $S \equiv Mn(OH)_4^0$ as: $A_1 = {}_3\beta_2 \times {}_sK_1 + {}_4\beta_1 + {}_5\beta_0 \times {}_sK_2$, $A_2 = {}_3\beta_3 \times {}_sK_1 + {}_4\beta_2 + {}_5\beta_1 \times {}_sK_2$ and $A_3 = {}_4\beta_3 + {}_5\beta_2 \times {}_sK_2$. Substituting the total sorbed metal and total surface sorption site concentrations into the definition of the distribution coefficient (Equation (2.3)) gives

$$ {}_iK_{Mn} = \frac{[MS_i]_T}{M_T[Mn]_T} = \frac{[M^{3+}](A_1[H^+]^{-1} + A_2[H^+]^{-2} + A_3[H^+]^{-3})}{M_T({}_sK_1[H^+] + 1 + {}_sK_2[H^+]^{-1})} \quad (2.8) $$

It was previously shown under similar conditions that the pH-dependent sorption of metal hydroxides (MOH^{2+}) does not change the model equation, only its interpretation, while sorption of metal chlorides (MCl^{2+}) is constant and after the introduction of an A_0 term in the model, the total dissolved concentration, M_T, is mathematically indistinguishable from the free dissolved concentration, $[M^{3+}]$ (Schijf and Marshall, 2011). To obtain the final equation under the current conditions, the only alteration of the model equation is the addition of an A_0 term in the numerator to describe metal chloride sorption on positively charged groups:

$$ {}_iK_{Mn} = \frac{A_0 + A_1[H^+]^{-1} + A_2[H^+]^{-2} + A_3[H^+]^{-3}}{{}_sK_1[H^+] + 1 + {}_sK_2[H^+]^{-1}} \quad (2.9) $$

This equation is the same as the one used for YREE sorption on hydrous ferric oxides (Schijf and Marshall, 2011).

2.5. Results and discussion

Distribution coefficients, ${}_iK_{Mn}$, were determined as a function of pH over the range 3.71-7.83 (0.5 M NaCl, T=25°C) (Table 2.2). The pH window was limited by HMO dissolution at low pH and dissolved YREE depletion at high pH. Precipitation of

YREE hydroxides did not occur at high pH, as has been previously documented (Diakonov et al., 1998), since strong sorption on HMO maintained low dissolved YREE concentrations at elevated pH. The influence of colloidal interactions on YREE sorption was checked by ultracentrifugation of a sorption sample from pH ~ 6.5 that indicated colloid-bound YREE were not significant during these experiments, as found on hydrous Fe oxides (Schijf and Marshall, 2011). More than 90% of dissolved YREE were non-colloidal (< 3 kDa) and thus truly dissolved at this pH for all YREE. The high Na^+ concentration in this work may have caused neutralization of the negative surface charge on HMO leading to particle coagulation thus removing any colloids, as was visually apparent during the 0.5 M NaCl pre-equilibration period before each sorption experiment. However, in similar experiments performed with *Ulva lactuca*, a marine macroalgae, as the sorbent, colloids had a strong effect on YREE sorption, even in 5.0 M NaCl solutions (Schijf and Zoll, 2011). Differences in the influence of colloidal sorption between these systems may reflect an inherent distinction between inorganic and organic colloids, or that HMO colloids simply did not form in my solutions.

2.5.1. Linear regression of distribution coefficients as a function of pH

Sorption was initially described as a function of pH by linear regression (Figure 2.1). The resulting slope was approximately 0.5 for all YREE, except cerium, indicating that ~ 0.5 protons were released on average for each YREE sorbed over the experimental pH range. The average proton exchange is less than one due to the combination of sorption reactions releasing 0, 1 and 2 protons over the entire experimental pH range. Sorption occurred only with surface hydroxyl groups since the HMO was highly amorphous, unlike the interaction with structural oxygen atoms found on crystalline Mn

oxides (Appelo and Postma, 1999). Also, extended X-ray absorption fine structure (EXAFS) work has suggested that YREE sorption on hydrous manganese oxides is associated with surface hydroxyl groups (Ohta et al., 2009b). Ohta et al. (2009a, b) used EXAFS to determine coordination numbers of 8 for HREE and 10 for LREE consisting of 6 short and 4 long M-O bonds. The bond length of La-O was similar to that of Ba-O in tridentate complexes above a site vacancy on lacustrine Mn oxides (Manceau et al., 2007) while Lu-O lengths were similar to those of Pb-O bound at the surface and edge of δ-MnO_2 (Takahashi et al., 2007). Ohta et al. (2009b) interpreted this information as well as the similar bonding angles of all analyzed YREE on hydrous ferric and manganese(IV) oxides to indicate that YREE are bound to HMO edges through bidentate or distorted tridentate complexes for the LREE (La, Pr, Nd and Sm) whereas the HREE form bidentate structures. Although LREE and HREE experience different total coordinations, the similar proton exchange associated with their sorption (Figure 2.1) indicates that all YREE sorb on similar sites. Increased LREE coordination may thus be due to additional bonding with water that also alters M-O bond lengths.

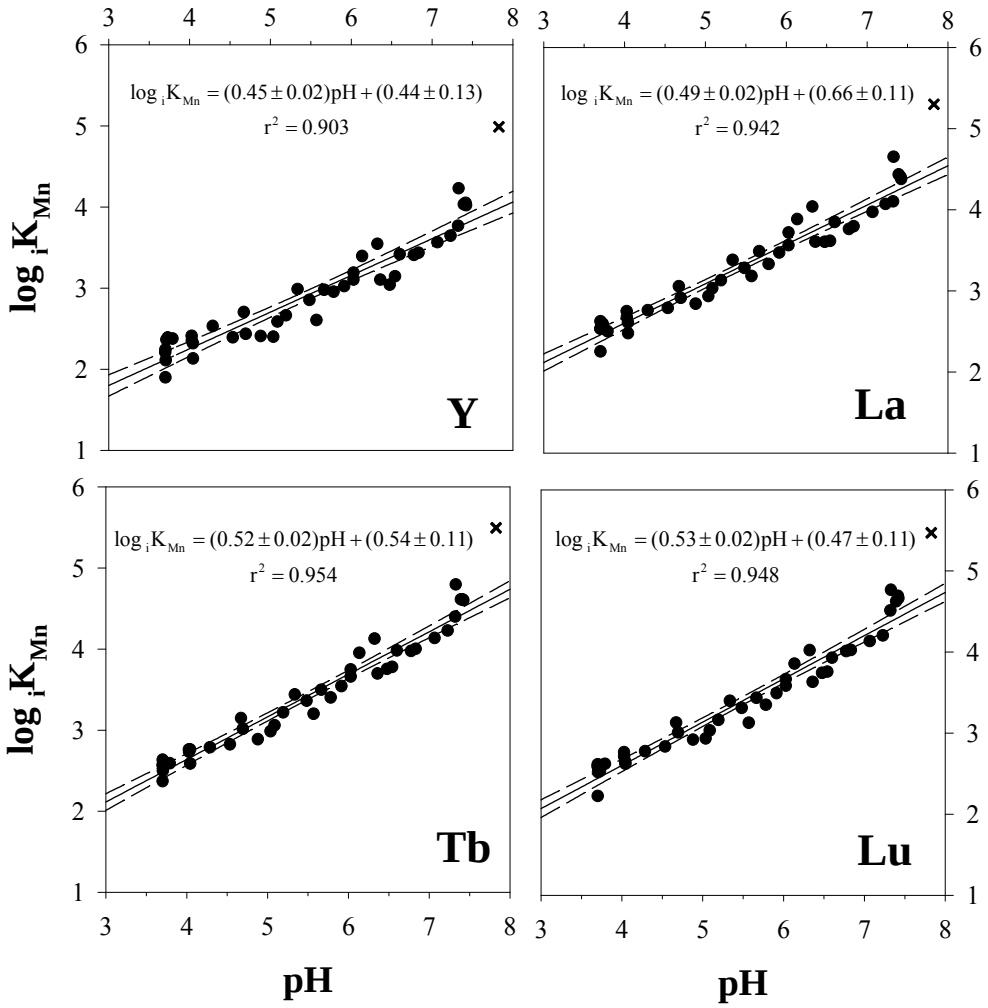

Figure 2.1. Linear regression of Y, La, Tb and Lu distribution coefficients *vs.* pH where slopes indicate the average number of protons released per YREE cation sorbed on HMO over the experimental pH range (0.5 M NaCl, 25°C). The highest pH point is represented by an 'x' and was not considered in the linear regression since it deviates from linearity for all YREE. Dashed lines represent the 95% confidence interval of the regression. Uncertainties are one standard error of the mean.

2.5.2 Non-linear regression as a function of pH and model parameters

The data were also fit with the non-electrostatic surface complexation model (Equation (2.9)) to account for specific sorption reactions. Cerium data were not considered during model development because Ce sorption was strongly influenced by non-equilibrium oxidation processes (see Section 2.4.4). The model parameters were

optimized by fitting the data in SigmaPlot which yielded ${}_sK_1 = 0$ and $A_0 = 0$ indicating that $S \equiv Mn(OH)_3^+$ did not exist in the pH range (3.71-7.83) and consequently there was no MCl^{2+} sorption on $S \equiv Mn(OH)_3^+$. However, sorption of metal chlorides on neutral and negative surface groups cannot be dismissed. Including the A_3 term in the model did not statistically improve its fit, meaning that under the current experimental conditions, sorption reactions exchanging three protons from neutral surface groups or two protons from negative surface groups were not observed. This could result from sparse data at elevated pH (> 7.5) where reactions with greater proton exchange that are described by A_3 and formation of MOH^{2+} species that releases an additional proton are more likely. Equation (2.9) was accordingly altered to the final model:

$$ {}_iK_{Mn} = \frac{A_1[H^+]^{-1} + A_2[H^+]^{-2}}{1 + {}_sK_2[H^+]^{-1}} \tag{2.10} $$

The ${}_sK_2$ value is a property of the HMO surface and as such should be the same for all YREE. However when fits were performed with an adjustable ${}_sK_2$ parameter each YREE gave a slightly different value due to the correlation of adjustable parameters and higher degree of freedom in the model. The ${}_sK_2$ parameter was therefore optimized via a series of regressions by fixing $\log {}_sK_2$ at values near its average found for all YREE when $\log {}_sK_2$ was left as a free parameter. Each YREE was individually fit with Equation (2.10) using $\log {}_sK_2$ values between -3.9 and -4.6 going down in 0.1 increments and then in 0.01 increments from -4.24 to -4.30. The optimum value (-4.27) gave the lowest combined residual sum of squares for all the YREE and the data were refit with this fixed value (Figure 2.2). The ${}_sK_2$ value indicates that the HMO surface has an equal amount of neutral and negatively charged surface groups near pH 4.27 under the experimental

conditions. Literature pH_{pzc} values range from 1-3 (Tonkin et al., 2004; Tan et al., 2008) such that based on this optimized $_sK_2$, the $_sK_1$ value under these conditions would be below the pH range, less than 1.7, supporting the lack of $S \equiv Mn(OH)_3^+$ in this experiment.

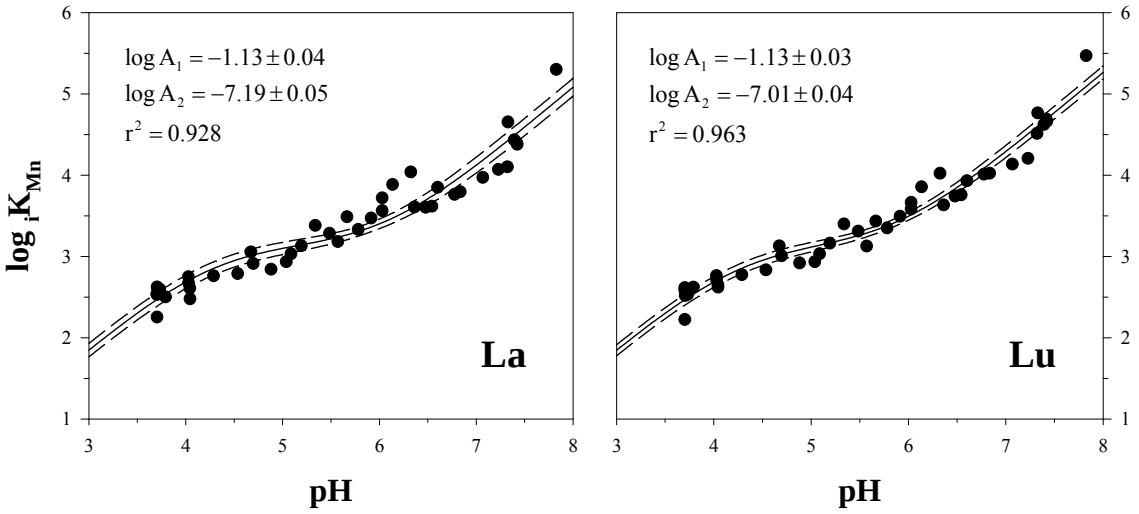

Figure 2.2. Non-electrostatic surface complexation model (Equation (2.10)) regressions for La and Lu sorption on HMO (0.5 M NaCl, 25°C). The data are fit better with this model than in linear regressions (Figure 2.1). Listed parameters are conditional stability constants, A_1 and A_2, obtained while fitting the data with Equation (2.10) using p_sK_2 = 4.27. See Table 2.3 for more information. Dashed lines represent the 95% confidence interval of the regression. Uncertainties are one standard error of the mean.

The model fits the data better for most YREE (Figure 2.2) than linear regressions (Figure 2.1). Stability constants, A_1 and A_2, obtained from the model are similar for all YREE but there is some fractionation among the elements, especially in A_2 (Table 2.3 and Figure 2.3). The A_n values are composite constants that describe sorption reactions on both neutral and negatively charged surface groups. The A_1 term describes YREE sorption on neutral surface groups releasing one proton and on negative groups with no proton release, while A_2 represents a two proton exchange from a neutral group and a one proton release from a negative group. Sorption occurs equally through net exchanges of

one and two protons relative to a neutral group when $pH = \log(A_2/A_1)$ which has an average of 5.85 for all YREE, excluding Ce (Table 2.3).

Linear free-energy relations (LFER) utilize known complexation constants for dissolved ligands to explain metal complexation by analogous surface ligands. Hydroxide ions are similar to the negatively charged surface groups on HMO and thus likely control YREE complexation behavior in a similar manner. Linear free-energy relations between the first hydrolysis constant of YREE, β^*_1, and the stability constants, A_1 and A_2, gave poor fits (data not shown) since these stability constants are composite terms that describe sorption on both neutral and negative surface sites. A strong LFER with the first hydrolysis constant of YREE should only exist with an A_n term that describes sorption on a site analogous to a dissolved hydroxyl ion, $S \equiv Mn(OH)_5^-$. Since the model does not contain such a stability constant, A_1 and A_2 have shapes that are distinctly not 'hydrolysis-like' (Figure 2.3) resulting in poor LFER.

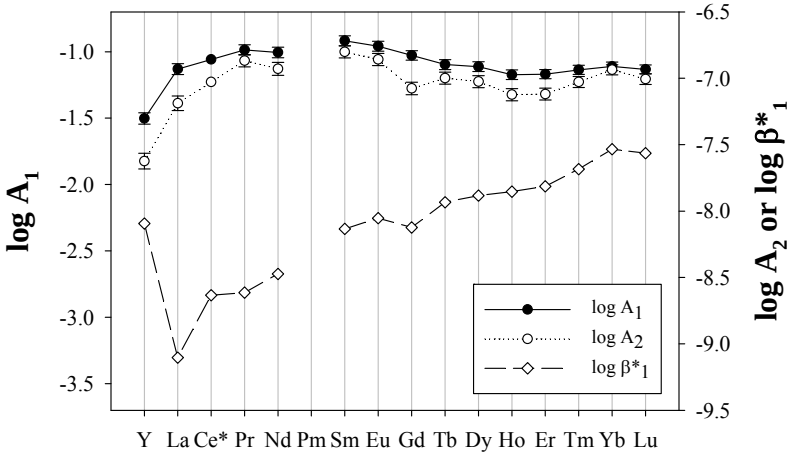

Figure 2.3. Composite stability constants, A_1 and A_2, for all YREE obtained during model regressions (Equation (2.10)) of the experimental data (0.5 M NaCl, 25°C) and the first hydrolysis constant, log β^*_1 (Klungness and Byrne, 2000), shown for comparison. Cerium values (Ce*) of stability constants were calculated by interpolation of those for La and Pr. Error bars represent one standard error of the mean.

2.5.3. Validity of the model

A model is only useful if it can faithfully predict behaviors in a variety of situations. I have therefore tested the quality of the model by investigating its ability to predict sorption over a range of solution conditions. The usefulness of YREE investigations derives from their coherent group behavior, so although the composite model cannot predict absolute sorption values under varying conditions, it is most important that the relative behavior of the YREE can be estimated for many solution compositions. The model was evaluated first by its ability to describe the experimental data reported here and then to reproduce sorption patterns found by others. Since Ce sorption occurs by non-equilibrium processes, Ce values were linearly interpolated from La and Pr sorption in the model and represent only Ce(III) sorption. Cerium sorption and oxidation will be discussed in the following section.

Sorption for all YREE is reproduced well by the model under the current experimental conditions (0.5M NaCl, 25°C). The ratio of predicted to measured distribution coefficients had a mean near one for all elements (Figure 2.4). The model slightly over-predicts sorption at pH < 5 and pH > 6.5 while under-predicting between pH 5 and 6.5 in most samples. Even so, the change in sorption behavior with pH is captured by the model (Figure 2.5) where at low pH there is little fractionation but as pH increases sorption is different for each YREE, as shown previously (Ohta and Kawabe, 2001). Increased fractionation may be caused by a transition toward sorption reactions that exchange more protons, described by stability constant A_2, with increasing pH since the A_2 pattern showed more structure among the YREE than the A_1 pattern (Figure 2.3).

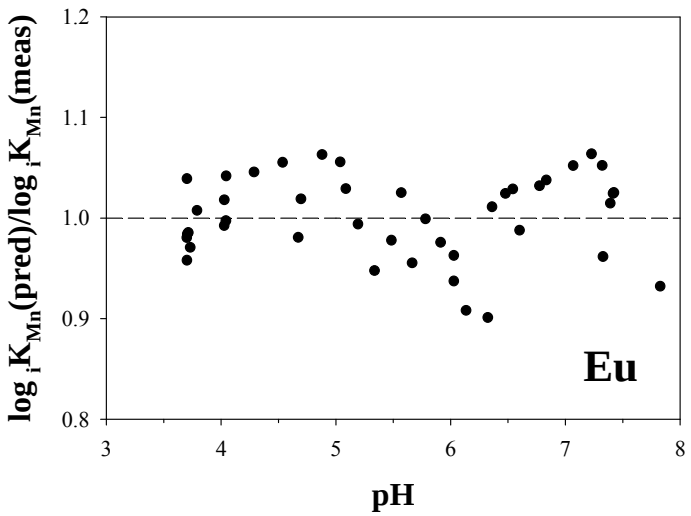

Figure 2.4. Model quality over the investigated pH range for europium. Predicted values were calculated with the proposed model (Equation (2.10)) using best fit parameters (stability constants in Table 2.3 and $p_sK_2 = 4.27$). Ratios of predicted to measured distribution coefficients, log $_iK_{Mn}$(pred)/log $_iK_{Mn}$(meas), are greater than 1 at pH values between 4 and 5 and above 6.5 (slight over-prediction of sorption) while between pH 5 and 6.5 they are less than 1 (slight under-prediction of sorption). Over the entire pH range the average ratio is near unity (mean = 1.002) and no trend with pH, supporting the validity of the model.

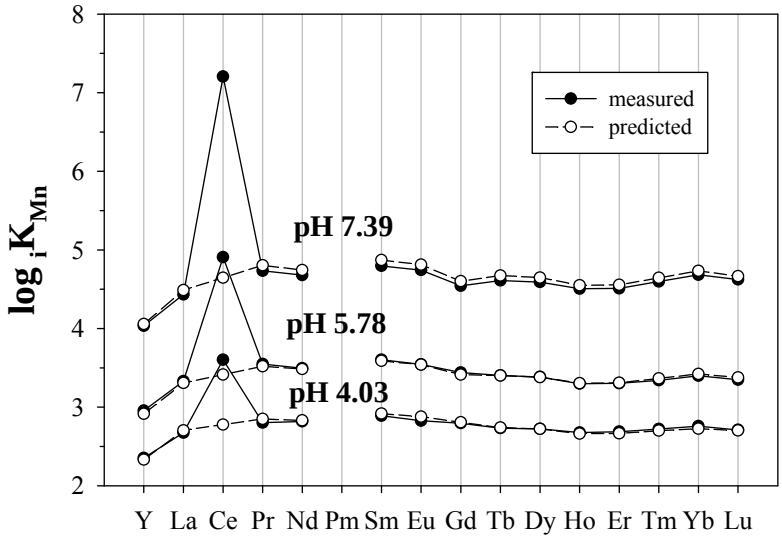

Figure 2.5. Distribution coefficients, log $_iK_{Mn}$, at low, intermediate and high pH for each YREE (0.5 M NaCl, 25°C). The predicted values are calculated from the model (Equation (2.10)) using best fit parameters from Table 2.3. Predicted values for Ce were estimated from the average values of La and Pr and therefore represent only Ce(III) sorption.

A more complete test of the quality of the model is its ability to explain sorption data from the literature. There are no applicable field studies but there are four appropriate laboratory investigations. The experimental conditions of Ohta and Kawabe (2001) were quite similar to mine (0.5 M NaCl, 25°C), with the difference that CO_2 was not removed from their solutions. The work of De Carlo et al. (1998) described YREE sorption on similarly produced HMO over a range of ionic strengths in the presence of CO_2. Davranche et al. (2005, 2008) performed YREE sorption on crystalline MnO_2 (Aldrich) in 0.001 M NaCl solutions containing CO_2 at pH 5 and under the same conditions over a range of pH. Here I compare my model predictions with data from Ohta and Kawabe at pH 5.59 and 6.8, De Carlo et al. at pH 5.75 in 0.7 *m* $NaNO_3$ and seawater solutions and from Davranche et al. at pH 5 and 6. All data were converted from the authors' calculation of distribution coefficients to my definition of $\log {}_iK_{Mn}$ (Equation (2.3)) for comparison. In Figure 2.6, model predictions have been vertically transposed along the arrows to give the best overlap with the measured literature patterns. For the Ohta and Kawabe (2001) data, the model quantitatively represented YREE sorption at pH 5.59 and 6.8, so the predicted patterns were not moved. Sorption was under-predicted for the De Carlo et al. (1998) data by approximately 1.5 log units in 0.7 *m* $NaNO_3$ and 2 log units in seawater. At pH 6, the model prediction was near experimental values of Davranche et al. (2008) and was not shifted. At pH 5, the measured values of Davranche et al. (2005, 2008) are separated by about 1 log unit which may have been caused by ageing of the crystalline MnO_2 surface or different MnO_2 batches with slightly altered surface properties between the studies. Nonetheless, my model pattern falls between the measured values and exhibits sorption behavior similar to those in Davranche et al.

(2005, 2008), supporting the model's utility as a predicting tool. The sorption patterns of YREE are quite similar over the range of experimental conditions while differences in solution conditions likely caused the variations in absolute log ${}_iK_{Mn}$ values between the model and experimental data (Kanungo et al., 2004). The amount of sorption can be influenced by varying YREE speciation in the different media due to YREE solution complexation by carbonate and nitrate anions in addition to competition from other cations (Ca^{2+}, Mg^{2+}) for sorption sites in seawater. The relative YREE sorption behavior, as described by sorption patterns, provides important insights into the relevant mechanisms which are largely unchanged over the range of ionic strengths (0.001-0.7 M) and solution compositions covered by these datasets.

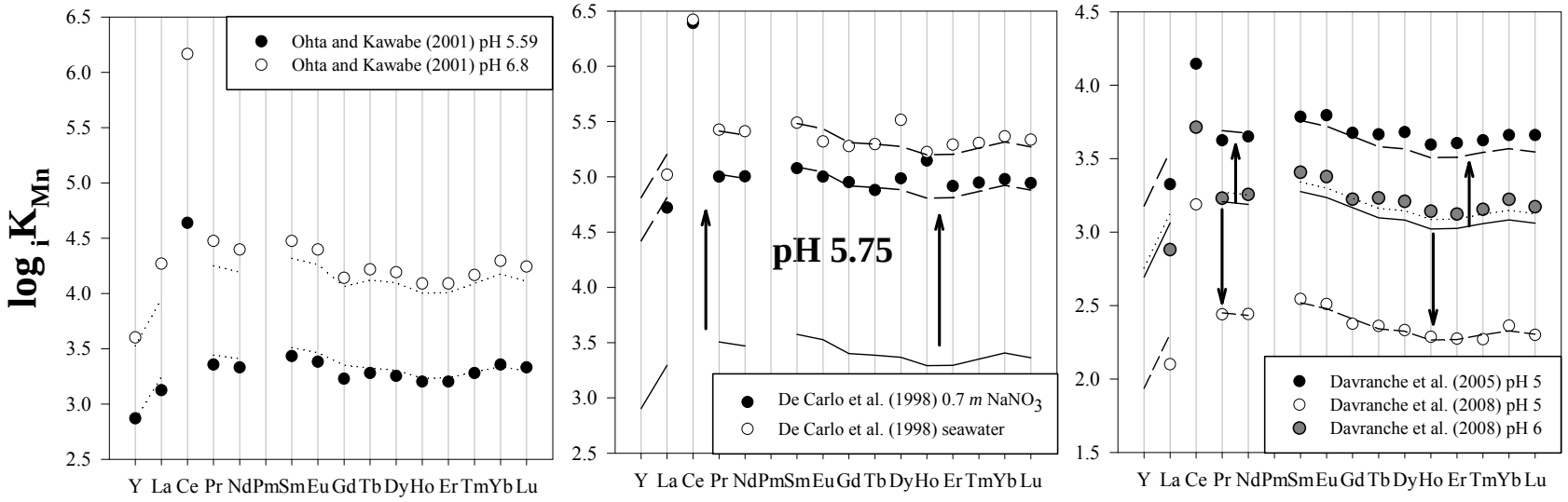

Figure 2.6. Comparison of model predictions of sorption with literature data (De Carlo et al., 1998; Ohta and Kawabe, 2001; Davranche et al., 2005, 2008) converted to my definition of $_iK_{Mn}$ (Equation (2.3)). The model predictions (solid line) were calculated at matching pH values using Equation ((2.10)) and the best fit parameters from Table 2.3. Cerium sorption was not modeled since it occurs via oxidative processes (section 2.4.4). The predicted values were adjusted vertically along the arrows to give the best overlap with literature values and are shown as dashed lines. The model predictions at pH 5.59, 6.8 and 6 (dotted lines) were not adjusted.

2.5.4. Cerium anomaly

Sorption of cerium occurred with higher log $_iK_{Mn}$ values than the remaining YREE and an average release of one proton per Ce cation sorbed over the pH range, compared to 0.5 protons exchanged for the other YREE (Figure 2.7). Cerium sorption was also less linear than sorption of the remaining YREE with a sudden increase in Ce removal from solution near pH 5.5. Below pH 5.5, proton exchange associated with Ce sorption was similar to the other YREE with an average of 0.52 protons exchanged per Ce cation sorbed. Above pH 5.5, elevated proton exchange occurred with 1.33 protons released on average per Ce sorbed. The sudden shift in Ce sorption at pH 5.5 was not observed for the other YREE and is the focus of this section.

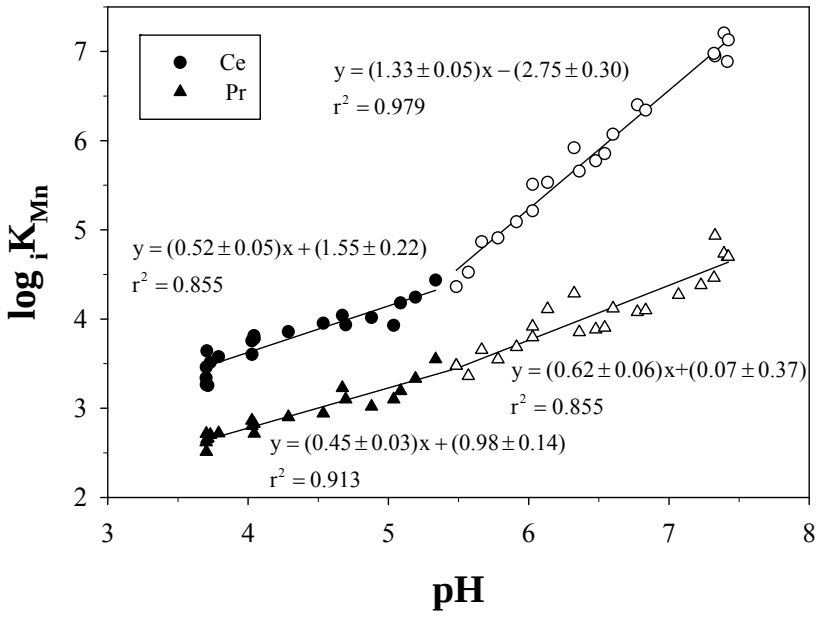

Figure 2.7. Linear regression of cerium (circles) and praseodymium (triangles) sorption at pH < 5.5 (closed points) and pH > 5.5 (open points) where the slope indicates the average number of protons released for each metal sorbed over the pH range. The proton exchange associated with Ce sorption increases by 0.81 above pH 5.5, while that of Pr sorption increases only 0.17 units above pH 5.5.

Cerium sorption occurs via non-oxidative mechanisms similar to the other YREE but also by oxidative processes that lead to its differentiation from the remaining YREE. Cerium(III) is initially sorbed on HMO and then is oxidized to Ce(IV), as confirmed by X-ray Absorption Near Edge Structure analyses (Takahashi et al., 2002). Cerium oxidation lowers surface-bound Ce(III) concentrations which consequently encourages more Ce sorption. The influence of Ce oxidation can be determined by normalizing Ce sorption to the linear interpolation of La and Pr sorption (Equation (1.2)). Relative Ce enrichment, defined as $\log(K_{Ce}/K_{Ce^*}) > 0$ or a positive Ce anomaly, occurred on HMO over the entire pH range, as found previously (De Carlo et al., 1998; Ohta and Kawabe, 2001), indicating that Ce oxidation was favorable under these conditions. At low pH, cerium is more likely oxidized by a strong oxidant, such as HMO, than any traces of dissolved O_2 that may have existed in experimental solutions (e.g., Yu et al., 2006). Cyclic voltammetry analyses at pH ~ 3 indicate that HMO is reduced during Ce oxidation supporting the oxidative role of HMO (De Carlo et al., 1998). The Ce anomaly, and presumably Ce oxidation by HMO, increased approximately 50-fold over the investigated pH range (3.71-7.83) including an abrupt rise near pH 5.5 as previously documented (Ohta and Kawabe, 2001) (Figure 2.8). The cerium anomaly increase with pH found here is larger than in the literature (Ohta and Kawabe, 2001) but the pattern of the anomaly is very similar even though distribution coefficients (K_{La}, K_{Ce} and K_{Pr}) used to determine Ce anomalies were calculated by Ohta and Kawabe as mole fractions unlike my ${}_iK_{Mn}$ calculations (Equation (2.3)). Lowered Ce anomalies were found at the upper pH ranges of both datasets due to increased La and Pr sorption while detection limitations of low dissolved Ce concentrations made Ce sorption appear fairly constant.

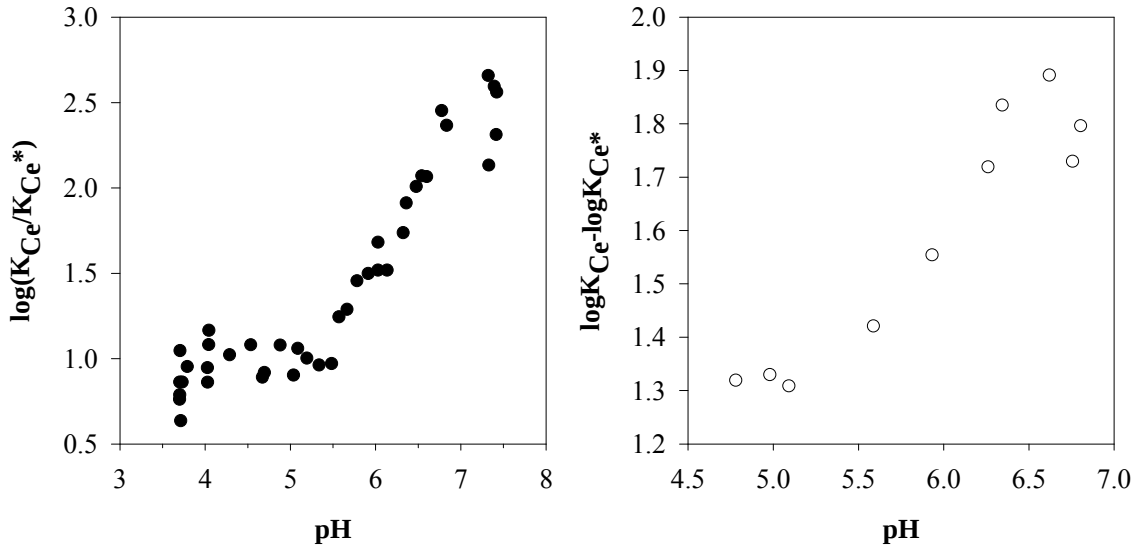

Figure 2.8. Cerium anomalies over experimental pH ranges from the current data (left panel) calculated as $\log(K_{Ce}/K_{Ce^*})$ and Ohta and Kawabe (2001) (right panel) calculated as $\log K_{Ce}-\log K_{Ce^*}$. Experimental conditions were similar in both studies (0.5 M NaCl, 25°C), except Ohta and Kawabe did not purge their solutions with inert gas. Distribution coefficients, K_d, are calculated as mole fractions by Ohta and Kawabe (2001) unlike in the current investigation (Equation (2.3)). In both datasets, Ce anomalies indicate Ce oxidation over the entire investigated pH range (values greater than 1) with a steady increase in oxidation above pH 5.5.

The abrupt shifts in proton exchange and Ce anomalies associated with Ce sorption near pH 5.5 can be attributed to changes in Ce speciation since HMO sorption sites gradually deprotonate with increasing pH, which should discourage electron transfer to HMO during Ce oxidation. Initial sorption of Ce(III) likely occurs via the same mechanism as the other trivalent YREE. Since the proton exchange associated with Ce sorption below pH 5.5 is similar to that of the other YREE, Ce oxidation at low pH must not release any additional protons. Oxidation below pH 5.5, thus likely occurs via a simple charge transfer between Ce and Mn. At elevated pH, the increased prevalence of YREE-hydroxides produces the slightly greater proton-exchange sorption of strictly trivalent YREE (Figure 2.7). Cerium most likely initially sorbes by this same mechanism, releasing on average approximately 0.6 protons per Ce cation. Thus, oxidative pathways

must lead to additional proton exchange to achieve the appropriate total exchange of 1.33 for Ce sorption above pH 5.5. Cerium oxidation on HMO may occur by many reactions with different proton exchanges, as found for Ce oxidation in solutions (Hayes et al., 2002; Yu et al., 2006). A shift in the Ce oxidation mechanism on HMO likely either occurs due to sorption of Ce(III) hydroxide species, instead of free Ce^{3+}, or a change in the electron transfer between Ce and HMO such that H_2O or hydroxyl groups are involved and release protons. Therefore, the shifts in proton exchange and amount of oxidation during Ce sorption are most likely due to changes in the reactants over the experimental pH range.

2.6. Summary

Hydrated manganese oxides (HMO) contain highly reactive surface hydroxyl groups that can influence the fate and transport of many environmentally relevant elements through sorptive proton exchange and redox reactions. The chemical coherence of YREE was exploited to identify these mechanisms. A non-electrostatic surface complexation model was created to explain YREE non-oxidative sorption on hydrous manganese oxides by adapting a previous model for YREE sorption on hydrous ferric oxides and accounting for known HMO surface characteristics. Deprotonation of HMO occurred at low pH (~ 4.3) which increases its sorption capacity for dissolved cations over a wider pH range relative to other surfaces in seawater. The model describes my experimental data and literature YREE sorption patterns well over a range of ionic strength (0.001-0.7M). Cerium oxidation by HMO occurred through two different types of reactions over the pH range that consequently produced a sudden shift near pH 5.5 in the proton exchange associated with Ce sorption and the magnitude of Ce anomalies.

Cerium was likely oxidized at low pH via a simple charge transfer between Ce and Mn(IV), whereas more complicated interactions with HMO likely oxidized Ce at higher pH. Manganese-oxide-rich environments thus have an elevated tendency to contain oxidized species.

The sorption mechanisms of all YREE, except Ce, are similar on hydrous iron (Schijf and Marshall, 2011) and manganese oxides. EXAFS analyses (Ohta et al., 2009b) suggest that sorption occurs through the formation of inner-sphere bidentate or distorted tridentate complexes for LREE and bidentate structures for HREE on hydrous Mn oxides. The same investigations on hydrous Fe oxides found that inner-sphere monodentate and bidentate binding occurs for all YREE. This similarity in YREE bonding is somewhat expected since these surfaces are amorphous and only contain hydroxyl groups, but also suggests that my non-electrostatic surface complexation model may be able to describe sorption processes on any amphoteric surface with one type of functional group.

Cerium was oxidized by hydrous manganese oxides under anaerobic conditions indicating that Ce anomalies are not an indicator of bottom water conditions at the time of their formation, as required for their use as a paleo-redox proxy (German and Elderfield, 1990). The variability of sedimentary Ce anomalies may be influenced by shifts in particulate Mn fluxes that contain 'preformed' Ce anomalies, independent of dissolved O_2, that are delivered to sediments. Interpretations of sedimentary Ce anomaly profiles therefore likely overestimate dissolved O_2 concentrations in paleo-basins when Mn oxides were present.

The mechanisms of Ce oxidation by components other than Mn oxides still require more research. The relative influence of Mn oxides in more natural mixed

particulates will be investigated in the next chapter via similar sorption experiments with mixed sorbents containing varying amounts of hydrous Fe and Mn oxides. Since Ce oxidation occurs on Mn oxides but not on Fe oxides, sedimentary records of Ce anomalies may partly reflect the ambient mixture of Fe and Mn present during YREE sorption.

2.7. Data tables

Table 2.1. Reproducibility of Mn oxidation state determination as calculated from Equation (2.2). Concentration of Mn was determined by ICP-MS analysis of a subsample from each iodometric titration. Titrations were standardized by analyzing Aldrich $Mn_2O_{3(s)}$ and $MnO_{2(s)}$ which yielded O:Mn ratios of 1.500 ± 0.003 and 1.99 ± 0.02, respectively.

MnO_x (g wet weight)	$[Na_2S_2O_3]$ (mmol)	[Mn] (mmol)	Oxidation state
22.6	0.0239	0.0110	2.088
34.2	0.0372	0.179	2.041
56.8	0.0590	0.0300	1.983
61.0	0.0635	0.0330	1.961
87.1	0.0918	0.0462	1.994
97.7	0.0894	0.0458	1.977
			2.01 ± 0.05

Table 2.2. Distribution coefficients, log $_{i}K_{Mn}$, for YREE sorption on HMO in 0.5 M NaCl ($[M]_T \sim 50$ μg·L^{-1} except $[Ce]_T \sim 500$ μg·L^{-1}, $[Mn]_T \sim 0.13$ mM, pH ≥ 3.7 , T = 25.0 ± 0.1°C).

	Experiment 1								Experiment 2					
time[a]									*		*			*
pH	3.71	4.04	4.54	5.09	5.57	6.36	7.07	7.23	3.79	4.29	4.88	5.78	6.48	6.78
Y	2.11	2.13	2.39	2.59	2.61	3.10	3.57	3.65	2.38	2.53	2.41	2.96	3.04	3.41
La	2.53	2.48	2.79	3.03	3.18	3.61	3.97	4.07	2.50	2.76	2.84	3.33	3.60	3.76
Ce	3.64	3.78	3.95	4.18	4.52	5.66	---[b]	---[b]	3.58	3.86	4.02	4.91	5.77	6.40
Pr	2.65	2.72	2.94	3.19	3.36	3.85	4.27	4.38	2.72	2.90	3.02	3.55	3.88	4.08
Nd	2.59	2.73	2.93	3.17	3.32	3.80	4.22	4.32	2.61	2.79	2.94	3.50	3.83	4.02
Pm[c]														
Sm	2.68	2.77	2.98	3.24	3.42	3.91	4.35	4.44	2.77	2.94	3.11	3.60	3.95	4.16
Eu	2.69	2.77	2.97	3.21	3.37	3.85	4.28	4.38	2.69	2.90	3.06	3.54	3.89	4.10
Gd	2.70	2.75	2.94	3.14	3.24	3.69	4.09	4.18	2.75	2.90	3.00	3.44	3.74	3.92
Tb	2.50	2.59	2.82	3.06	3.20	3.70	4.14	4.23	2.59	2.79	2.89	3.40	3.75	3.98
Dy	2.50	2.59	2.80	3.04	3.17	3.66	4.12	4.20	2.58	2.74	2.92	3.38	3.73	3.96
Ho	2.48	2.54	2.74	2.98	3.09	3.57	4.02	4.10	2.53	2.70	2.82	3.30	3.64	3.87
Er	2.51	2.57	2.78	2.98	3.09	3.57	4.03	4.11	2.56	2.73	2.82	3.30	3.64	3.88
Tm	2.51	2.56	2.81	3.02	3.13	3.63	4.11	4.19	2.56	2.76	2.88	3.34	3.72	3.97
Yb	2.47	2.61	2.84	3.06	3.18	3.70	4.21	4.28	2.58	2.77	2.93	3.40	3.80	4.08
Lu	2.52	2.62	2.83	3.03	3.13	3.63	4.13	4.20	2.62	2.78	2.92	3.35	3.74	4.01

[a]Samples collected after more than 12 h equilibrations are indicated with asterisks; [b]Concentrations were too low to accurately calculate a distribution coefficient; [c]not measured

Table 2.2. (*continued*)

	Experiment 3						Experiment 4					Experiment 5					
time[a]		*		*		*		*		*			*		*		*
pH	3.73	4.04	5.19	5.91	7.42	7.39	3.70	4.03	5.67	6.03	7.33	3.70	4.03	5.04	6.54	6.83	7.32
Y	2.39	2.32	2.66	3.02	4.05	4.03	2.24	2.41	2.98	3.19	4.23	1.90	2.35	2.40	3.15	3.44	3.77
La	2.59	2.61	3.13	3.47	4.40	4.43	2.62	2.75	3.49	3.72	4.65	2.25	2.67	2.93	3.62	3.80	4.10
Ce	3.51	3.81	4.24	5.09	6.89	7.20	3.46	3.76	4.87	5.51	6.95	3.26	3.60	3.93	5.85	6.34	6.98
Pr	2.70	2.83	3.33	3.69	4.70	4.74	2.72	2.86	3.65	3.92	4.94	2.51	2.80	3.10	3.90	4.10	4.46
Nd	2.79	2.85	3.31	3.65	4.65	4.68	2.73	2.87	3.60	3.87	4.88	2.49	2.82	3.06	3.85	4.05	4.41
Pm[c]																	
Sm	2.78	2.96	3.41	3.76	4.77	4.80	2.79	2.94	3.71	3.97	4.99	2.60	2.89	3.18	3.98	4.19	4.56
Eu	2.74	2.89	3.36	3.69	4.72	4.74	2.76	2.90	3.65	3.92	4.94	2.54	2.83	3.12	3.92	4.13	4.51
Gd	2.54	2.82	3.22	3.54	4.53	4.54	2.70	2.85	3.51	3.75	4.73	2.41	2.80	3.00	3.74	3.94	4.30
Tb	2.59	2.76	3.22	3.54	4.61	4.61	2.63	2.76	3.50	3.75	4.80	2.37	2.73	2.99	3.78	4.00	4.40
Dy	2.64	2.69	3.18	3.50	4.60	4.59	2.64	2.77	3.47	3.72	4.77	2.33	2.72	2.95	3.75	3.98	4.40
Ho	2.53	2.58	3.07	3.41	4.53	4.51	2.58	2.75	3.40	3.63	4.68	2.32	2.68	2.87	3.67	3.90	4.27
Er	2.52	2.59	3.07	3.43	4.54	4.51	2.59	2.71	3.39	3.62	4.67	2.27	2.69	2.87	3.66	3.91	4.33
Tm	2.58	2.65	3.14	3.49	4.65	4.60	2.63	2.78	3.44	3.67	4.75	2.30	2.72	2.93	3.74	3.99	4.46
Yb	2.59	2.63	3.18	3.53	4.75	4.68	2.62	2.81	3.49	3.72	4.83	2.42	2.76	3.01	3.83	4.09	4.58
Lu	2.53	2.65	3.16	3.49	4.69	4.62	2.61	2.76	3.43	3.66	4.77	2.22	2.71	2.93	3.76	4.02	4.51

[a]Samples collected after more than 12 h equilibrations are indicated with asterisks; [c]not measured

Table 2.2. (*continued)*

	Experiment 6						Experiment 7					
time[a]		*		*				*		*		*
pH	3.70	4.70	5.48	6.03	6.60	7.42	3.71	4.67	5.34	6.14	6.32	7.83
Y	2.21	2.44	2.85	3.10	3.42	4.02	2.36	2.70	2.99	3.40	3.55	4.99
La	2.53	2.91	3.28	3.56	3.85	4.38	2.57	3.06	3.38	3.88	4.04	5.30
Ce	3.34	3.94	4.36	5.21	6.07	7.13	3.26	4.04	4.44	5.53	5.92	---[b]
Pr	2.62	3.10	3.48	3.80	4.12	4.70	2.67	3.23	3.55	4.11	4.29	5.60
Nd	2.62	3.06	3.44	3.75	4.07	4.65	2.67	3.22	3.52	4.07	4.24	5.55
Pm[c]												
Sm	2.73	3.19	3.56	3.87	4.19	4.78	2.72	3.30	3.61	4.17	4.34	5.64
Eu	2.69	3.14	3.50	3.81	4.14	4.72	2.69	3.25	3.56	4.11	4.29	5.62
Gd	2.62	3.04	3.38	3.66	3.95	4.52	2.46	3.14	3.42	3.92	4.09	5.42
Tb	2.57	3.02	3.36	3.66	3.98	4.60	2.62	3.15	3.44	3.95	4.13	5.49
Dy	2.57	3.00	3.34	3.62	3.95	4.59	2.60	3.13	3.41	3.91	4.09	5.47
Ho	2.51	2.93	3.27	3.54	3.86	4.51	2.52	3.06	3.35	3.82	3.98	5.39
Er	2.52	2.94	3.27	3.53	3.85	4.52	2.53	3.07	3.35	3.81	3.97	5.38
Tm	2.53	2.98	3.31	3.59	3.92	4.62	2.57	3.13	3.39	3.86	4.03	5.46
Yb	2.58	3.04	3.35	3.64	3.99	4.72	2.58	3.16	3.44	3.91	4.09	5.51
Lu	2.59	3.01	3.31	3.58	3.93	4.66	2.56	3.13	3.40	3.86	4.02	5.47

[a]Samples collected after more than 12 h equilibrations are indicated with asterisks; [b]Concentrations were too low to accurately calculate a distribution coefficient; [c]not measured

Table 2.3. Best-fit parameters for the non-linear regression of log ${}_iK_{Mn}$ *vs.* pH (Table 2.2) using the non-electrostatic surface complexation model (Equation (2.10)) with ${}_sK_1 = 0$ and $pK_2 = 4.27$. Uncertainties are one standard error of the mean.

M^{3+}	log A_1	log A_2	-log (A_2/A_1)
Y	-1.50 ± 0.04	-7.62 ± 0.06	6.12
La	-1.13 ± 0.04	-7.19 ± 0.05	6.06
Ce*[a]	-1.06	-7.03	5.97
Pr	-0.99 ± 0.04	-6.87 ± 0.05	5.88
Nd	-1.01 ± 0.04	-6.93 ± 0.05	5.92
Pm[b]			
Sm	-0.92 ± 0.04	-6.80 ± 0.05	5.88
Eu	-0.96 ± 0.04	-6.86 ± 0.05	5.90
Gd	-1.03 ± 0.04	-7.08 ± 0.05	6.05
Tb	-1.10 ± 0.04	-7.00 ± 0.05	5.90
Dy	-1.11 ± 0.04	-7.03 ± 0.04	5.91
Ho	-1.17 ± 0.04	-7.12 ± 0.05	5.95
Er	-1.17 ± 0.03	-7.12 ± 0.04	5.95
Tm	-1.14 ± 0.03	-7.03 ± 0.04	5.89
Yb	-1.11 ± 0.03	-6.94 ± 0.04	5.83
Lu	-1.13 ± 0.03	-7.01 ± 0.04	5.87

[a] interpolated; [b] not measured

Chapter 3: The relative influence of Fe(III) and Mn(IV) on YREE sorption and Ce oxidation on hydrous ferromanganese oxides in 0.5 M NaCl solutions

3.1. Abstract

The partitioning of YREE between 0.5 M NaCl solutions and hydrous ferromanganese oxides under anaerobic conditions was quantified by distribution coefficients, ${}_{i}K_{FeMn}$, over a range of pH (4-8) at 25 °C. Three ferromanganese sorbents containing varying proportions of Fe and Mn (3:1, 1:1 and 1:9 mol Fe:mol Mn) were individually investigated and compared with previous findings of YREE sorption on pure hydrous ferric and manganese(IV) oxides to determine the relative influence of Fe and Mn on YREE fractionation. A composite complexation model was developed to further describe experimental and literature data by additively combining non-electrostatic surface complexation models of metal sorption on hydrous Fe and Mn oxides.

Sorption of YREE was greater on hydrous FeMn oxides than on hydrous Fe and Mn oxides separately. On 3:1 and 1:9 FeMn oxides, relative YREE sorption, excluding Ce, was directly related to the Fe and Mn oxide content of each sorbent with associated proton exchange similar to that found on hydrous Fe and Mn oxides, respectively. On 1:1 FeMn oxides, YREE sorption, excluding Ce, caused more protons to be released than for any of the other pure or mixed sorbents.

Cerium was enriched on all hydrous FeMn oxides with Ce anomalies and their pH dependence similar to those found for hydrous Mn oxide alone. The observation of anaerobic Ce oxidation even in the presence of ferromanganese oxides with only a small

fraction of Mn (27%) supports my previous conclusion that the use of sedimentary Ce anomalies as a proxy for bottom water O_2 content may not be appropriate.

3.2. Introduction

Iron and Mn are the 4th and 10th most abundant elements in Earth's crust with an average crustal Fe:Mn ratio of 50:1. However, this proportion is rarely found in seawater due to fractionation of Fe and Mn caused by differences in their chemical properties including oxidation rates and solubility. Even so, the coexistence of Fe and Mn in ferromanganese deposits is quite common. Ferromanganese oxides are complex mixtures that may consist of ferric, manganese(IV) and manganese(III) oxides, carbonates, phosphates, silicates, and trace metals. Based on the lower pH_{pzc} of Mn oxides than Fe oxides, it has been proposed that metal cations such as Co^{3+}, Cd^{2+} and Ag^{+} associate primarily with Mn portions while anions such as PO_4^{3-}, SeO_4^{2-} and AsO_4^{3-} are more likely to associate with Fe sections of ferromanganese minerals (Li, 1982). The surface and redox properties of Fe and Mn oxides can also influence biological productivity through a Mn-Fe-P shuttle whereby dissolved Fe^{2+} is oxidized by Mn oxides resulting in Fe(III) precipitation and the formation of FeMn oxides that encourage phosphorus (P) removal from solution (Dellwig et al., 2010). Phosphorus may either coprecipitate with Fe on Mn oxides or bind to FeMn oxides after their formation. This pump controls P distributions, and thus primary productivity, by preventing P diffusion to surface waters in anoxic zones, except when reduced sulfur promotes Fe removal from the system as iron sulfides. Ferromanganese oxides are thus highly reactive minerals that influence trace metal and nutrient distributions.

Marine ferromanganese minerals are found worldwide in areas with low sedimentation rates and thought to contain important records of oceanic conditions. A review of the basic properties of FeMn deposits has been compiled by Glasby (2000). Ferromanganese oxides form near the seafloor as oblong formations consisting of concentric growth rings around a precipitation nucleus that is often a fragment of bone, shell or another FeMn oxide. Ferromanganese minerals grow via deposition from the water column above, sedimentary diagenesis from below or by a combination of these pathways. Average expansion rates are approximately 1-10 mm My^{-1} (Heath, 1981) meaning that individual rings can represent thousands of years of bottom water conditions. Relative concentrations of Fe and Mn in these deposits vary from approximately 1:1 to 1:4 in the Pacific Ocean (Goldberg, 1954). Since abiotic Fe oxidation is much faster than that of Mn, Mn^{2+} is more mobile than Fe^{2+} leading to FeMn oxides that contain different ratios of Fe and Mn based on their genetic origins. The mineral forms of Fe and Mn within oxides also vary among the formation pathways. Hydrogenous minerals, consisting of hydrous ferric and manganese(IV) oxides, form in the water column and thus have Fe and Mn contents similar to that of seawater with Fe:Mn ratios near 1:1 and the slowest FeMn growth rates of approximately 2 mm My^{-1}. Diagenetic nodules grow primarily in siliceous oozes of sediments at rates near 10-100 mm My^{-1} where Mn exists as todorokite (10 Å manganate) and the increased mobility of Mn^{2+} results in lower Fe:Mn ratios of 1:2 to 1:5 during oxic diagenesis while under suboxic conditions ratios can reach 1:50. Hydrothermal concretions are the least prevalent but fastest growing FeMn oxides with growth rates near 1000 mm My^{-1} and Fe:Mn ratios from 1:10 to 1:5000 due to the elevated incorporation of Fe in iron sulfides

rather than in ferromanganese minerals under these conditions. Variations within each type of ferromanganese oxide occur due to differing bottom water currents, sedimentation rates and proximity to various sources.

The incorporation of economically and environmentally important metals into FeMn minerals has received a great deal of attention (e.g., Goldberg, 1954; Li, 1982; Balistrieri and Murray, 1984; Dymond et al., 1984; Sato et al., 1989; Manceau and Charlet, 1992; Peacock and Sherman, 2007; Zhang et al., 2007; Turner et al., 2008). Analogous to the varying amounts of Fe and Mn, trace metals also have different abundances in the three FeMn oxide types due to the chemical properties of individual metals and their source signatures under the three deposition environments. Oxidation by Mn oxides leads to preferential enrichment of trace metals in Mn components while metals remaining in their lower oxidation states may be primarily incorporated in Fe portions of FeMn minerals (Takahashi et al., 2007). Certain metals may exist at higher concentrations in seawater, porewater or hydrothermal plumes resulting in their greater abundances in hydrogenous, diagenetic or hydrothermal FeMn oxides, respectively. Since Ni, Cu and Co are more concentrated in porewaters than in seawater, the genetic origins of FeMn minerals have been determined by their Ni, Cu and Co contents such that diagenetic nodules contain more of these metals than hydrogenetic oxides (Bonatti et al., 1972). However, since Co is oxidized by and preferentially associates with Mn oxides, Zn has been substituted for Co to identify hydrogenetic, oxic diagenetic and suboxic diagenetic ferromanganese oxides (Dymond et al., 1984). Ferromanganese deposits have been classified through comparison of their Co/(Ni+Cu) ratios and Ce anomalies since both Co and Ce exhibit elevated concentrations in Mn portions of hydrogenetic oxides

while Ni, Cu and trivalent rare earth elements are more concentrated in porewaters and diagenetic nodules (Ohta et al., 1999). Spatial variability of trace metals has also been used to determine the genetic origins of ferromanganese oxides. Some trace metals may preferentially concentrate in the basal parts of FeMn deposits indicating elevated diagenetic inputs while those in upper mineral portions signal a greater hydrogenetic or hydrothermal influence (Calvert and Price, 1977). Shifts in depositional environments over geologic time periods can thus be mapped by interpreting changes in metal abundances of FeMn growth rings.

Yttrium and REE are directly removed from seawater by FeMn minerals forming distributions in FeMn oxides that mirror those in seawater (German and Elderfield, 1990 and references therein). Relative YREE distributions in FeMn oxides may thus be related to the ambient YREE concentrations during mineral formation. Since HREE are more stabilized in seawater solution by carbonate complexation than LREE, changes in marine carbonate concentrations have been inferred from shifts in relative abundances of LREE and HREE in FeMn deposits (Piper, 1974; De Carlo et al., 2000). Interpretations of Y concentrations are not as straightforward since Y behaves similarly to Ho in seawater, but Y concentrations are lower than those of Ho in hydrogenetic and diagenetic FeMn oxides (Ohta et al., 1999). Cerium fractionation in ferromanganese oxides appears to be even more complicated. Relative Ce enrichment often decreases based on the genetic origin of FeMn oxides such that hydrogenetic oxides have positive Ce anomalies, diagenetic nodules contain small positive or no Ce anomalies (e.g., Ohta et al., 1999) and some hydrothermal formations have negative anomalies (Usui et al., 1997; Mascarenhas-Pereira and Nath, 2010). Based on the lower Ce anomalies of diagenetic nodules (lower

Fe:Mn) than hydrogenetic oxides (higher Fe:Mn), it was proposed that Ce is predominantly incorporated directly from seawater into Fe components of FeMn deposits (Elderfield et al., 1981b). However, these same authors noted that the relative Fe content in FeMn oxides only controlled Ce anomalies in diagenetic todorokite-bearing nodules since the covariance between Ce and Fe concentrations was much weaker in hydrogenous oxides (Elderfield et al., 1981a). Additionally, Mn oxides are known to preferentially concentrate Ce through oxidation (Chapter 2). It has been suggested that Ce anomalies covary with Fe and Mn concentrations in FeMn oxides due to different YREE source concentrations in each environment and growth rates for each ferromanganese mineral class instead of the relative Mn content (Takahashi et al., 2007).

Sorption of YREE on synthetic ferromanganese oxides must be studied under controlled conditions to determine specific mechanisms of metal incorporation in natural FeMn deposits but this has received limited attention. Only one study of YREE co-precipitation at intermediate pH has been performed to provide insight into their associations with FeMn oxides (Kawabe et al., 1999). This chapter describes YREE sorption on hydrous ferromanganese oxides with special emphasis on the formation of Ce anomalies over a range of pH (4-8) and sorbent Fe:Mn ratios. The relative influence of Fe and Mn components in FeMn oxides is determined through comparisons of YREE sorption data on mixed FeMn oxides with those on pure Fe and Mn oxides (Schijf and Marshall, 2011; Chapter 2).

3.3. Materials and methods

All solutions were prepared in a class-100 laminar flow hood with Milli-Q water (18.2 MΩ·cm) from a Millipore Direct-Q 3UV purification system. Solids of $NaMnO_4$

(97+% purity), $MnCl_2$ (99.99+% purity), $FeCl_2$ (99.99% purity), KI (99+% ACS reagent) and NaCl (Reagent-Plus) were purchased from Sigma-Aldrich. Solutions of concentrated HNO_3 and H_2SO_4 (TraceMetal grade) and 1 M NaOH were obtained from Fisher while certified HCl (1.0011 M) was purchased from Brinkmann (Westbury, NY). Stock solutions of 100 $\mu g \cdot L^{-1}$ Co, 100 $\mu g \cdot L^{-1}$ Mn, 100 $\mu g \cdot L^{-1}$ Fe and a mixed stock solution containing 83.3 $mg \cdot L^{-1}$ Ce and 8.33 $mg \cdot L^{-1}$ of all other YREE were made from 1000 $mg \cdot L^{-1}$ single-element standards purchased from SPEX/CertiPrep (Metuchen, NJ). Cobalt, manganese and iron stock solutions were used to make the FeMn calibration line. The YREE calibration line was created from a premixed standard containing 10 $mg \cdot L^{-1}$ of each YREE (plus Sc and Th). All plastic equipment was acid cleaned and thoroughly rinsed with Milli-Q water before use. Small Teflon parts were cleaned in sub-boiling 8 M HNO_3 for at least 24 h while 1 L Teflon bottles and non-Teflon parts were cleaned in cold 4 M HCl for at least 1 week.

3.3.1. Mixed oxide synthesis

Mixed amorphous precipitates of Fe and Mn oxides were made externally in an anaerobic chamber using the strong oxidant $NaMnO_4$ to oxidize $FeCl_2$ and $MnCl_2$ in a basic solution by the following reaction

$$\begin{aligned} &3aFeCl_2 + 3bMnCl_2 + (a+2b)NaMnO_4 + (5a+4b)NaOH \rightarrow \\ &3aFe(OH)_3(s) + (a+5b)MnO_2(s) + (6a+6b)NaCl + (2b-2a)H_2O \end{aligned} \quad (3.1)$$

where the stoichiometry is based on the precipitation of Mn as only Mn(IV) oxides, as found previously in a similar reaction (Chapter 2). The values of a and b were chosen to produce particles with varying amounts of Fe and Mn. For example, to create solids with equal amounts of Fe and Mn the following molar quantities were selected: a = 5 and

b = 2. In a 1 L polyethylene bottle a degassed solution of the reductants ($MnCl_2$ and $FeCl_2$) was quickly mixed with a Teflon stir bar before the addition of alkaline $NaMnO_4$ causing the precipitation of Fe and Mn oxides. This solution was stirred rapidly for 3 h and then slowly for an additional 21 h to ensure reaction completion before removal from anaerobic conditions. Since $NaMnO_4$ is more soluble than the other reactants, a slight excess of $NaMnO_4$ was added to ensure proper rinsing of the product and complete oxidation of $MnCl_2$ and $FeCl_2$ before transferring the solution to an oxic environment. Once produced, the solids were rinsed thoroughly with Milli-Q water to remove any excess reactants. Rinsed particles were stored in suspension with Milli-Q water at 2°C in polypropylene centrifuge tubes to retard aging. All experiments were performed within one month of mixed oxide synthesis.

3.3.2. Fe:Mn ratio determination

The relative concentration of Fe and Mn in each type of mixed particulate was verified by dissolving two subsamples and measuring their Fe and Mn contents by ICP-MS. Oxides were dissolved through the sequential addition of 85 mL Milli-Q water, 5 mL 50% H_2SO_4 and 10 mL alkaline 2 M KI with stirring, as done previously for hydrous manganese oxides (Chapter 2) and sediment samples (Kalhorn and Emerson, 1984). Upon dissolution, subsamples (100 µL) were collected, diluted at least 1,000-fold with 1% HNO_3 to reduce matrix affects, spiked with 5 $\mu g \cdot L^{-1}$ Co as an internal standard and analyzed for Fe and Mn content by ICP-MS, as described below, using an external calibration line (0, 0.5, 1, 2 and 5 $\mu g \cdot L^{-1}$).

3.3.3. X-ray powder diffraction (XRD)

X-ray powder diffraction was performed on an air-dried subsample of the 1:1 FeMn oxides to determine their degree of crystallinity and characterize any crystal structures. Since the 1:1 FeMn oxides contained the highest concentrations of both Fe and Mn, these particles were most likely of all the oxides to have detectible peaks representative of Fe or Mn oxides. Hydrous mixed oxides were dried in a laminar flow hood for 5 days in preparation for their analysis by the same methods as discussed in relation to hydrous manganese oxides (Section 2.3.3).

3.3.4. YREE sorption experiments

Sorption experiments were performed similar to those on hydrous manganese oxides (Chapter 2), except that the initial pH in mixed oxide experiments was set slightly higher (pH ~ 4) before particle addition to prevent oxide dissolution. The influence of colloid-bound YREE was not considered in mixed oxide experiments since colloidal YREE species were insignificant in end-member datasets (Schijf and Marshall, 2011; Chapter 2). All other sorption experiment details were discussed in Section 2.3.4.

3.2.5. ICP-MS analyses

Dissolved Fe and Mn concentrations in particle dissolution samples and dissolved YREE concentrations in sorption samples were measured on an Agilent 7500cx ICP-MS. For Fe and Mn detection, the Octopole Reaction System was used with He carrier gas to remove ArO interferences on Fe masses, especially for ^{56}Fe. A High Matrix Introduction accessory was used during YREE analysis since these samples contained high NaCl concentrations. The remaining analytical details were discussed in Section 2.3.5. Sorption

is described by distribution coefficients calculated from dissolved YREE concentrations, $[M]_{diss}$, as

$$ {}_{i}K_{FeMn} = \frac{[M]_{init} - [M]_{diss}}{[M]_{diss} \times ([Fe]_T + [Mn]_T)} \quad (3.2) $$

where $[Fe]_T$ and $[Mn]_T$ are the total concentrations of Fe and Mn added as determined from the average content of each metal in the mixed oxide corrected for water content in each batch experiment.

3.4. Results and discussion

The mixed oxides are considered amorphous since X-ray powder diffraction of air-dried 1:1 FeMn oxides did not produce any significant peaks. All mixed oxides were analyzed for their relative Fe and Mn concentrations to confirm the stoichiometry of Reaction (3.1). Since the percentages of Fe and Mn in mixed oxides (Table 3.1) agree with the proposed redox mechanism, Fe and Mn existed in their most oxidized states (+III and +IV, respectively). The Fe:Mn molar ratios of mixed oxides were 3:1, 1:1 and 1:9 which represent particles with high Fe concentrations, equal Fe and Mn concentrations as in hydrogenous oxides and high Mn concentrations as in diagenetic nodules. Distribution coefficients, ${}_{i}K_{FeMn}$, were calculated over the experimental pH range for each set of mixed oxides (3:1 oxides pH 3.91-8.05, 1:1 oxides pH 4.01-7.59, 1:9 oxides pH 4.27-7.34) (Tables 3.2-3.4). The third experiment with 3:1 FeMn oxides was performed with a 10-fold higher sorbent concentration (~1 g wet weight) to increase YREE sorption at low pH. As in the investigations with pure sorbent phases (Schijf and Marshall, 2011; Chapter 2), the experimental pH window was limited by particle dissolution at low pH and depletion of dissolved YREE at high pH. Distribution

coefficients, log $_iK_{FeMn}$, in the mixed oxide datasets are higher than those found on either end-member, possibly due to greater concentrations of sorption sites on mixed oxides as previously suggested for mechanical mixtures of hydrous Fe and Mn oxides (Tripathy and Kanungo, 2005).

3.4.1. Linear regression of distribution coefficients as a function of pH

The proton exchange associated with YREE sorption was investigated by performing linear regressions of distribution coefficients (log $_iK_{FeMn}$) as a function of pH (Figure 3.1). Since all mixed sorbents are considered amorphous, all hydroxyl groups associated with Fe and Mn oxides were available for sorption. Samples collected at elevated pH (> 7.60) were not considered in linear regressions since these consistently deviated from linearity. The slopes resulting from linear regressions (Table 3.5) indicate, for all YREE, the largest proton release during sorption on the 1:1 FeMn oxides followed by the 3:1 FeMn oxides and then the 1:9 FeMn oxides which released the fewest protons. Proton exchange on 3:1 FeMn oxides is similar to that on hydrous Fe oxides (Schijf and Marshall, 2011) while on 1:9 FeMn oxides it is analogous to that on hydrous Mn oxides (Chapter 2). Elevated proton release from surfaces with higher Fe concentrations is reasonable since deprotonation constants (Schijf and Marshall, 2011; Chapter 2) indicate that on average more YREE sorption reactions on Fe oxides (p_sK_2 = 6.16) will involve proton exchange than on Mn oxides (p_sK_2 = 4.27). Sorption on 1:1 FeMn oxides exchanged more protons than on any other investigated oxide and thus cannot be fully explained by the end-members.

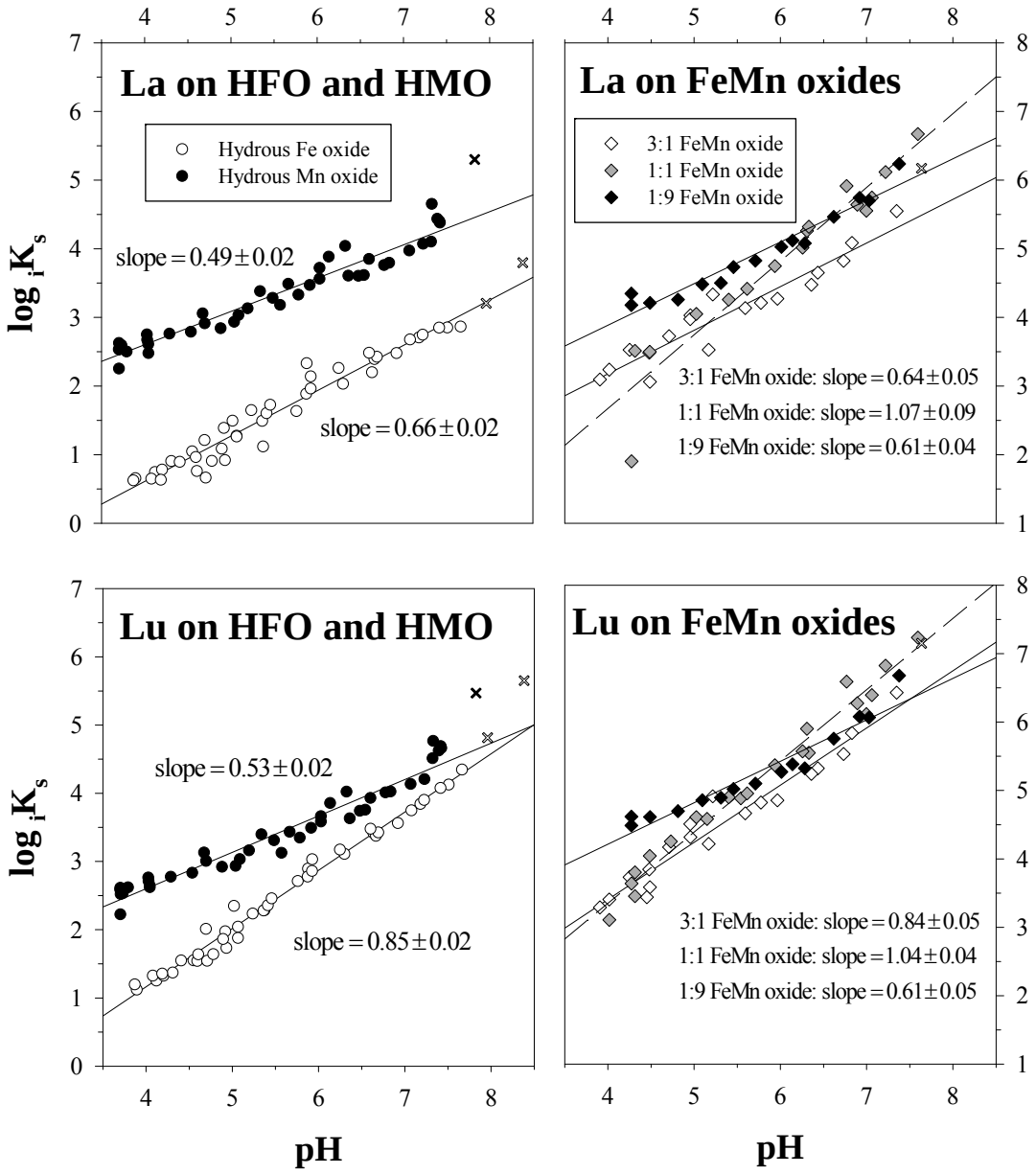

Figure 3.1. Linear regression of La (top) and Lu (bottom) distribution coefficients (log $_iK_s$) *vs.* pH for sorption on hydrous ferric oxide (HFO, open circles), hydrous manganese oxide (HMO, closed circles) in the left panel and on 3:1 FeMn mixed oxide (open diamonds), 1:1 FeMn mixed oxides (gray diamonds) and 1:9 FeMn mixed oxide (closed diamonds) in the right panel. The resulting slopes (Table 3.5) indicate the average number of protons released per YREE cation sorbed over the experimental pH range (0.5 M NaCl, 25°C) increased with increasing Fe content of the sorbent (excluding 1:1 FeMn oxides, which had the highest proton exchange). Distribution coefficients obtained at pH > 7.60 (shown as an 'x') were excluded from linear regression since these points consistently deviated from linearity. The two highest pH points in the HFO dataset as well as the highest pH points in the HMO and 3:1 FeMn oxide datasets consequently did not affect the regressions.

Cerium sorption and its associated proton exchange were greater than those of the other YREE. In addition, a sudden shift in the proton exchange at pH 5.5 on 1:9 FeMn oxides of 0.70 units is similar to the shift for Ce sorption on pure hydrous Mn oxides of 0.81 units (Figure 3.2). The transition on hydrous Mn oxides was attributed to a different Ce oxidation mechanism at elevated pH (Section 2.5.4). Cerium sorption on the other mixed particles does not exhibit this same shift either because there is no such change or the data are too variable to identify the transition.

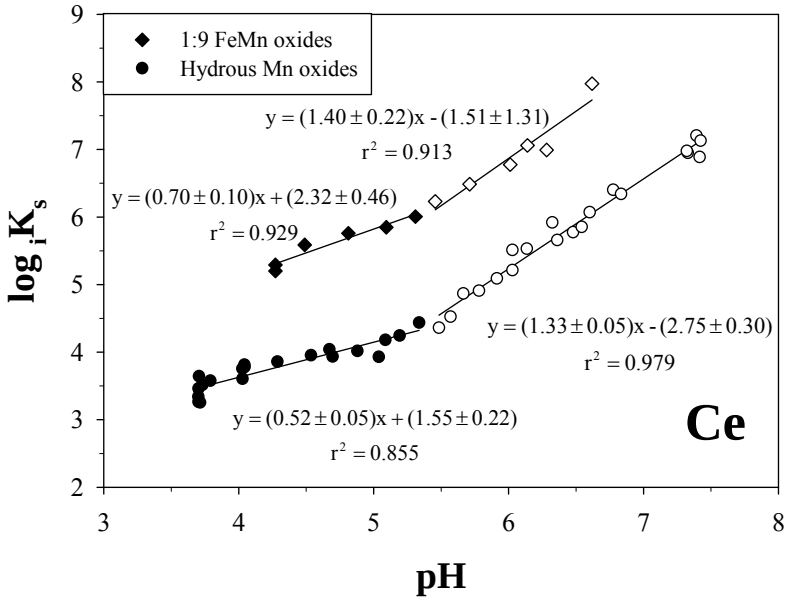

Figure 3.2. Linear regression of Ce distribution coefficients on hydrous manganese oxide (HMO, circles) and 1:9 FeMn oxides (diamonds) at pH < 5.5 (closed symbols) and pH > 5.5 (open symbols). The change in slope near pH 5.5 of 0.70 units on 1:9 mixed oxides is similar to the shift found previously of 0.81 units on HMO (Chapter 2).

3.4.2. Comparisons between sorbents (LREE/HREE, Ce/Ce and Y/Ho)*

The chemical coherence of YREE allows fundamental processes to be identified through comparisons of their relative distributions. In controlled environments, systematic variations in abundances across the YREE group can be directly related to their solution and surface complexation. Since my experimental conditions contain only

dissolved ligands (Cl^- and OH^-) whose impact on YREE interactions with the end-members is well understood, comparisons of distribution coefficients highlight differences in the sorption sites of the oxides. The relative influence of Fe and Mn concentrations in mixed FeMn oxides can thus be investigated by comparing YREE distribution coefficients.

The reactivity of YREE increases throughout the group with decreasing ionic radius such that surface and solution complexation of HREE are more favorable than those of LREE. In the absence of strong solution ligands, as in my experiments, HREE are generally more susceptible to sorption reactions than LREE. To investigate gradual changes in sorption across the YREE series, distribution coefficients from each sorbent dataset have been shifted so that all have equal values for Yb at an intermediate pH of 6.35 ± 0.08 (Figure 3.3). When thus arranged, the distribution coefficient patterns of the mixed oxides are bracketed above by hydrous Mn oxide and below by hydrous Fe oxide. The pH chosen for this comparison is above the deprotonation constant for both end-members, where moderate sorption occurs resulting in the highest quality data. Sorbent comparisons at low and high pH are less clear but it appears that at lower pH all mixed sorbents behave similarly while at elevated pH the 1:1 FeMn oxide patterns resemble those of hydrous Mn and 1:9 FeMn oxides. The pattern of distribution coefficients for 1:1 FeMn oxides is not shown in Figure 3.3 since it is very similar to that of the 3:1 FeMn oxides. Near pH 6.4, all sorbents containing Mn oxides are Ce enriched and when Ce is excluded, all sorbents display the typical inter-element fractionation pattern known as the tetrad effect (e.g., Kawabe et al., 1991), but the slope of these patterns differs between the sorbents. As expected in the absence of strong dissolved ligands, HREE are preferentially

sorbed on hydrous ferric oxides; however, on surfaces containing Mn there is slightly greater removal of LREE than HREE. Light REE enrichment is proportional to the Mn content of the mixed precipitates such that 1:9 FeMn oxides are more LREE enriched than 1:1 and 3:1 FeMn oxides. The relative degree of YREE sorption on 3:1 and 1:1 FeMn oxides falls between that of the end-members, resulting in a distribution coefficient pattern with very little fractionation, except for Ce. Preferential uptake of LREE by Mn-rich oxides may result from increased coordination of LREE relative to HREE on hydrous Mn oxides (Ohta et al., 2009b; Chapter 2).

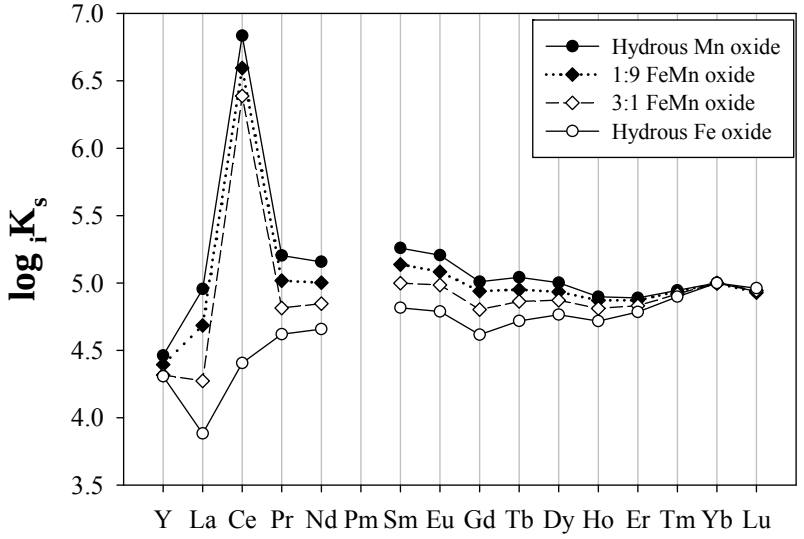

Figure 3.3. Distribution coefficients (log $_iK_s$) of all YREE at intermediate pH (~ 6.4) on hydrous Fe, Mn and FeMn oxides. Coefficients have been vertically adjusted to have equal Yb values in order to emphasize relative YREE behaviors between the sorbents.

All sorbents containing Mn were Ce enriched relative to the other YREE such that Ce accumulation does not appear to be altered much by differing amounts of Fe or Mn in the mixed oxides (Figure 3.3). Positive Ce anomalies, log (Ce/Ce*) > 0, existed on all FeMn oxides over the experimental pH ranges with Ce/Ce* values near those found on

hydrous Mn oxide but no Ce anomaly, log (Ce/Ce*) ~ 0, was produced on hydrous Fe oxides (Figure 3.4). Since no Ce anomaly was found on Fe oxides under the same anaerobic conditions, all anomalies can be attributed to Ce oxidation by Mn oxide components in the mixed oxides. Lowered Mn concentrations in 3:1 and 1:1 FeMn oxides did not considerably influence Ce anomalies. In fact, even a small amount of Mn oxide in a sorbent (~27% in 3:1 FeMn particles) produced a Ce anomaly nearly as large as found on pure hydrous Mn oxides at intermediate pH. Cerium anomalies, and thus Ce oxidation, associated with 3:1 and 1:1 mixed oxides appear to increase less with pH than on hydrous Mn oxides, while anomalies on the 1:9 FeMn oxides are more similar to those on hydrous Mn oxides. On 3:1 FeMn oxides, Ce anomalies are higher than those on hydrous Mn oxides at low and intermediate pH but lower at elevated pH (> 6.5), possibly due to decreased availability of Mn sorption sites compared to sorbents with higher Mn content. Cerium anomalies on 1:1 FeMn oxides are the most variable and difficult to interpret.

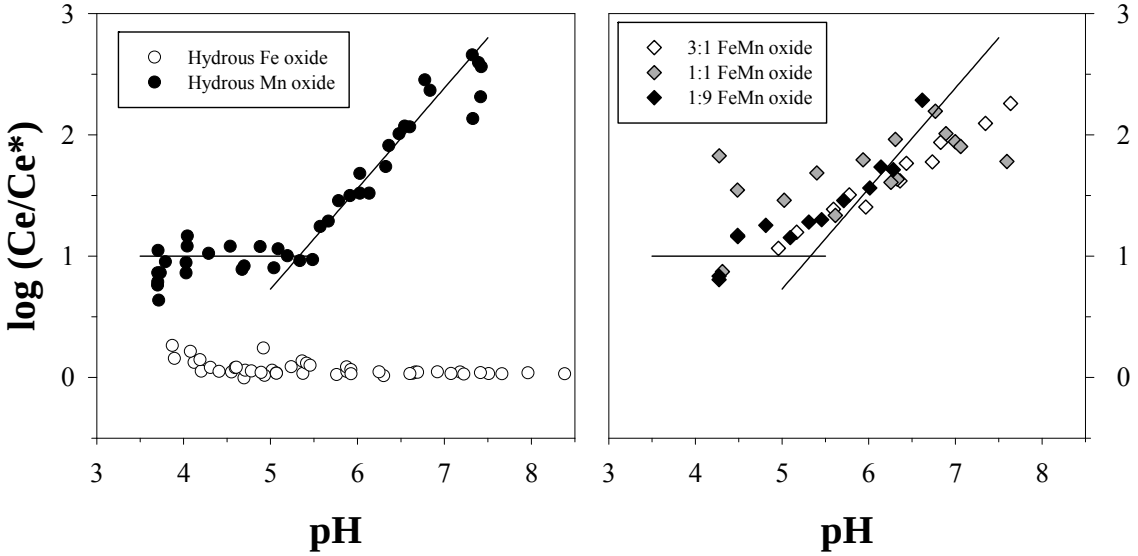

Figure 3.4. Cerium anomalies formed on pure (left panel) (Schijf and Marshall, 2011; Chapter 2) and mixed oxide (right panel) sorbents over the experimental pH range. Positive Ce anomalies, log(Ce/Ce*) > 0, indicate enhanced Ce sorption due to Ce oxidation whereas Ce is not oxidized when anomalies are near zero. For reference, the regression lines of the HMO data were added to the right side panel.

Distributions of yttrium and holmium are often compared since these elements have similar ionic radii but differing electronic configurations that can result in their fractionation from each other. Elements containing more electrons have more polarizable electron clouds leading to stronger covalent than ionic interactions with ligands. Since all REE, except La, have additional 4f electrons not present in Y, differentiation between Y and rare earth elements is often attributed to their varying degrees of covalent bonding (Mioduski, 1993). Complexation of Y is more favorable through ionic than covalent binding with ligands, due to its lack of f-electrons, but Y has an ionic radius similar to those of HREE which prefer covalent interactions. The combination of bonding preferences and ionic radii leads to similar sorption of Y and Ho during ionic interactions and increased Ho scavenging relative to Y through covalent bonds with surfaces. Yttrium may consequently behave similar to LREE or HREE depending on the covalent character of its binding with sorbents and ligands (e.g., Borkowski and Siekierski, 1992; Quinn et al., 2004). Holmium appears to be scavenged more than Y by natural ferromanganese oxides in a variety of settings (Bau et al., 1996; Bau et al., 1997; Bau and Dulski, 1999) independent of solution complexation influences (Bau and Koschinsky, 2009), suggesting that FeMn oxides form fairly covalent bonds with YREE. To investigate the covalency of YREE interactions with sorption sites, fractionations between Y and Ho on hydrous Fe, Mn and FeMn oxides were calculated as the ratio of their distribution coefficients, ${}_iK_s(Y)/{}_iK_s(Ho)$, and presented with respect to pH in Figure 3.5. Mixed FeMn oxides (not shown) form Y/Ho ratios that are more variable but mostly intermediate to pure end-member values indicating a combined influence of Fe and Mn on the covalent nature of bonding with mixed oxides. As anticipated, enhanced sorption of Ho relative to Y

(Y/Ho < 1) occurred on all surfaces and at every pH. At low pH (< 4.5), Y/Ho ratios were highest on hydrous Fe oxides while fractionation of Y from Ho was greatest on hydrous Mn oxides, suggesting that YREE bonding was more ionic with hydrous Fe oxides but more covalent with hydrous Mn oxides. On all sorbents, Y/Ho ratios decreased gradually with increasing pH to a single minimum value of approximately 0.3 at pH > 6, as found previously on synthetic hydrous Fe oxides (Bau, 1999). Therefore, Y behavior was most similar to that of Ho, representing the most ionic interactions, at low pH on hydrous ferric oxides than at any other pH or on any of the other surfaces. Decreasing Y/Ho ratios with increasing pH indicate that YREE bonding on all oxides became less ionic and more covalent. The nature of YREE bonds with hydroxyl ligands is considered to be a mixture of ionic and covalent interactions that may explain these lowered Y/Ho ratios. Strong linear free-energy relations (LFER) between YREE distribution coefficients and hydrolysis constants exist at elevated pH on hydrous Fe oxides (Schijf and Marshall, 2011). However, no such strong LFER were found for the hydrous Mn oxide dataset (Chapter 2), even though Y/Ho ratios suggest that hydrous Mn oxides behave more covalently with YREE than do hydrous Fe oxides. Therefore, with increasing pH, sorption sites on hydrous Fe oxides appear to become more hydroxyl-like while those associated with hydrous Mn oxides interact more covalently but are not hydroxyl-like.

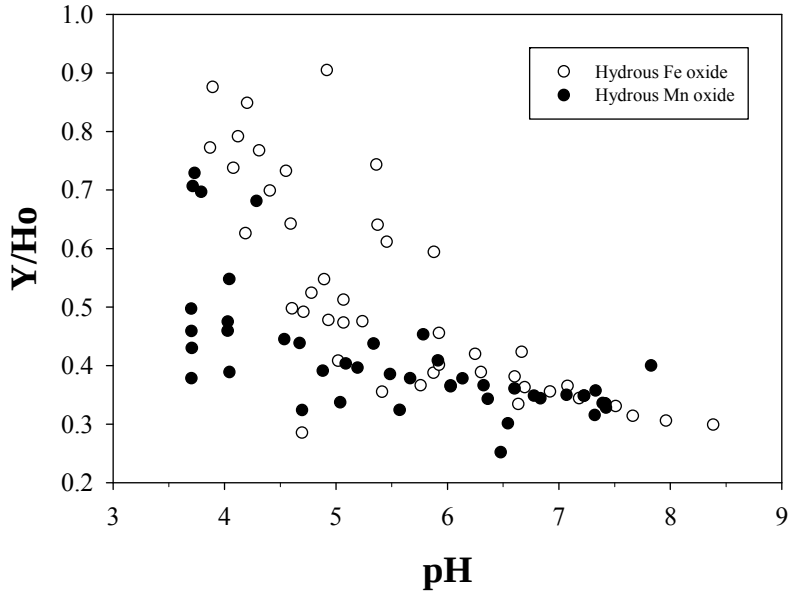

Figure 3.5. Fractionation of Y from Ho, as determined by the ratio of their distribution coefficients, on each of the pure oxides (Schijf and Marshall, 2011; Chapter 2) over the experimental pH range. Values from mixed oxide datasets are intermediate to those shown here.

3.4.3. Component Additivity modeling

Component additivity models, as described by Davis et al. (1998), combine known mechanisms of relatively simple systems to explain phenomena in more complicated and environmentally relevant settings. This approach has several advantages for sorption investigations in that it builds upon previous findings so that data are more easily interpreted and new models are not required for the many diverse natural surfaces. Component additivity models predict sorption on mixed surfaces from the sum of sorption on each end-member by assuming that surface deprotonation and complexation constants as well as reaction stiochiometries of the modeled sorbent are a linear combination of the end-member values (e.g., Turner et al., 1996; Arnold et al., 2001; Prikryl et al., 2001). Consequently, these models can only explain behaviors that fall between those of the end-members. Moreover, Ce sorption on FeMn oxides cannot be

described by the composite model used here since Ce sorption on hydrous Mn oxides is non-equilibrium (Chapter 2).

Previously developed non-electrostatic surface complexation models of YREE interactions with hydrous Fe and Mn oxides were combined here to explain sorption processes on more complex hydrous ferromanganese oxides. Based on their distribution patterns (Figure 3.3), sorption of trivalent YREE on mixed FeMn oxides appears to be directly related to the amount of Fe and Mn present in the sorbents. Therefore, YREE distribution coefficients on each of the mixed oxides were predicted from pure end-member models of sorption as

$$ {}_{i}K_{FeMn} = R \times {}_{i}K_{Fe} + (1-R) \times {}_{i}K_{Mn} + c \qquad (3.3) $$

where the pure oxide models, ${}_{i}K_{Fe}$ and ${}_{i}K_{Mn}$, are weighted by the fraction of Fe and Mn, R and (1-R), respectively, in a given mixed oxide and c is a constant. Equation (3.3) contains only two free parameters, R and c. Basically, c is a correction factor that allows the model to fit the higher experimental distribution coefficients found on mixed FeMn oxides compared to those on the end-members and R is a measure of the contribution from the hydrous Fe oxide model to distribution coefficients calculated by the composite model. The value of c reflects the offset of composite model predictions from experimentally measured mixed oxide distribution coefficients due to differences in sorbent characteristics (e.g., sorption site concentration) between pure and mixed oxides that should influence all elements on a single sorbent similarly. However, the covariance of R and c when both are free parameters in the regression equation led to slightly different values of c for each element. Model equations for each oxide type were accordingly optimized by determining the fixed value of c resulting in the lowest

combined residual sum of squares for all YREE in a given dataset when R remained a free parameter. Distribution coefficients in each FeMn oxide dataset were then refit with Equation (3.3) containing the optimized c values of 2.22, 3.16 and 1.91 for 3:1, 1:1 and 1:9 FeMn oxides, respectively (Table 3.6).

Composite model regressions of distribution coefficients on mixed FeMn oxides fit the data fairly well for each sorbent (Figure 3.6). Regressions of 1:1 FeMn oxide data (not shown) cannot be meaningfully interpreted since proton release from this surface was greater than that of the end-members (Figure 3.1 and Table 3.5). The curvature in HREE data on 3:1 FeMn oxides that may be indicative of YREE-hydroxide sorption on hydrous Fe oxides at high pH, as described by the A_3 term of the Fe model (Schijf and Marshall, 2011), was captured in these fits. While the models fit each sorbent dataset well, regressions of 1:9 FeMn data gave the overall highest r^2 and lowest errors for all YREE.

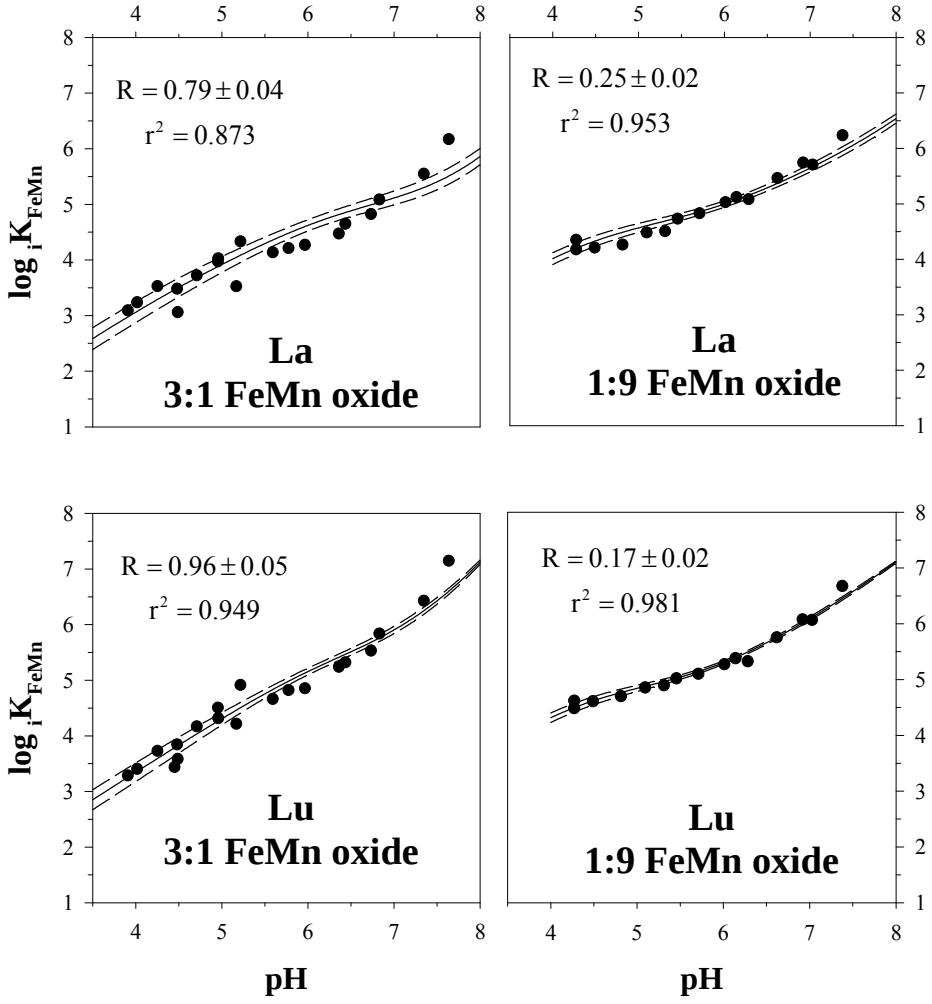

Figure 3.6. Model regressions (Equation (3.3)) of La (top panels) and Lu (bottom panels) sorption on 3:1 and 1:9 mixed oxide sorbents over the experimental pH ranges. The relative effect of Fe and Mn on metal interaction with a given sorbent is determined by the resulting R values (Table 3.6) such that higher numbers indicate greater contribution from Fe. Dashed lines indicate the 95% confidence interval and uncertainties are one standard error of the mean.

Modeling also provided R values (Table 3.6 and Figure 3.7) that are indicative of the relative effect of Fe sorption sites in each of the mixed oxides. For the 3:1 FeMn oxides, LREE (excluding Ce) had R values near 0.8 which reflect the Fe content of the sorbent (73%); however, Y and HREE regressions gave R values closer to 1 suggesting that these elements may have preferentially sorbed on Fe sites over Mn sites. Fits of the

1:9 FeMn oxide data gave R values near 0.20 for Y, La, Pr and Nd and from ~ 0.18 to 0.15 for the remaining elements which are higher than expected from the Fe content of these sorbents (8%). Compared to the other YREE, HREE appear to more preferentially sorb on the most available sorption site, hydrous Fe oxides in 3:1 FeMn oxides and hydrous Mn oxides in 1:9 FeMn oxides. Yttrium seems to favor sorption on hydrous Fe oxides on both mixed oxides, likely due to the ionic nature of bonding with hydrous Fe oxides (Section 3.4.2).

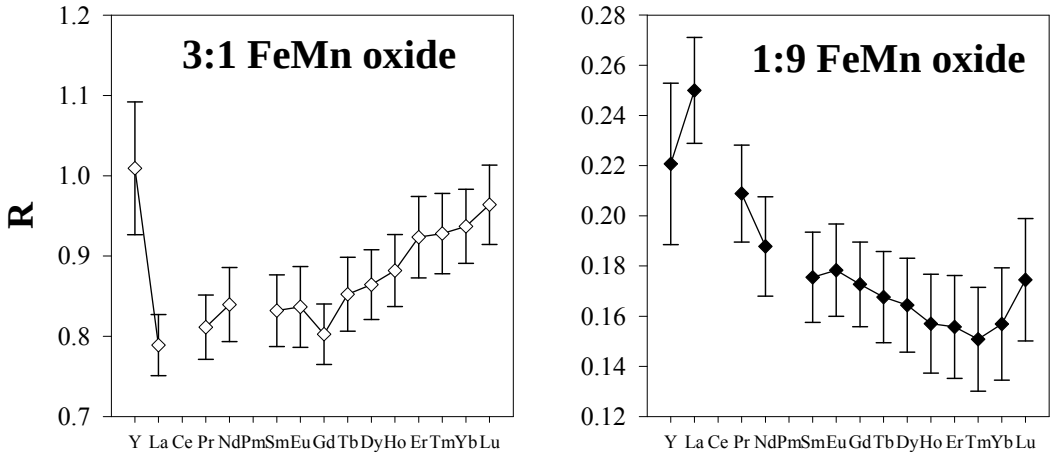

Figure 3.7. Best fit values of R (Equation (3.3)) for all YREE, except Ce, on 3:1 and 1:9 FeMn oxides. Higher values of R reflect greater contribution from Fe sites while lower R values indicate a greater contribution from Mn sites to sorption. Uncertainties are one standard error of the mean.

3.4.4. Evaluation of model quality

The composite model assumes that mixed FeMn oxides are composed of independent Fe and Mn sorption sites and that YREE sorption on mixed oxides is analogous to that on pure Fe and Mn oxides, as suggested by data for the strictly trivalent YREE. These assumptions are evaluated by determining the skill of the model in reproducing experimental data. The ability of the composite model to describe YREE

sorption on FeMn oxides was tested by comparing model predictions first with my experimental data and then with that of Kawabe et al. (1999).

The model performs well over the investigated pH ranges with an average ratio of predicted to measured distribution coefficients near unity for all strictly trivalent YREE. However, predictions are not of equal quality for each of the sorbents or at every pH, as shown for Sm in Figure 3.8. Sorption on 3:1 FeMn oxides is mostly over-predicted at pH less than 6.5 and under-predicted above pH 6.5. The predicted sorption behavior on 1:9 FeMn oxides is more accurate than the other sorbents with only a slight under-prediction above pH 7.

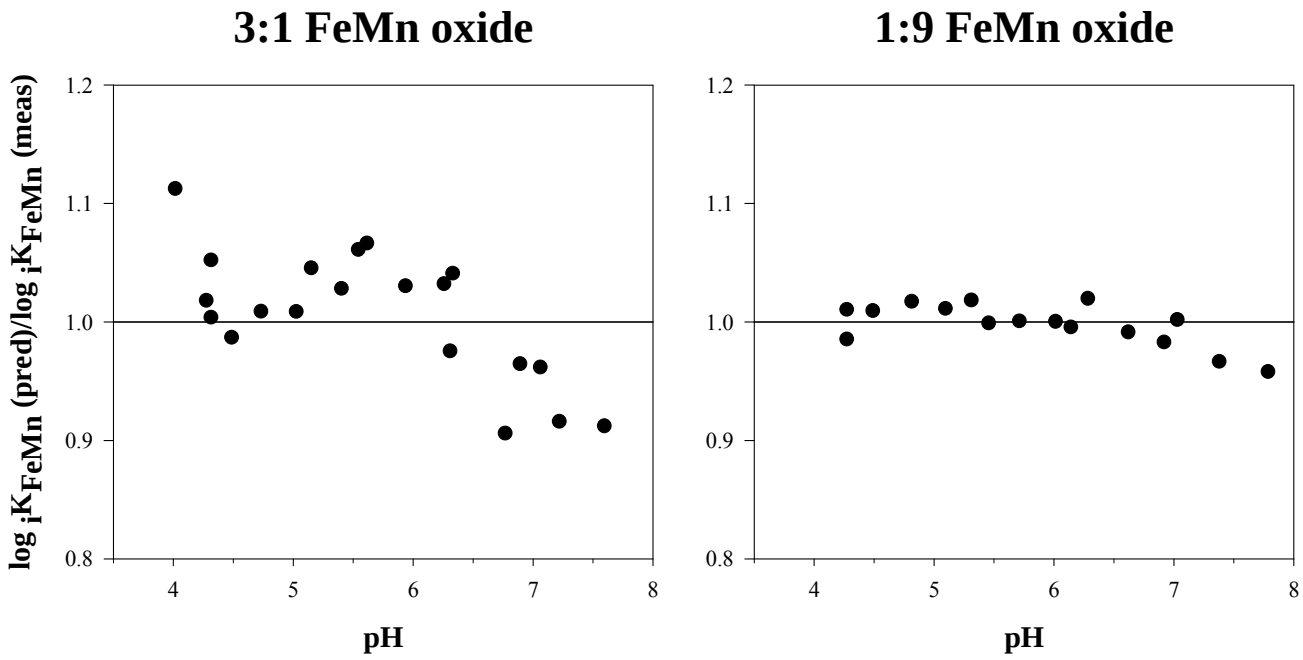

Figure 3.8. The ability of the model (Equation (3.3)) to predict samarium sorption on each modeled mixed oxide over the investigated pH range. The average ratio of predicted to measured distribution coefficients is near unity for all YREE (mean = 0.997 and 0.995 for 3:1 and 1:9 FeMn oxides, respectively), but model skill varies with pH and sorbent.

Sorption patterns of model predictions are compared with those measured experimentally on each FeMn oxide in Figure 3.9. Relative values of strictly trivalent distribution coefficients are reproduced very well in 3:1 and 1:9 FeMn sorbent datasets. Cerium sorption, which occurs by non-equilibrium processes not included in the model, is estimated as only Ce(III) sorption which is much lower than the measured Ce sorption on all FeMn oxides and at all pH. Even under conditions least favorable for Ce oxidation, lowest Mn sorbent content and low pH (3:1 FeMn oxide at pH 4.96), Ce sorption is under-predicted by approximately 1 log unit. On 1:9 FeMn oxides at pH 7.03, a best-case scenario for Ce oxidation, Ce sorption is under-predicted by ~ 2.5 log units. Thus, significant Ce oxidation occurred on all mixed oxides, even those with relatively little Mn (~ 27% in 3:1 FeMn oxides).

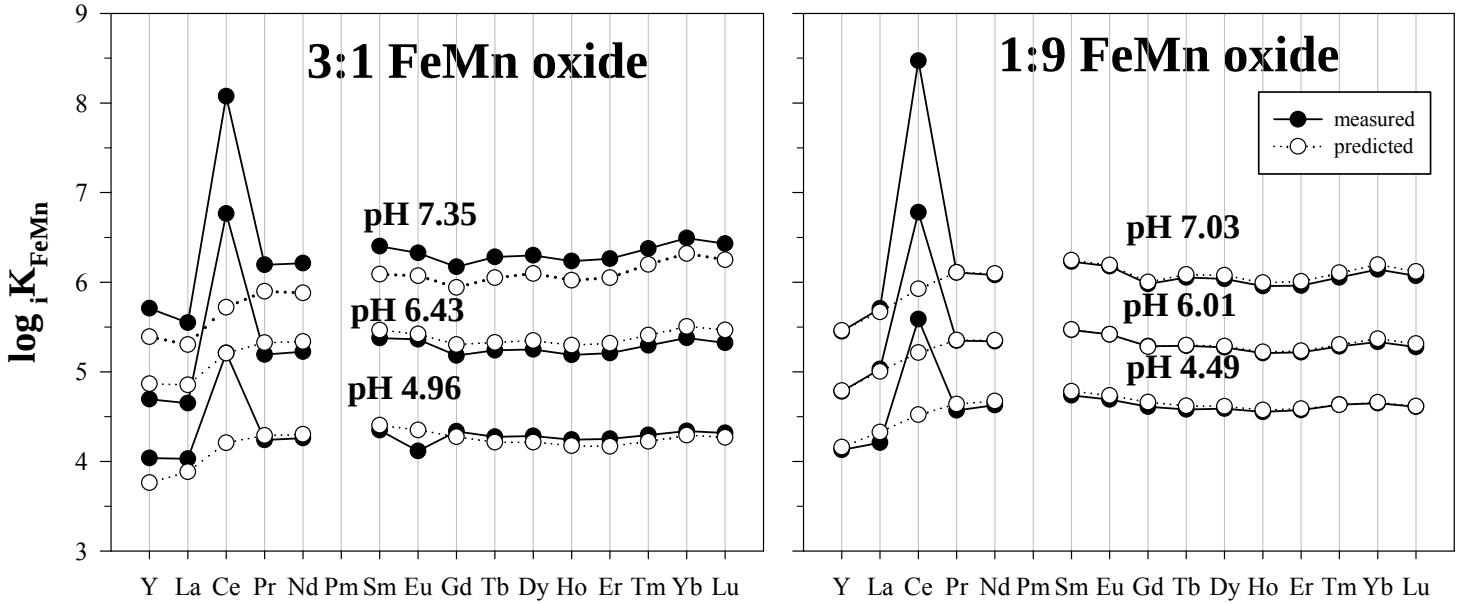

Figure 3.9. Comparison of measured (closed circles) and predicted (open circles) patterns of YREE sorption on each of the mixed oxides at three values of pH. Predicted patterns were calculated using Equation (3.3) with appropriate c constants and R values (Table 3.6). The model accurately reproduces relative and absolute sorption behavior of strictly trivalent YREE on 1:9 FeMn oxides (right panel) and relative behavior on 3:1 FeMn oxides (left panel). Cerium distribution coefficients are predicted from only Ce(III) sorption which is much lower than measured values on all FeMn oxides.

There has been a great deal of research on YREE distributions in ferromanganese oxides (e.g., De Carlo, 1991; De Carlo and McMurtry, 1992; Nagender Nath et al., 1992; Bau et al., 1996; Bayon et al., 2004; Bau and Koschinsky, 2009); however, most of these studies have been performed on natural field samples precluding the evaluation of true distribution coefficients as defined in Equations (2.3) and (3.2). One notable exception is the work of Kawabe et al. (1999) that described YREE sorption on ferromanganese oxides in 0.53 M NaCl solutions with CO_2 and O_2 present. Their data were converted to my definition of distribution coefficient (Equation (3.2)) and compared with predictions from the composite (Equation (3.3)) and hydrous Mn oxide (Equation (2.10)) models (Figure 3.10). Since the relative Fe and Mn sorbent concentrations were not reported by Kawabe et al. (1999), it is assumed that all dissolved Fe^{3+} and Mn^{2+} precipitated due to their moderately high experimental pH (~ 6). The resulting Fe:Mn ratios suggest the formation of hydrous 1:5 FeMn oxides with a relative Fe content of approximately 17%. Accordingly, R = 0.17 was used for all YREE in the composite model while the constant c was ignored since the FeMn oxides discussed here were of a different composition than those used to optimize the c term. Composite and Mn model predictions were about 0.9 and 0.7 units lower, respectively, than those found in the literature and were accordingly shifted to emphasize similarities between the literature and modeled distribution coefficients (Figure 3.10). Sorption was better predicted by the composite model than the Mn model alone, especially for HREE, supporting the strength of the mixed model. Consistent under-prediction of the literature data by both models is likely due to differences between the sorbent surface and model end-members, hydrous Fe(III) and Mn(IV) oxides. Since Kawabe et al. (1999) formed FeMn oxides from the precipitation

of Fe^{3+} and Mn^{2+}, it is likely that at least some Mn(III) oxides were present in the sorbent (Hem and Lind, 1983). Slight variations in distribution patterns may also be attributed to differences in analytical techniques since Kawabe et al. (1999) concentrated YREE by sorption on additional hydrous Fe oxide to improve ICP-AES (Inductively Coupled Plasma-Atomic Emission Spectroscopy) detection.

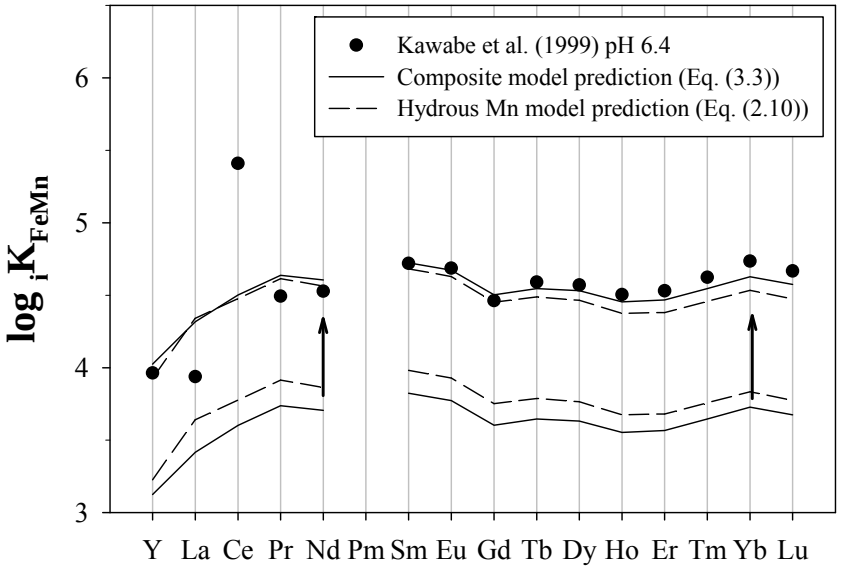

Figure 3.10. Comparison of model predictions of sorption with literature data at pH 6.4 (Kawabe et al., 1999) converted to my definition of ${}_iK_{FeMn}$ (Equation (3.2)). The composite model prediction (solid line) was calculated at pH 6.4 using Equation (3.3) with R as the fraction of Fe in the experiment (~ 0.17) and without c. The hydrous Mn model prediction (dashed line) was calculated at pH 6.4 using Equation (2.10) and best-fit parameters (Table 2.3). The predicted values were adjusted upward along the arrows to give the best overlap with literature values. Sorption behavior is described better by the composite than hydrous Mn model, especially for HREE.

3.5. Summary

Ferromanganese oxides are heterogeneous deposits of varying composition that exist in marine sediments throughout the world. Their affinities for trace metals and metal distributions within concentric growth rings have been of great interest for many decades. Ferromanganese oxide growth rates and metal distributions have been used to infer past deep-ocean conditions; yet, the pathways of metal incorporation in these oxides are not

fully understood. Accordingly, YREE sorption was investigated here on hydrous ferromanganese oxides with varying Fe and Mn concentrations under anaerobic conditions and over a range of pH (4-8) to identify important mechanisms.

Hydrous ferromanganese oxides scavenge trivalent YREE through reactions similar to those of its components such that sorption can be interpolated from the known behavior of hydrous ferric and manganese oxide end-members. Proton exchange during sorption is proportional to the relative Fe and Mn content of each sorbent, except on 1:1 FeMn oxides which experience enhanced proton release. Light REE are enriched relative to HREE on ferromanganese oxides with greater Mn content, while HREE enrichment is associated with hydrous Fe oxides. Fractionation of Y from Ho on FeMn oxides appears to be related to characteristics of Fe and Mn sorption sites which behave more covalently with YREE at elevated pH. The composite model accurately predicts experimental sorption patterns on 3:1 and 1:9 FeMn oxides in addition to estimating literature sorption data (Kawabe et al., 1999) better than the hydrous Mn model alone. The combined influence of Fe and Mn components in FeMn oxides on strictly trivalent YREE sorption suggests that distributions of other trace metals on ferromanganese oxides may be predicted similarly by considering their behaviors on pure Fe and Mn oxide components, supporting the utility of the Component Additivity approach.

Cerium anomalies formed on all ferromanganese oxides under anaerobic conditions due to Ce oxidation by hydrous Mn oxides, even when small amounts of Mn oxide were present. Cerium oxidation enhanced Ce sorption, relative to neighboring YREE, approximately 10-fold on 3:1 and 1:9 FeMn oxides at pH ~ 5 and 4.5, respectively, and more than 300-fold under the most favorable Ce oxidation conditions

(1:9 FeMn oxides, pH ~ 7). Since positive Ce anomalies associated with FeMn oxides containing a range of Mn (27-92%) were similar, the relative amount of Ce enrichment in natural ferromanganese oxides is likely often quite large and independent of Mn content, as previously suggested (Takahashi et al., 2007).

3.6. Application of cerium anomalies as a paleo-redox proxy

Cerium oxidation, and the formation of Ce anomalies, is not simply influenced by dissolved O_2 as many paleoceanographers have assumed (e.g., Wright et al., 1987), but occurs through more complicated pathways involving multiple factors. The exact mechanism of Ce oxidation is not clear, but my data support previous findings (De Carlo et al., 1998; Ohta and Kawabe, 2001; Davranche et al., 2005, 2008) that oxidation occurs on hydrous manganese oxides under abiotic anaerobic conditions (Chapter 2). Substantial Ce anomalies, similar to those on pure hydrous Mn oxides, exist even on particulates with low Mn content, such as 3:1 FeMn oxides. Consequently, surfaces with small amounts of Mn oxide are likely to significantly affect sedimentary Ce anomalies independent of ambient O_2 concentrations. Manganese oxides are common throughout the marine environment and likely oxidize Ce in the water column as well as within sediments, so it can be assumed that Ce is often oxidized in deep waters regardless of ambient O_2 concentrations. Sedimentary Ce anomalies reflect the elevated transport of Ce to sediments relative to the other YREE due to Ce oxidation in bottom waters, which in the presence of hydrous Mn oxides are probably not related to dissolved O_2. Moreover, sedimentary Ce anomalies cannot be corrected for heightened Ce deposition due to oxidation by hydrous Mn oxides since it is unlikely that Mn oxide influences on YREE fractionation were constant during the formation of a given sediment or that a lasting

record of Mn oxide abundance exists, as Mn is fairly mobile. In fact, under Mn-reducing conditions, hydrous Mn oxides are dissolved whereas sedimentary Ce anomalies may increase (Murray et al., 1991). Sedimentary Ce anomalies are therefore not an indicator of the instantaneous bottom water conditions at the time of their formation, as required for their use as a paleo-redox proxy (German and Elderfield, 1990).

Cerium anomaly signals in marine sediments are influenced by a variety of factors not directly related to ambient O_2 content. In marine ferromanganese deposits, the indirect relation of Ce anomalies with bottom water O_2 conditions was used to describe shifts in trace metal distributions from the Cretaceous-Tertiary boundary (De Carlo, 1991). However, since Mn oxides can exist under suboxic conditions, inferences based on sedimentary Ce anomalies can at most only signify transitions between anoxic Mn reducing and suboxic or oxic conditions within sediments. Consequently, the interpretation of sedimentary Ce anomalies remains very difficult, especially when Mn oxides are present, and may lead to incorrect explanations of changes in marine processes over Earth's history, such as global ocean circulation patterns or sea level.

3.7. Future work

This thesis provides new information on the mechanisms of YREE sorption, especially for Ce, on hydrous Fe, Mn and FeMn oxides. However, questions remain regarding the surface characteristics of hydrous Mn(IV) and ferromanganese oxides and the role of ferromanganese oxides in more natural systems. Sorption site concentrations for hydrous Mn and FeMn oxides should be measured so load factors can be determined and the proposal of elevated sorption site concentrations on hydrous FeMn oxides can be confirmed. Further characterization of hydrous FeMn oxides by ζ-potential analysis to

examine their pH_{pzc} will determine if these values are in fact set by their relative amounts of Fe and Mn oxides, as previously proposed for other oxide mixtures (Parks, 1967). Sorption site concentration and pH_{pzc} analyses will also provide insight into the elevated proton release found on 1:1 FeMn oxides. Sorption experiments similar to those described in this thesis could be performed over a wider range of solution conditions to obtain more realistic conditions. Additional seawater cations, such as Ca^{2+} and Mg^{2+}, could be included to investigate their competitive influence on YREE sorption processes. Experiments could also be performed over a range of CO_2 and O_2 partial pressures to identify their effects on YREE sorption and Ce oxidation. Particulate organic matter often fractionates YREE with middle REE enrichment and without Ce anomalies, so the combined effect of organic matter with hydrous FeMn oxides would be very interesting. Since YREE complexation with a marine macroalgae, *Ulva lactuca*, has been characterized (Zoll and Schijf, in prep.), degraded algal debris could be combined with hydrous FeMn oxides to create an even more heterogeneous and relevant sorbent surface for future experiments.

3.8. Data tables

Table 3.1. Stoichiometry of mixed oxide synthesis (Reaction (3.1)) and the measured percentages of Fe and Mn present in each type of oxide. The agreement of measured Fe and Mn contents with the proposed reaction mechanism indicates that Fe and Mn exist as fully oxidized Fe(III) and Mn(IV) oxides.

mol Fe:mol Mn	a	b	Expected %Fe	Expected %Mn	Actual % Fe	Actual % Mn
3:1	1	0	75.0	25.0	73.3	26.8
1:1	5	2	50.0	50.0	49.8	50.2
1:9	5	8	10.0	90.0	8.0	92.0

Table 3.2. Distribution coefficients, log ${}_iK_{FeMn}$, for YREE sorption on 3:1 FeMn oxides in 0.5 M NaCl ($[M]_T$ ~50 µg·L^{-1} except $[Ce]_T$ ~500 µg·L^{-1}, ~0.1 g FeMn oxide L^{-1}, pH ≥ 3.91, T = 25.0 ± 0.1°C). Experiment 3 was performed with higher particle concentration (~1 g FeMn oxide L^{-1}).

	Experiment 1						Experiment 2								Experiment 3						
time[a]			*			*			*		*	*		*					*		*
pH	4.49	4.96	5.59	5.78	6.43	6.83	4.45	5.17	5.97	6.36	6.73	7.35	7.64	8.05	3.91	4.02	4.25	4.48	4.71	4.96	5.22
Y	2.67	4.04	4.18	4.31	4.69	5.19	2.08	3.63	4.38	4.55	4.90	5.71	6.39	7.41	3.07	3.11	3.44	3.31	3.65	4.00	4.40
La	3.06	4.03	4.14	4.21	4.65	5.09	---[b]	3.53	4.27	4.48	4.82	5.55	6.17	7.14	3.09	3.24	3.53	3.48	3.73	3.97	4.33
Ce	4.42	5.21	5.78	6.03	6.77	7.40	4.34	5.25	6.02	6.52	6.98	8.08	8.90	---[c]	---[d]	---[d]	---[d]	---[d]	---[d]	---[d]	---[d]
Pr	3.38	4.24	4.55	4.71	5.19	5.66	3.88	4.28	4.81	5.11	5.41	6.19	6.87	8.34	3.25	3.47	3.75	3.88	4.16	4.46	4.86
Nd	3.51	4.26	4.59	4.75	5.22	5.70	3.52	4.17	4.79	5.11	5.42	6.21	6.88	8.16	3.30	3.50	3.79	3.91	4.20	4.51	4.91
Pm[e]																					
Sm	3.66	4.35	4.72	4.89	5.38	5.86	3.62	4.28	4.93	5.28	5.57	6.40	7.09	8.32	3.37	3.58	3.87	4.02	4.32	4.64	5.05
Eu	3.59	4.12	4.55	4.74	5.36	5.83	---[b]	---[b]	4.67	5.18	5.44	6.33	6.90	7.31	3.28	3.46	3.77	4.07	4.34	4.64	5.03
Gd	3.60	4.33	4.61	4.75	5.18	5.65	3.52	4.24	4.80	5.08	5.37	6.17	6.85	8.09	3.34	3.51	3.79	3.86	4.15	4.45	4.85
Tb	3.48	4.27	4.61	4.77	5.24	5.73	3.21	4.14	4.79	5.14	5.44	6.28	6.98	8.36	3.25	3.43	3.73	3.83	4.14	4.47	4.88
Dy	3.49	4.28	4.61	4.77	5.25	5.75	3.38	4.11	4.79	5.16	5.45	6.30	7.00	8.35	3.25	3.39	3.71	3.81	4.13	4.46	4.87
Ho	3.46	4.24	4.56	4.72	5.19	5.68	3.31	4.10	4.75	5.11	5.39	6.24	6.93	8.05	3.22	3.36	3.67	3.76	4.08	4.41	4.82
Er	3.40	4.25	4.58	4.74	5.21	5.71	3.16	4.10	4.75	5.12	5.41	6.26	6.96	8.09	3.23	3.36	3.67	3.77	4.09	4.42	4.83
Tm	3.52	4.29	4.64	4.80	5.30	5.80	3.20	4.19	4.83	5.21	5.50	6.37	7.09	8.39	3.27	3.39	3.72	3.83	4.15	4.49	4.90
Yb	3.60	4.34	4.71	4.87	5.38	5.90	3.56	4.25	4.90	5.30	5.59	6.49	7.22	9.20	3.27	3.41	3.73	3.87	4.20	4.54	4.95
Lu	3.59	4.32	4.66	4.82	5.32	5.84	3.44	4.22	4.85	5.24	5.53	6.43	7.15	8.50	3.29	3.41	3.73	3.85	4.17	4.51	4.92

[a]Samples equilibrated longer than 12 h before sampling are indicated with an asterisk; [b]Value not reported due to instrument error; [c]Concentration below instrument detection limit; [d]Values not reported since Ce distribution coefficients increased at lower load factor; [e]Not measured.

Table 3.3. Distribution coefficients, log $_{i}K_{FeMn}$, for YREE sorption on 1:1 FeMn oxides in 0.5 M NaCl ($[M]_T \sim 50$ µg·L^{-1} except $[Ce]_T \sim 500$ µg·L^{-1}, ~ 0.1g FeMn oxide L^{-1}, pH ≥ 4.02 , T = 25.0 ± 0.1°C).

	Experiment 1							Experiment 2								Experiment 3					
time[a]		*		*		*			*		*		*		*		*		*		*
pH	4.31	4.49	5.03	5.40	5.94	6.31	6.77	4.31	4.73	5.15	5.54	6.33	6.89	7.22	7.00	4.02	4.27	5.61	6.26	7.06	7.59
Y	3.49	3.62	4.20	4.31	4.82	5.35	6.01	3.28	3.75	4.07	4.23	5.01	5.71	6.21	5.57	---[b]	2.27	4.44	5.07	5.82	6.73
La	3.51	3.50	4.05	4.26	4.75	5.26	5.91	---[b]	---[b]	---[b]	---[b]	5.32	5.64	6.12	5.55	---[b]	1.90	4.42	5.02	5.75	6.67
Ce	4.53	5.31	5.77	6.28	6.88	7.58	8.48	4.40	5.39	5.70	6.16	7.02	7.98	---[c]	7.82	4.22	5.08	6.03	6.92	7.99	8.75
Pr	3.76	3.93	4.48	4.79	5.27	5.81	6.49	3.45	4.10	4.45	4.77	5.45	6.15	6.68	6.06	2.68	3.54	4.86	5.49	6.27	7.14
Nd	3.79	4.03	4.53	4.83	5.30	5.83	6.51	3.43	4.18	4.50	4.80	5.47	6.17	6.71	6.07	3.52	3.67	4.89	5.52	6.30	7.16
Pm[d]																					
Sm	3.82	4.09	4.64	4.97	5.45	5.99	6.68	3.64	4.29	4.62	4.96	5.62	6.33	6.88	6.23	3.14	3.72	5.00	5.64	6.44	7.28
Eu	3.75	4.02	4.56	5.03	5.46	5.97	6.57	3.56	4.27	4.61	4.93	5.60	6.30	6.86	6.19	3.11	3.68	5.00	5.62	6.43	7.26
Gd	3.73	4.07	4.56	4.82	5.27	5.79	6.47	3.53	4.22	4.51	4.81	5.45	6.13	6.66	6.02	3.23	3.76	4.88	5.48	6.25	7.12
Tb	3.72	3.95	4.54	4.85	5.33	5.87	6.56	3.47	4.17	4.52	4.83	5.51	6.22	6.77	6.09	3.07	3.47	4.92	5.54	6.34	7.18
Dy	3.75	3.96	4.54	4.85	5.34	5.87	6.55	3.43	4.15	4.53	4.84	5.52	6.22	6.77	6.09	1.95	3.54	4.92	5.54	6.35	7.19
Ho	3.72	3.92	4.50	4.80	5.28	5.81	6.49	3.43	4.13	4.49	4.80	5.46	6.16	6.70	6.03	3.09	3.49	4.88	5.49	6.28	7.14
Er	3.71	3.91	4.52	4.82	5.29	5.82	6.51	3.45	4.18	4.51	4.80	5.47	6.18	6.71	6.03	2.59	3.57	4.89	5.50	6.30	7.15
Tm	3.79	4.03	4.59	4.88	5.36	5.89	6.59	3.48	4.20	4.56	4.88	5.54	6.26	6.80	6.11	2.80	3.46	4.94	5.56	6.37	7.23
Yb	3.77	4.02	4.63	4.94	5.42	5.96	6.66	3.57	4.27	4.62	4.94	5.61	6.33	6.89	6.18	2.65	3.66	5.00	5.62	6.46	7.29
Lu	3.80	4.04	4.61	4.90	5.37	5.90	6.59	3.45	4.25	4.58	4.88	5.55	6.27	6.82	6.11	3.11	3.64	4.96	5.57	6.39	7.23

[a]Samples equilibrated longer than 12 h before sampling are indicated with an asterisk; [b]Value not reported due to instrument error; [c]Concentration below instrument detection limit; [d]Not measured.

Table 3.4. Distribution coefficients, log $_iK_{FeMn}$, for YREE sorption on 1:9 FeMn oxides in 0.5 M NaCl ($[M]_T \sim 50$ µg·L^{-1} except $[Ce]_T \sim 500$ µg·L^{-1}, ~ 0.1 g FeMn oxide L^{-1}, pH ≥ 4.27 , T = 25.0 ± 0.1°C).

	Experiment 1								Experiment 2						
time[a]		*		*		*		*		*		*		*	
pH	4.27	4.49	5.09	5.46	6.14	6.62	6.92	7.38	4.27	4.81	5.31	5.71	6.01	6.28	7.03
Y	4.06	4.13	4.42	4.43	4.85	5.18	5.48	6.03	4.24	4.13	4.36	4.54	4.78	4.79	5.45
La	4.18	4.21	4.48	4.73	5.12	5.47	5.74	6.24	4.35	4.26	4.50	4.83	5.03	5.08	5.70
Ce	5.20	5.59	5.85	6.23	7.06	7.97	---[b]	---[b]	5.29	5.76	6.00	6.48	6.78	6.99	---[b]
Pr	4.50	4.57	4.83	5.06	5.46	5.83	6.14	6.67	4.59	4.66	4.87	5.16	5.34	5.41	6.10
Nd	4.54	4.63	4.86	5.06	5.45	5.81	6.11	6.64	4.63	4.70	4.88	5.16	5.34	5.40	6.08
Pm[c]															
Sm	4.61	4.74	4.99	5.19	5.57	5.95	6.25	6.79	4.73	4.84	5.03	5.30	5.46	5.53	6.23
Eu	4.59	4.69	4.91	5.15	5.53	5.90	6.20	6.74	4.68	4.79	4.99	5.24	5.41	5.48	6.17
Gd	4.49	4.61	4.85	5.03	5.37	5.71	6.00	6.53	4.62	4.73	4.90	5.12	5.28	5.33	5.98
Tb	4.46	4.58	4.83	5.02	5.40	5.77	6.07	6.62	4.60	4.68	4.89	5.11	5.29	5.35	6.05
Dy	4.48	4.59	4.84	5.02	5.39	5.75	6.06	6.62	4.58	4.67	4.89	5.09	5.27	5.33	6.03
Ho	4.46	4.55	4.80	4.97	5.33	5.67	5.98	6.54	4.54	4.62	4.81	5.04	5.21	5.27	5.95
Er	4.48	4.57	4.82	4.98	5.33	5.68	5.98	6.55	4.54	4.61	4.83	5.04	5.21	5.27	5.96
Tm	4.52	4.63	4.86	5.05	5.39	5.76	6.07	6.65	4.58	4.69	4.87	5.11	5.28	5.33	6.05
Yb	4.56	4.65	4.91	5.09	5.45	5.83	6.15	6.75	4.61	4.72	4.93	5.17	5.33	5.39	6.14
Lu	4.49	4.61	4.86	5.02	5.38	5.76	6.08	6.68	4.62	4.70	4.89	5.10	5.27	5.32	6.07

[a]Samples equilibrated longer than 12 h before sampling are indicated with an asterisk; [b]Concentration below instrument detection limit; [c]Not measured.

Table 3.5. Relative proton exchange associated with sorption over the experimental pH range as determined from slopes of distribution coefficients as a function of pH (pH < 7.6). Excluding Ce values, proton exchanges on 3:1 and 1:9 FeMn oxides are similar to those found for hydrous Fe and Mn oxides, respectively, while 1:1 FeMn oxides exhibit heightened proton release. Proton-exchange for Ce sorption was greater on sorbents containing Mn due to oxidation. Uncertainties are one standard error of the mean.

M^{3+}	Hydrous Fe oxide	3:1 FeMn oxide	1:1 FeMn oxide	1:9 FeMn oxide	Hydrous Mn oxide
Y	0.73 ± 0.02	0.79 ± 0.09	1.02 ± 0.06	0.55 ± 0.05	0.45 ± 0.02
La	0.66 ± 0.02	0.64 ± 0.05	1.07 ± 0.09	0.61 ± 0.04	0.49 ± 0.02
Ce	0.70 ± 0.02	1.21 ± 0.05	1.24 ± 0.06	0.99 ± 0.08	0.96 ± 0.04
Pr	0.75 ± 0.02	0.76 ± 0.05	1.06 ± 0.04	0.63 ± 0.04	0.53 ± 0.02
Nd	0.74 ± 0.02	0.76 ± 0.05	0.99 ± 0.03	0.61 ± 0.04	0.52 ± 0.02
Pm[a]					
Sm	0.78 ± 0.02	0.79 ± 0.05	1.04 ± 0.04	0.62 ± 0.04	0.53 ± 0.02
Eu	0.80 ± 0.02	0.76 ± 0.06	1.05 ± 0.03	0.62 ± 0.04	0.53 ± 0.02
Gd	0.77 ± 0.02	0.74 ± 0.04	0.98 ± 0.03	0.57 ± 0.04	0.49 ± 0.02
Tb	0.83 ± 0.02	0.81 ± 0.05	1.05 ± 0.03	0.61 ± 0.04	0.53 ± 0.02
Dy	0.84 ± 0.02	0.82 ± 0.05	1.13 ± 0.07	0.60 ± 0.04	0.52 ± 0.02
Ho	0.83 ± 0.02	0.81 ± 0.05	1.03 ± 0.03	0.59 ± 0.04	0.51 ± 0.02
Er	0.83 ± 0.02	0.82 ± 0.05	1.07 ± 0.04	0.59 ± 0.04	0.51 ± 0.02
Tm	0.86 ± 0.02	0.84 ± 0.05	1.07 ± 0.04	0.60 ± 0.05	0.53 ± 0.02
Yb	0.88 ± 0.02	0.85 ± 0.05	1.09 ± 0.05	0.62 ± 0.05	0.55 ± 0.02
Lu	0.85 ± 0.02	0.84 ± 0.05	1.04 ± 0.04	0.61 ± 0.05	0.53 ± 0.02
Average[b]	0.80 ± 0.06	0.79 ± 0.05	1.05 ± 0.04	0.60 ± 0.02	0.52 ± 0.03

[a]Not measured; [b]Ce not included.

Table 3.6. Best-fit R values for regressions of log ${}_iK_{FeMn}$ *vs.* pH using the composite non-electrostatic surface complexation model (Equation (3.3)) where R indicates the relative influence of hydrous Fe and Mn oxides during metal sorption on mixed oxides such that larger values reflect greater effect of Fe oxides than Mn oxides. Uncertainties are one standard error of the mean.

M^{3+}	3:1 FeMn oxide	1:1 FeMn oxide	1:9 FeMn oxide
Y	1.01 ± 0.08	1.62 ± 0.08	0.22 ± 0.03
La	0.79 ± 0.04	1.19 ± 0.08	0.25 ± 0.02
Ce*[a]	0.80	1.27	0.23
Pr	0.81 ± 0.04	1.34 ± 0.06	0.21 ± 0.02
Nd	0.84 ± 0.05	1.34 ± 0.06	0.19 ± 0.02
Pm[b]			
Sm	0.83 ± 0.04	1.37 ± 0.05	0.18 ± 0.02
Eu	0.84 ± 0.02	1.38 ± 0.05	0.18 ± 0.02
Gd	0.80 ± 0.04	1.33 ± 0.04	0.17 ± 0.02
Tb	0.85 ± 0.05	1.41 ± 0.04	0.17 ± 0.02
Dy	0.86 ± 0.04	1.52 ± 0.06	0.16 ± 0.02
Ho	0.88 ± 0.04	1.48 ± 0.04	0.16 ± 0.02
Er	0.92 ± 0.05	1.57 ± 0.05	0.16 ± 0.02
Tm	0.93 ± 0.05	1.60 ± 0.05	0.15 ± 0.02
Yb	0.94 ± 0.05	1.66 ± 0.05	0.16 ± 0.02
Lu	0.96 ± 0.05	1.67 ± 0.05	0.17 ± 0.02

[a] Interpolated; [b]Not measured.

Appendix*

Marine Chemistry 123 (2011) 32–43

Contents lists available at ScienceDirect

Marine Chemistry

journal homepage: www.elsevier.com/locate/marchem

YREE sorption on hydrous ferric oxide in 0.5 M NaCl solutions: A model extension

Johan Schijf *, Kathleen S. Marshall

University of Maryland Center for Environmental Science, Chesapeake Biological Laboratory, P.O. Box 38, Solomons, MD 20688, USA

ARTICLE INFO

Article history:
Received 11 June 2010
Received in revised form 11 September 2010
Accepted 14 September 2010
Available online 22 September 2010

Keywords:
Rare earth elements
Hydrous ferric oxide
Sorption
ICP-MS
Surface complexation model

ABSTRACT

Distribution coefficients, ${}_iK_{Fe}$, were measured for sorption of yttrium and the rare earth elements (YREEs) on hydrous ferric oxide (HFO) in 0.5 M NaCl solutions over the pH range 3.9–8.4 ($T = 25$ °C). An existing, non-electrostatic model [Quinn, K.A., Byrne, R.H., Schijf, J., 2006. Sorption of yttrium and rare earth elements by amorphous ferric hydroxide: influence of pH and ionic strength. Mar. Chem. 99, 128–150] was modified to account for sorption of YREE–chloride complexes, as well as YREE–hydroxide complexes at elevated pH. The extended model, which allows calculation of ${}_iK_{Fe}$ as a function of $[H^+]$, contains two parameters, ${}_sK_1$ and ${}_sK_2$, to describe the equilibrium between positive, neutral, and negative forms of the hydroxyl functional groups on the HFO surface. In addition, it contains several composite, conditional stability constants, A_n, that represent YREE bonding to the neutral groups with release of n protons and/or to the negatively charged groups with release of $n-1$ protons.

In 0.5 M NaCl solutions, YREE sorption on HFO is weaker and less pH dependent, yielding only 0.7–0.9 protons per YREE cation on average, vs. about 1.5 at low ionic strength. This is due to enhanced deprotonation of the HFO surface (${}_sK_1 \sim 0$, $p_sK_2 = 6.16$), leading to an increase in the proportion of negatively charged groups, which release fewer protons per YREE cation sorbed. On a logarithmic scale, ${}_iK_{Fe}$ is a nearly linear function of pH, except at pH > 8 where cumulative sorption of YREE–hydroxide complexes causes it to rise more rapidly, especially for the heavy REEs. Both our own data and prior results from the literature are well described by the extended model, using only three adjustable parameters, A_1–A_3. The constant A_3, representing YREE bonding to the negatively charged groups with release of two protons, shows an excellent linear free-energy relation when plotted against the first YREE hydrolysis constant, β_1^*. There is no evidence for YREE bonding to the positively charged groups (i.e., $A_0 = 0$).

1. Introduction

The inorganic portion of marine sediments is a complex mixture of minerals, a large fraction of which may comprise hydrated oxides of trivalent and tetravalent metals like aluminum, silicon, titanium, iron, and manganese (Chester, 1990). The solid–solution interface of hydrated oxides harbors an abundance of hydroxyl functional groups in various steric configurations. Hydroxyl functional groups of individual mineral components predominantly protonate (become positively charged) at pH values below their first deprotonation constant (pK_{a1}) and deprotonate (become negatively charged) above their second deprotonation constant (pK_{a2}). At the pH of the point-of-zero-charge ($pH_{pzc} = \frac{1}{2}[pK_{a1} + pK_{a2}]$), each group holds one proton on average and the surface as a whole is neutral. Negatively charged surfaces have a pronounced affinity for dissolved metal cations, which may bond to functional groups through a combination of electrostatic attraction and surface complexation mechanisms, collectively termed 'sorption'. Proton exchange may allow metal cations to be sorbed on neutral surfaces or even on positively charged ones if the electrostatic repulsion can be overcome. In short, oxide minerals are very reactive with respect to metal sorption from aqueous solution and this process is likely to be strongly pH dependent.

One group of metals for which sorption has been widely studied is yttrium and the rare earth elements (YREEs), since they have certain properties that make them uniquely suitable for such investigations. Notably, the YREEs serve as chemical analogs of the actinides, whose mobility in nuclear waste repositories is a matter of grave concern yet unfit for direct testing due to severe radioactive and toxic hazards (Krauskopf, 1986). The tendency of metal cations to be sorbed on solids and colloids generally goes up with increasing charge and down with increasing ionic radius (Whitfield and Turner, 1979; Sverjensky, 2006). All YREEs are trivalent in aqueous solution, but their ionic radii decrease gradually across the lanthanide series from La to Lu, a phenomenon called 'lanthanide contraction'. The affinity of free YREE ions (M^{3+}) for hydrated oxide minerals should therefore increase in the same direction. Conversely, the ionic radius of Y ($Z = 39$) is almost identical to that of Ho ($Z = 67$) hence one might expect little or no fractionation between them (e.g., Bau et al., 1995; Nozaki et al., 1997). In practice Y shows a broad spectrum of behaviors, alternately resembling a pseudo-heavy or a pseudo-light REE, implying a varying

* Corresponding author. Tel.: +1 410 326 7387; fax: +1 410 326 7341.
E-mail address: schijf@cbl.umces.edu (J. Schijf).

0304-4203/$ – see front matter © 2010 Elsevier B.V. All rights reserved.
doi:10.1016/j.marchem.2010.09.003

level of covalence in its chemical interactions (Borkowski and Siekierski, 1992). Finally, YREE (inorganic) solution speciation is quite well known (e.g., Wood, 1990; Byrne and Sholkovitz, 1996). By simultaneously observing all YREEs in a single solution, sorption processes can be understood in terms of relative behavior, which requires information about comparative YREE properties only, whereas absolute behavior requires detailed knowledge of particle characteristics that may be difficult to measure, quantify, or keep constant, for example their size distribution, degree of crystallinity, and specific surface area (Byrne and Kim, 1990).

Despite these advantages it is challenging to study YREE sorption on natural sediments and suspended particles, because they are usually composites of finely interspersed minerals wherein the components may have different crystal structures, pH_{pzc}, equilibrium deprotonation constants ($pK_{a1,2}$) etc. (Schindler and Stumm, 1987). Each component may contain oxides of multiple metals, such as Fe and Mn in ferromanganese concretions, or Al, Si, and Fe in clays. Another complication is that inorganic surfaces can acquire organic coatings, which substantially alters their functional groups and charge (Loder and Liss, 1985). Composite substrates are hard to characterize and their sorptive properties difficult to model on a molecular scale. Various approaches have been taken to tackle the problem. Some use relatively well-defined natural materials (Tang and Johannesson, 2005; Tertre et al., 2008; Bau and Koschinsky, 2009), trading off structural simplicity for greater environmental relevance. Others prefer pure minerals of moderate complexity, for instance commercial-grade illite and kaolinite clays (Aagaard, 1974; Coppin et al., 2002; Tertre et al., 2006). A third school of thought favors single-metal (hydr)oxides – freshly prepared to constrain key surface properties – subscribing to the premise that their individual contributions to YREE sorption on sediments and particulate matter must be additive, at least to some extent (Quinn et al., 2004; Davranche et al., 2005; Piasecki and Sverjensky, 2008). Among such synthetic phases, Fe oxide is probably the most noteworthy. It naturally occurs in several crystal structures, including hematite (α-Fe_2O_3), goethite (α-FeOOH), and lepidocrocite (γ-FeOOH). What first precipitates from solution however, is an amorphous hydroxide referred to as hydrous ferric oxide (HFO) whose features have been extensively studied, especially its proton-exchange equilibria and concomitant pH-dependent surface charge (Dzombak and Morel, 1990; Pretorius and Linder, 1998).

De Carlo and co-workers pioneered systematic investigations of YREE sorption on Fe and Mn oxides, highlighting its kinetic aspects (Koeppenkastrop et al., 1991; Koeppenkastrop and De Carlo, 1992, 1993; De Carlo et al., 1998). The experiments were conducted with externally prepared precipitates, many in UV-oxidized, filtered seawater at low temperature (2 °C) and a single pH (7.8), whereby CO_2 was allowed to enter the solution. They noted that YREE sorption on goethite is very fast (>80% within 5 min) and not substantially retarded in the presence of carbonate, which was attributed to the formation of ternary Fe–O–MCO_3 surface complexes. No evidence of Ce oxidation was found. Bau (1999) precipitated HFO directly from YREE solutions in 0.01 M HCl and assessed sorption over a limited pH range (3.6–6.2) by titrating with NH_4OH, making no provisions to exclude CO_2. He similarly found YREE sorption to attain equilibrium in ~7 min and to increase strongly with pH. One incongruous observation was a prominent positive Ce anomaly (enhanced sorption) at low pH, which Bau interpreted as Ce oxidation on the HFO surface. This result has not been independently confirmed. Japanese scientists (Kawabe et al., 1999; Ohta and Kawabe, 2000a) unsuccessfully attempted to employ YREE sorption on HFO in $NaHCO_3$-enriched NaCl solutions as a means to deduce YREE-carbonate stability constants (see Luo and Byrne, 2004). Ohta and Kawabe (2001) then compared YREE sorption on Fe and Mn oxides in pure NaCl solutions (without purging CO_2) and showed definitively that Ce is oxidized on the surface of Mn oxide, but not HFO. A French group (Davranche et al., 2004, 2005, 2008) has focused on how YREE sorption on Fe and Mn oxides is affected by humic acids. Pending better data on the stability of YREE–humate complexes, it is not straightforward to evaluate their findings in the context of the aforementioned research.

Starting from basic stoichiometric principles, Quinn et al. (2006a) were the first to develop a non-electrostatic surface complexation model that successfully describes YREE sorption on HFO as a function of pH (3.9–7.0) in dilute NH_4Cl solutions, where the ionic strength dependence was found to be minor. Quinn et al. (2007) also derived enthalpy values by repeating the experiments at different temperatures (10–40 °C). The model was subsequently extended to incorporate the influence of P_{CO_2} by expressly postulating the existence of ternary Fe–O–MCO_3 surface complexes (Quinn et al., 2006b). In the present work, we report new measurements of YREE sorption on HFO at higher ionic strength (0.5 M NaCl) and over a wider pH range (3.9–8.4), in the absence of carbonate or other strong solution ligands. Comparison with the results of Quinn et al. (2006a) demonstrates that under these conditions YREE sorption on HFO is weaker and less pH dependent. A modification of the original model accurately accounts for both effects, indicating that the observed distinctions are primarily caused by changes in HFO properties, whereas the fundamental interactions between YREEs and the hydroxyl functional groups i.e., the formation of either monodentate (Fe–O–M) or bidentate (Fe–O_2–M and (Fe–O–)$_2$M) surface complexes (Quinn et al., 2006a), remain the same.

It should be emphasized that the purpose of this paper is not to present a quantitative and fully functional model of YREE sorption in seawater under natural conditions. New insights gained here may ultimately contribute to such a goal, yet the process comprises many steps of increasing complexity that must by necessity use a greatly simplified version of reality as its point of departure. With these investigations we took a small step, albeit an important one, namely extending the model of Quinn et al. (2006a) to higher ionic strength without compromising its ability to describe dilute solutions. Future steps may accommodate other attributes of seawater, such as competing cations or YREE complexation with additional inorganic anions and specific organic ligands. Although built on the model of Quinn et al. (2006a), whom we cite frequently, this study not only stands on its own but in a sense supersedes their work. Our unconventional method of conducting batch experiments as a function of pH at constant metal concentration (*cf.* Davis and Leckie, 1978) is one of several approaches (e.g., sorption isotherms, kinetic studies and spectroscopic analysis), together weaving a rich tapestry of complementary information, that we hope to carry to an advanced level of sophistication. The extended model essentially probes the *mechanism* underlying YREE sorption on HFO in seawater (as illustrated by its eminent prediction of YREE fractionation). In that regard our results, while apt to be useful to marine geochemists and applicable in both pelagic and benthic environments, will be of particular interest to physical and surface chemists.

2. Materials and methods

All standards and experimental solutions were made inside a class-100 laminar flow bench with Milli-Q water (18.2 MΩ cm) from a Millipore Direct-Q 3UV purification system. Solutions of Fe(III) (40% w/v $FeCl_3$ in HCl), concentrated HNO_3 (TraceMetal grade), and 1 M NaOH were purchased from Fisher. Certified HCl (1.0011 M) was obtained from Brinkmann (Westbury, NY) and NaCl salt (Reagent-Plus) from Sigma-Aldrich. A stock solution containing 66.7 mg/L of each YREE was blended from 1000 mg/L single-element standards. The ICP-MS calibration line was fashioned from a premixed standard containing 10 mg/L of each YREE (plus Sc and Th). Primary YREE and other metal standards were supplied by SPEX/CertiPrep (Metuchen, NJ). Plastic laboratory materials were acid cleaned and thoroughly rinsed with Milli-Q water before use. Small Teflon items were

immersed in sub-boiling 8 M HNO_3 for 24 h. Teflon bottles and non-Teflon items were soaked in cold 4 M HCl for at least one week.

Two Teflon wide-mouth bottles were placed inside jacketed glass beakers connected to a recirculating water bath (LAUDA-Brinkmann RE-106) to maintain a temperature of 25.0 ± 0.1 °C. One bottle was filled with 1 L of 0.5 M NaCl containing 500 μg/L of each YREE to which 100 μL of Fe(III) solution was added. The other was filled with 1 L of 1.00 mM HCl (pH 3.00) in 0.5 M NaCl, constituting the pH standard. Solution pH was measured with an Orion glass combination electrode (no. 810200) connected to a PerpHecT 350 millivolt meter. The internal electrolyte (3 M NaCl) was replaced every day. The electrode was checked regularly for proper Nernstian slope (59.16 mV/pH at 25 °C) by titrating a 0.5 M NaCl solution with 1 M HCl. The YREE solution was sparged with N_2 at low pH to eliminate carbonate and kept under an N_2 atmosphere throughout the experiment. The UHP-grade gas was first passed through an in-line trap (Supelco) that captures any residual traces of CO_2. The two bottles were fitted with custom PTFE caps, containing ports for the pH electrode and gas line, as well as for adding titrants. Both were continuously stirred with Teflon-coated magnetic stir bars, the one in the YREE solution being of a 'floating' design that does not grind the HFO particles.

A filtered sample of the YREE solution was taken after addition of the Fe(III) solution, as described below, to determine the initial dissolved YREE concentration, $[M]_{init}$ (pH<3). The experiment was then started by titrating the YREE solution with 1 M NaOH from a 2 mL Gilmont micrometer buret via a Teflon needle, causing abrupt HFO precipitation around pH 3.5. Titration was slowly continued until a preselected pH value was reached as indicated by the electrode. After an equilibration period of 6–24 h, stirring was briefly discontinued to allow the precipitate to settle. Two 5 mL aliquots were removed from the solution with a pipette and sequentially forced through a 13 mm HDPE filter cartridge (0.22 μm PVDF membrane) with an all-plastic Luer-Lok syringe (National Scientific). The first aliquot was discarded, serving only to prevent YREE loss by saturating sorption sites on the filter membrane, while the second was collected in a 15 mL polypropylene centrifuge tube and acidified with a small amount of concentrated HNO_3. Stirring was resumed, the YREE solution titrated to the next pH value, and the entire procedure repeated. To ensure minimal aging of HFO, each experiment was terminated after 4–5 days during which 5–10 samples were collected.

The acidified samples were readied for analysis by spiking with an internal standard solution (2 μg/L each of In, Cs, and Re) after 100-fold dilution with 1% HNO_3 to suppress NaCl matrix effects. Dissolved YREE concentrations were measured on an Agilent 7500cx ICP-MS equipped with a High Matrix Introduction accessory, against an external calibration line (0, 0.5, 1, 2 and 5 μg/L) matrix-matched to the samples (5 mM NaCl). The instrument was tuned for maximum signal across the YREE mass range (50–200 amu), as well as for minimum production of metal-oxide ions (CeO^+ at 156 amu vs. Ce^+ at 140 amu) and double-charged ions (Ce^{2+} at 70 amu vs. Ce^+ at 140 amu). Standards, blanks, and samples were injected in triplicate via a MicroMist concentric nebulizer (0.4 mL/min) and a Scott-type double-pass spray chamber, Peltier-cooled to 2 °C. A 1% HNO_3 rinse solution was aspirated before and after every autosampler position to clean the sample introduction system. Concentrations were determined from the mean of two suitable isotopes for each element, except for monoisotopic Y, Pr, Tb, Ho, and Tm. Fluctuations in sensitivity were compensated for by normalizing ^{89}Y to ^{115}In and each REE isotope to a virtual internal standard (VIS) value derived from linear interpolation between ^{133}Cs and ^{187}Re.

Distribution coefficients, ${}_iK_{Fe}$, were calculated from dissolved YREE concentrations, $[M]_{diss}$, as follows:

$$ {}_iK_{Fe} = \frac{[M]_{init} - [M]_{diss}}{[M]_{diss} \times [Fe]_T} \quad (1) $$

where $[Fe]_T$ is the initial dissolved Fe(III) concentration (~0.25 mM), assuming this is entirely converted to HFO. The assumption is reasonable because $[Fe]_T$ for NaCl solutions in equilibrium with HFO is about $10^{-6.2}$ M at pH 3.9 (Liu and Millero, 1999), indicating that HFO precipitation is >99.97% complete at the lowest pH of our experiments (supplementary data, Table S.2). Dzombak and Morel (1990) stated that the entire mass of HFO, being an amorphous solid with an open structure, is considered available for participation in surface reactions.

Every batch of samples was analyzed twice in random order and replicate concentrations were typically equal to within 1%. To avoid systematic errors, $\log {}_iK_{Fe}$ values were calculated from each individual ICP-MS run and averaged. A total of ten experiments was completed, spanning the pH range 3.9–8.4. Preliminary data for pH<5 were of inferior quality due to very weak YREE sorption and consequently rejected (including all of experiments 6 and 7). The issue was resolved in two final experiments (9 and 10) by adding ten times more Fe(III) to the YREE solution, thereby lowering the load factor ($[M]_{init}/[Fe]_T$) and raising the amount of YREE sorbed for a given value of ${}_iK_{Fe}$. In experiment 8, the YREE solution was quickly brought up to pH 6 and then titrated downward with 1 M HCl. In experiment 3, an additional 15 mL aliquot was filtered at pH ~ 5.5 to gauge the contribution to $[M]_{diss}$ of HFO colloids that might elude the 0.22 μm filter. The filtrate was sequentially forced through two 50 mL Millipore Amicon ultrafiltration tubes (30 kDa and 3 kDa MWCO, respectively) in a Hettich EBA 21 centrifuge. Retentates were subsequently recovered by centrifuging 10 mL of 1% HNO_3 through each tube.

3. The extended non-electrostatic surface complexation model

3.1. Derivation of the model equation

In accordance with the strategy and notation of Quinn et al. (2006a), we consider three distinct chemical forms of the hydroxyl functional group on the HFO surface: a positive form that predominates at low pH, a negative form that predominates at high pH, and a neutral form that predominates at intermediate pH. We will write these forms, respectively, as $S{\equiv}Fe(OH)_2^+$, $S{\equiv}Fe(OH)_4^-$, and $S{\equiv}Fe(OH)_3^0$, where the triple-bond sign merely indicates that the Fe atoms are tightly bound at the surface S of the HFO particle. In the final equation, all reactions will be expressed in terms of the neutral form, $S{\equiv}Fe(OH)_3^0$. Since amorphous HFO is regarded as having no long-range order, we will assume that there are no structural types of each form that are identifiable by different crystal planes or by different locations on the plane ('corner' vs. 'edge'), as in crystalline ferric oxides (e.g., Ghose et al., 2010). Unlike Dzombak and Morel (1990), we also do not distinguish between 'high-affinity' and 'low-affinity' sites, which would have required measurement of isotherms (i.e., sorption as a function of YREE concentration at constant pH), an effort deemed beyond the scope of this study. Ours is effectively a 'one-site, two-pK' type model.

The three forms of the hydroxyl functional group transform into one another by equilibrium (de)protonation reactions:

$$ S{\equiv}Fe(OH)_3^0 + H^+ \rightleftharpoons S{\equiv}Fe(OH)_2^+ + H_2O \quad (2a) $$

$$ S{\equiv}Fe(OH)_3^0 + H_2O \rightleftharpoons S{\equiv}Fe(OH)_4^- + H^+ \quad (2b) $$

with corresponding equilibrium constants, ${}_sK_1$ and ${}_sK_2$:

$$ {}_sK_1 = \frac{[S{\equiv}Fe(OH)_2^+]}{[S{\equiv}Fe(OH)_3^0][H^+]} \quad (3a) $$

$$ {}_sK_2 = \frac{[S{\equiv}Fe(OH)_4^-][H^+]}{[S{\equiv}Fe(OH)_3^0]} \quad (3b) $$

Using Eqs. (3a) and (3b), we can express the total surface functional group concentration, $[S\equiv Fe]_T$, as

$$[S\equiv Fe]_T = [S\equiv Fe(OH)_2^+] + [S\equiv Fe(OH_3^0)] + [S\equiv Fe(OH)_4^-] = [S\equiv Fe(OH)_3^0]({}_SK_1[H^+] + 1 + {}_SK_2[H^+]^{-1}) \quad (4)$$

Next, we can describe YREE sorption in terms of specific reactions between single YREE ions, M^{3+}, and each of the three forms of the hydroxyl functional group, ranked according to the number of protons released. In agreement with Quinn et al. (2006a), we assume that electrostatic repulsion is too strong for M^{3+} to associate with $S\equiv Fe(OH)_2^+$ and we do not consider any YREE surface species with charges higher than 2+. For example, we do not include this reaction:

$$S\equiv Fe(OH)_3^0 + M^{3+} \rightleftharpoons S\equiv Fe(OH)_3M^{3+} \quad (5)$$

We can now tally as follows; reactions without proton release:

$$S\equiv Fe(OH)_4^- + M^{3+} \rightleftharpoons S\equiv Fe(OH)_4M^{2+} \quad (6)$$

reactions with release of one proton:

$$S\equiv Fe(OH)_3^0 + M^{3+} \rightleftharpoons S\equiv Fe(OH)_2OM^{2+} + H^+ \quad (7a)$$

$$S\equiv Fe(OH)_4^- + M^{3+} \rightleftharpoons S\equiv Fe(OH)_3OM^{+} + H^+ \quad (7b)$$

and reactions with release of two protons:

$$S\equiv Fe(OH)_3^0 + M^{3+} \rightleftharpoons S\equiv Fe(OH)O_2M^{+} + 2H^+ \quad (8a)$$

$$S\equiv Fe(OH)_4^- + M^{3+} \rightleftharpoons S\equiv Fe(OH)_2O_2M + 2H^+ \quad (8b)$$

These can be described with two generic stability constants:

$${}_3\beta_n = \frac{\left[S\equiv Fe(OH)_{3-n}O_nM^{(3-n)+}\right][H^+]^n}{\left[S\equiv Fe(OH)_3^0\right][M^{3+}]} \quad (9a)$$

$${}_4\beta_n = \frac{\left[S\equiv Fe(OH)_{4-n}O_nM^{(2-n)+}\right][H^+]^n}{\left[S\equiv Fe(OH)_4^-\right][M^{3+}]} = \frac{\left[S\equiv Fe(OH)_{4-n}O_nM^{(2-n)+}\right][H^+]^{n+1}}{{}_sK_2 \times \left[S\equiv Fe(OH)_3^0\right][M^{3+}]} \quad (9b)$$

where subscripts 3 and 4 refer to the neutral and negative forms of the hydroxyl functional group, respectively, while n is the number of protons released in each reaction.

Combining all five reactions we get the total sorbed YREE concentration, $[MS_i]_T$; subscript i denotes the involvement of multiple surface species:

$$[MS_i]_T = [S\equiv Fe(OH)_4M^{2+}] + [S\equiv Fe(OH)_2OM^{2+}] + [S\equiv Fe(OH)_3OM^{+}] + [S\equiv Fe(OH)O_2M^{+}] + [S\equiv Fe(OH)_2O_2M] \quad (10)$$

Substituting the stability constants from Eqs. (9a) and (9b) we find

$$[MS_i]_T = [S\equiv Fe(OH_3^0)][M^{3+}]({}_4\beta_0\times{}_SK_2[H^+]^{-1} + {}_3\beta_1[H^+]^{-1} + {}_4\beta_1\times{}_SK_2[H^+]^{-2} + {}_3\beta_2[H^+]^{-2} + {}_4\beta_2\times{}_SK_2[H^+]^{-3}) \quad (11a)$$

and after rearranging:

$$[MS_i]_T = \left[S\equiv Fe(OH)_3^0\right]\left[M^{3+}\right]\left\{({}_4\beta_0\times{}_SK_2 + {}_3\beta_1)[H^+]^{-1} + ({}_4\beta_1\times{}_SK_2 + {}_3\beta_2)[H^+]^{-2} + ({}_4\beta_2\times{}_SK_2)[H^+]^{-3}\right\} = \left[S\equiv Fe(OH)_3^0\right]\left[M^{3+}\right]\sum_{n=1}^{3}A_n[H^+]^{-n} \quad (11b)$$

with $A_1 = ({}_4\beta_0\times{}_SK_2 + {}_3\beta_1)$; $A_2 = ({}_4\beta_1\times{}_SK_2 + {}_3\beta_2)$; and $A_3 = ({}_4\beta_2\times{}_SK_2)$. The model equation is obtained by inserting Eqs. (4) and (11b) into the definition of the distribution coefficient, ${}_iK_{Fe}$:

$${}_iK_{Fe} = \frac{[MS_i]_T}{M_T\times[S\equiv Fe]_T} = \frac{\left[M^{3+}\right]\left(A_1[H^+]^{-1} + A_2[H^+]^{-2} + A_3[H^+]^{-3}\right)}{M_T({}_sK_1[H^+] + 1 + {}_sK_2[H^+]^{-1})} \quad (12)$$

An overview of stability constants appearing in the model is provided in Table 1.

3.2. The influence of YREE solution speciation

Quinn et al. (2006a) found no evidence for deprotonation of the neutral groups i.e., ${}_sK_2 \sim 0$, yielding $A_1 = {}_3\beta_1$, $A_2 = {}_3\beta_2$, and $A_3 = 0$. Furthermore, they assumed YREE solution complexation to be negligible under the conditions of their experiments ($[Cl^-] < 0.1$ M, pH ≤ 7.0), thus posing that $M_T = [M^{3+}]$ whence Eq. (12) simplifies to their Eq. (19):

$${}_iK_{Fe} = \frac{{}_3\beta_1[H^+]^{-1} + {}_3\beta_2[H^+]^{-2}}{{}_sK_1[H^+] + 1} \quad (13)$$

Under the conditions of the present experiments ($[Cl^-] = 0.5$ M, pH < 8.5) the assumption $M_T = [M^{3+}]$ is not obviously valid. At pH 4, about 20% of each YREE is actually present as MCl^{2+}, whereas the contribution of MOH^{2+} is negligible; at pH 8.4, MCl^{2+} and MOH^{2+} represent about 17% and 13% of total dissolved La, yet about 3% and 84% of total dissolved Lu, respectively (Klungness and Byrne, 2000; Luo and Byrne, 2001). It is quite plausible that the species MOH^{2+} interacts with the HFO surface much like M^{3+}, as was shown by Quinn et al. (2006b) for the species MCO_3^+. While it might be possible for the less positively charged MOH^{2+} to associate with $S\equiv Fe(OH)_2^+$, releasing one proton, in reality the former species occurs only at high pH and the latter only at low pH. The two therefore cannot coexist to any appreciable extent, ruling out this reaction. Nonetheless, the following two reactions could arise:

$$S\equiv Fe(OH)_3^0 + MOH^{2+} \rightleftharpoons S\equiv Fe(OH)_3OM^{+} + H^+ \quad (14a)$$

$$S\equiv Fe(OH)_3^0 + MOH^{2+} \rightleftharpoons S\equiv Fe(OH)_2O_2M + 2H^+ \quad (14b)$$

For this type of reaction we can define a new stability constant:

$${}_3\beta_n^* = \frac{\left[S\equiv Fe(OH)_{4-n}O_nM^{(2-n)+}\right][H^+]^n}{\left[S\equiv Fe(OH)_3^0\right][MOH^{2+}]} = \frac{\left[S\equiv Fe(OH)_{4-n}O_nM^{(2-n)+}\right][H^+]^{n+1}}{\beta_1^*\times\left[S\equiv Fe(OH)_3^0\right][M^{3+}]} \quad (15)$$

where

$$\beta_1^* = \frac{\left[MOH^{2+}\right][H^+]}{\left[M^{3+}\right]} \quad (16)$$

Table 1
Overview of stability constants used in the non-electrostatic surface complexation model.

Stability constant	Description	Corresponding equilibrium reaction	Defined in Eq.
${}_{s}K_1$	Protonation of a neutral HFO site	$S{\equiv}Fe(OH)_3^0 + H^+ \rightleftharpoons S{\equiv}Fe(OH)_2^+ + H_2O$	(3a)
${}_{s}K_2$	Deprotonation of a neutral HFO site	$S{\equiv}Fe(OH)_3^0 + H_2O \rightleftharpoons S{\equiv}Fe(OH)_4^- + H^+$	(3b)
${}_{3}\beta_n$	YREE sorption on a neutral HFO site releasing n protons	$S{\equiv}Fe(OH)_3^0 + M^{3+} \rightleftharpoons S{\equiv}Fe(OH)_{3-n}O_nM^{(3-n)+} + nH^+$	(9a)
${}_{4}\beta_n$	YREE sorption on a negatively charged HFO site releasing n protons	$S{\equiv}Fe(OH)_4^- + M^{3+} \rightleftharpoons S{\equiv}Fe(OH)_{4-n}O_nM^{(2-n)+} + nH^+$	(9b)
${}_{3}\beta_n^*$	Sorption of YREE–hydroxide complex on a neutral HFO site releasing n protons	$S{\equiv}Fe(OH)_3^0 + MOH^{2+} \rightleftharpoons S{\equiv}Fe(OH)_{4-n}O_nM^{(2-n)+} + nH^+$	(15)
β_1^*	First YREE hydrolysis constant	$M^{3+} + H_2O \rightleftharpoons MOH^{2+} + H^+$	(16)
${}_{2}^{Cl}\beta_1$	Sorption of YREE–monochloride complex on a positively charged HFO site releasing 1 proton	$S{\equiv}Fe(OH)_2^+ + MCl^{2+} \rightleftharpoons S{\equiv}Fe(OH)OMCl^{2+} + H^+$	(21)
${}_{Cl}\beta_1$	Formation of YREE–monochloride complex	$M^{3+} + Cl^- \rightleftharpoons MCl^{2+}$	(22)

is the stability constant of the hydrolysis reaction

$$M^{3+} + H_2O \rightleftharpoons MOH^{2+} + H^+ \tag{17}$$

Comparing Eqs. (15) and (9b) it is apparent that ${}_{3}\beta_n^* \times \beta_1^* = {}_{4}\beta_n \times {}_{s}K_2$, a corollary of the fact that the model, whose only variable is pH, cannot distinguish between reactions (14a) and (7b), each producing the same surface species and releasing the same number of protons, nor between (14b) and (8b). Including reactions (14a) and (14b) in the model thus changes the definition of the parameters A_2 and A_3, but not the algebraic form of Eq. (12). This subtle point was already made by Quinn et al. (2006a) who remarked that the model cannot distinguish either between reaction (8a) and the following:

$$S{\equiv}\left\{Fe(OH)_3^0\right\}_2 + M^{3+} \rightleftharpoons S{\equiv}\left\{Fe(OH)_2O\right\}_2M^+ + 2H^+ \tag{18}$$

In other words, the model does not reveal whether the two hydroxyl groups that each release a proton to bind the M^{3+} ion are attached to a single Fe atom as in reaction (8a), or to adjacent Fe atoms as in reaction (18).

Analogously, the following reaction cannot be distinguished from reaction (7a):

$$S{\equiv}Fe(OH)_3^0 + MCl^{2+} \rightleftharpoons S{\equiv}Fe(OH)_2OM^{2+} + H^+ + Cl^- \tag{19a}$$

or alternatively

$$S{\equiv}Fe(OH)_3^0 + MCl^{2+} \rightleftharpoons S{\equiv}Fe(OH)_2OMCl^+ + H^+ \tag{19b}$$

Accounting for these reactions, and similar ones involving $S{\equiv}Fe(OH)_4^-$, again does not alter the algebraic form of Eq. (12). However, we may need to consider the reaction:

$$S{\equiv}Fe(OH)_2^+ + MCl^{2+} \rightleftharpoons S{\equiv}Fe(OH)OMCl^{2+} + H^+ \tag{20}$$

with stability constant

$${}_{2}^{Cl}\beta_1 = \frac{\left[S{\equiv}Fe(OH)OMCl^{2+}\right][H^+]}{\left[S{\equiv}Fe(OH)_2^+\right][MCl^{2+}]} = \frac{\left[S{\equiv}Fe(OH)OMCl^{2+}\right]}{{}_{Cl}\beta_1 \times {}_{s}K_1 \times \left[S{\equiv}Fe(OH)_3^0\right][M^{3+}][Cl^-]} \tag{21}$$

where

$${}_{Cl}\beta_1 = \frac{\left[MCl^{2+}\right]}{[M^{3+}][Cl^-]} \tag{22}$$

is the stability constant of the complexation reaction

$$M^{3+} + Cl^- \rightleftharpoons MCl^{2+} \tag{23}$$

Including this surface species in the model introduces a new term in the numerator of Eq. (12):

$${}_{i}K_{Fe} = \frac{\left[M^{3+}\right]\left(A_0 + A_1[H^+]^{-1} + A_2[H^+]^{-2} + A_3[H^+]^{-3}\right)}{M_T\left({}_{s}K_1[H^+] + 1 + {}_{s}K_2[H^+]^{-1}\right)} \tag{24}$$

where $A_0 = {}_{2}^{Cl}\beta_1 \times {}_{Cl}\beta_1 \times {}_{s}K_1 \times [Cl^-]$. The term A_0 is diagnostic for interactions of MCl^{2+} with $S{\equiv}Fe(OH)_2^+$, provided the latter is indeed present. Quinn et al. (2006a) did not incorporate A_0, yet under the conditions to which their model was applied ($[Cl^-] \sim 0.025$ M) the contribution of reaction (20) to the term $[MS_i]_T$ is very small ($[MCl^{2+}]/M_T < 4.5\%$).

In conclusion, since the model cannot distinguish between sorption on HFO of the solution species M^{3+}, MCl^{2+}, or MOH^{2+}, YREE total and free-ion concentrations, M_T and $[M^{3+}]$, are mathematically interchangeable and calculated values of $\log {}_{i}K_{Fe}$, plotted as a function of pH, should conform to the relation

$$\log {}_{i}K_{Fe} = \log\left(\frac{A_0 + A_1 \times 10^{pH} + A_2 \times 10^{2\times pH} + A_3 \times 10^{3\times pH}}{{}_{s}K_1 \times 10^{-pH} + 1 + {}_{s}K_2 \times 10^{pH}}\right) \tag{25}$$

Note that, whereas $[Cl^-]$ is constant in our experiments and $[OH^-]$ depends directly on $[H^+]$, the assumption $M_T = [M^{3+}]$ is not generally tenable when YREE solution speciation is controlled by an additional variable, like P_{CO_2} (Quinn et al., 2006a,b). It must also be borne in mind that the constants A_n are composite, conditional, and have limited thermodynamic significance.

4. Results and discussion

4.1. Regression of the distribution coefficients as a function of pH

Distribution coefficients, ${}_{i}K_{Fe}$, were determined as a function of pH in the range 3.9–8.4 (0.5 M NaCl, T = 25 °C). The lower limit is imposed by HFO dissolution, which occurs around pH 3.5. Throughout our experiments, the load factor does not exceed ~10^{-2} so that even moderate co-precipitation of YREEs would not transmute the HFO surface. Benjamin and Leckie (1981) moreover stated that "Coprecipitation and adsorption studies are directly comparable […] since the two processes are indistinguishable with respect to both kinetic and equilibrium behavior of metal ion partitioning in aqueous suspensions of [HFO]." No YREE were present in the HFO-bound fraction ($[MS_i]_T$) at pH 3.9 (supplementary data, Table S.2), where HFO precipitation is virtually complete, indicating that co-precipitation did not occur.

Separation of the YREEs into 'dissolved' (M_T) and HFO-bound fractions was achieved by membrane filtration. Imperfect retention of HFO, being highly colloidal when newly precipitated, may cause the

ratio $[MS_i]_T/M_T$ in Eq. (12), and consequently the value of ${}_iK_{Fe}$, to be underestimated. To gauge the magnitude of this artifact, an ancillary experiment was done in which any HFO colloids were removed from the dissolved fraction by stepwise ultrafiltration to 3 kDa MWCO. The test revealed that colloid-bound YREEs retained at 3 kDa MWCO constitute no more than 3% of the <0.22 μm fraction, falling within the analytical uncertainty. Gammons et al. (2005a) found that dissolved Fe (<0.1 μm) in a Montana mountain stream affected by acid mine drainage contained no more than 5% colloids larger than 10 kDa MWCO. Dissolved YREE concentrations, $[M]_{diss}$, are thus properly defined as the part of $[M]_{init}$ that passes a 0.22 μm filter and ${}_iK_{Fe}$ was calculated from Eq. (1). Results are listed in the supplementary data (Tables S.1–S.2).

In Fig. 1, log ${}_iK_{Fe}$ values are plotted as a function of pH for four representative YREEs and compared with data of Quinn et al. (2006a) at low ionic strength (~0.025 M NH_4Cl). Although Eq. (24) is a polynomial in $[H^+]$, on these double-logarithmic plots (log ${}_iK_{Fe}$ vs. pH = −log $[H^+]$) the data appear to follow straight lines. Linear regressions were performed to determine their slopes, representing the number of protons released per YREE cation sorbed, averaged over the experimental pH range. At low ionic strength that ratio is close to 1.5 for all YREEs. In 0.5 M NaCl the slopes are clearly lower and more variable too, ranging from 0.66 for La to 0.85 for Lu. Data deviating from the linear trends near our upper pH limit, which exceeds that of Quinn et al. (2006a) by more than one unit, were omitted from the regressions (Fig. 1). These points were initially regarded with caution since progressive hydrolysis above pH 8 might have saturated the solution, specifically with respect to hydroxides of the heavy REEs for which the non-linearity appears strongest. Precipitation could have transferred dissolved YREEs to the solid phase by an irreversible process unaccounted for in the model, causing calculated ${}_iK_{Fe}$ to be overestimated.

In Fig. 2, the same data are shown for La and Lu only. Quinn et al. (2006a) were able to fit all their results with Eq. (13), requiring two terms in the numerator with stability constants ${}_3\beta_1$ and ${}_3\beta_2$ (Eq. (9a)) for ${}_sK_2 \sim 0$. They obtained excellent fits ($r^2 \geq 0.96$) over the entire pH range with log ${}_sK_1 = 4.76$ (we found a slightly higher value of log ${}_sK_1 = 4.83$, using an improved optimization procedure). Taken together, their observations signify that few negatively charged groups are present on the HFO surface under these conditions and that YREEs do not associate with positively charged groups, bonding exclusively to the neutral groups by forming either a monodentate species with release of one proton, or a bidentate species with release of two protons. It could not be determined if the bidentate species were of a mononuclear (edge-sharing) type as in reaction (8a), or of a binuclear (corner-sharing) type as in reaction (18).

Early attempts to fit our data with Eq. (13) were not satisfactory. In view of enhanced HFO deprotonation at elevated ionic strength (Dzombak and Morel, 1990) and the possible influence of YREE solution complexation with Cl^- and OH^-, non-linear regressions were performed with the extended model of Eq. (25). Good preliminary fits were obtained with ${}_sK_1 \sim 0$ and $A_0 \sim 0$, converting Eq. (24) to the final model equation:

$$ {}_iK_{Fe} = \frac{A_1[H^+]^{-1} + A_2[H^+]^{-2} + A_3[H^+]^{-3}}{1 + {}_sK_2[H^+]^{-1}} \tag{26}$$

The equilibrium constant ${}_sK_2$ is an HFO surface property and should not depend on the sorbate element, yet regressions with ${}_sK_2$ as an adjustable parameter gave slightly different values for each YREE. A thorough analysis of these fits revealed that this is a statistical artifact, jointly caused by the inevitable correlation of adjustable parameters and raising the degrees of freedom in the model, having no physicochemical

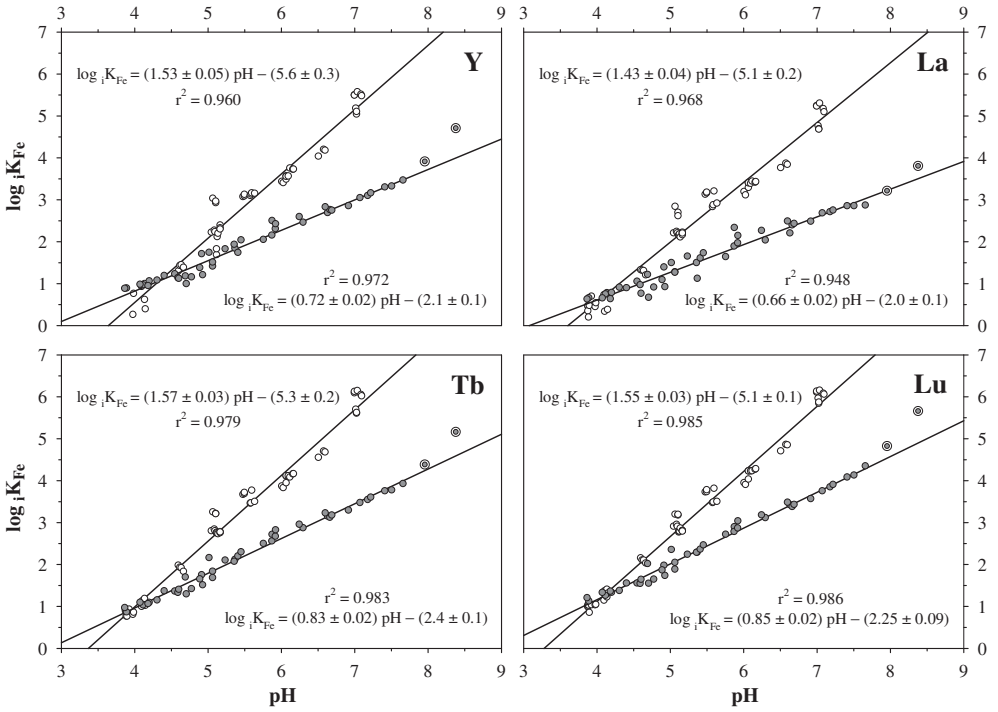

Fig. 1. Distribution coefficients, log ${}_iK_{Fe}$, for sorption of Y, La, Tb, and Lu on HFO as a function of solution pH. Open symbols are results from Quinn et al. (2006a) at low ionic strength (~0.025 M NH_4Cl). Closed symbols are results from this work (0.5 M NaCl). Data at the two highest pH values (ringed symbols) were omitted from the linear regressions (see text). The slope of each line equals the number of protons released per YREE cation sorbed, averaged over the experimental pH range.

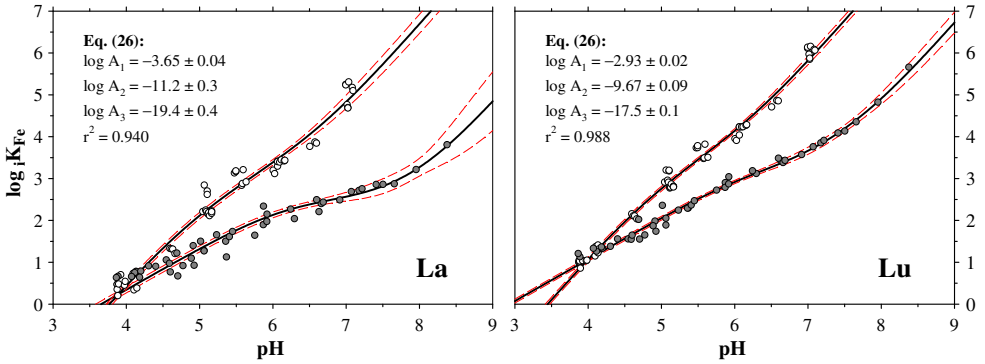

Fig. 2. Regressions of log $_iK_{Fe}$ vs. pH using the non-electrostatic surface complexation model (Eq. (26)). Listed best-fit parameters refer to the regressions of data from this work (closed symbols) where $_sK_1 = 0$ and log $_sK_2 = -6.16$, the optimized value for all YREEs (see also Table 2). Note the excellent fits of all data, including those omitted from the linear regressions in Fig. 1. Regressions of the low ionic strength data (open symbols) were performed using the same model with log $_sK_1 = 4.83$ and $_sK_2 = 0$. An improved procedure for optimizing $_sK_1$ and $_sK_2$ yielded a value of log $_sK_1$ slightly higher than the one reported by Quinn et al. (2006a). Dashed red curves are 95% confidence intervals.

meaning. A series of regressions was thus performed for all YREEs wherein log $_sK_2$ was fixed at values between −5.7 and −6.7 going up in 0.1-unit steps, and then between −6.13 and −6.19 going up in 0.01-unit steps. Adding the residual sums of squares of individual regressions after every step, a minimum was found for log $_sK_2 = -6.16$. Final regressions were performed with log $_sK_2$ fixed at this optimum value to determine A_1–A_3 for each YREE. The results are summarized in Table 2 and plotted in Fig. 3. It should be stressed that none of the patterns exhibit any Ce anomalies that could be construed as oxidation on the HFO surface.

Excellent fits were obtained for all YREEs ($r^2 \geq 0.94$; Fig. 2), including points omitted from the linear regressions in Fig. 1. The fact that the model accurately predicts this conspicuous 'non-linearity' confirms that it is caused by sorption of YREE–hydroxide complexes and not $M(OH)_3$ precipitation. A simple solubility argument supports this conclusion. The solubility product of the least soluble YREE hydroxide (Lu) is about $10^{-23.7}$ M^4 in non-complexing medium (0.1 M $NaClO_4$); we will use this as a worst case value, since the solubility of YREE hydroxides increases with ionic strength (Diakonov et al., 1998). It can then be estimated that Lu remains undersaturated with respect to hydroxide precipitation by at least a factor of 5 at the highest pH (8.4) attained in our experiments. YREE solubility rapidly diminishes with increasing pH, yet this effect is opposed by enhanced solution complexation and cumulative sorption, which conspire to keep free-ion concentrations low. Regressions were also done with

Table 2
Best-fit parameters for regressions of log $_iK_{Fe}$ vs. pH (supplementary data, Tables S.1–S.2) using the non-electrostatic surface complexation model (Eq. (26)) with $_sK_1 = 0$ and log $_sK_2 = -6.16$. The composite, conditional stability constants, A_1–A_3, represent YREE bonding to different forms of the hydroxyl functional group releasing one, two, or three protons, respectively (see text for details). Uncertainties are one standard error of the mean.

M^{3+}	log A_1	log A_2	log A_3	log(A_1/A_2)	log(A_2/A_3)
Y	−3.38 ± 0.03	−10.7 ± 0.2	−18.3 ± 0.2	7.28	7.68
La	−3.65 ± 0.04	−11.2 ± 0.3	−19.4 ± 0.4	7.52	8.20
Ce	−3.24 ± 0.03	−10.6 ± 0.2	−18.7 ± 0.3	7.40	8.08
Pr	−3.14 ± 0.02	−10.3 ± 0.1	−18.6 ± 0.2	7.20	8.26
Nd	−3.07 ± 0.02	−10.3 ± 0.1	−18.5 ± 0.2	7.24	8.14
Pm	–	–	–	–	–
Sm	−2.98 ± 0.02	−10.04 ± 0.09	−18.1 ± 0.2	7.06	8.06
Eu	−3.03 ± 0.02	−10.02 ± 0.08	−18.1 ± 0.2	6.99	8.07
Gd	−3.16 ± 0.02	−10.2 ± 0.1	−18.2 ± 0.2	7.07	7.98
Tb	−3.14 ± 0.02	−9.97 ± 0.08	−18.0 ± 0.2	6.83	8.04
Dy	−3.12 ± 0.02	−9.89 ± 0.08	−17.9 ± 0.2	6.77	8.05
Ho	−3.13 ± 0.02	−9.97 ± 0.09	−17.9 ± 0.2	6.84	7.96
Er	−3.08 ± 0.02	−9.91 ± 0.09	−17.8 ± 0.1	6.84	7.91
Tm	−3.02 ± 0.02	−9.74 ± 0.08	−17.6 ± 0.1	6.72	7.91
Yb	−2.94 ± 0.02	−9.59 ± 0.07	−17.5 ± 0.1	6.65	7.89
Lu	−2.93 ± 0.02	−9.67 ± 0.09	−17.5 ± 0.1	6.75	7.78

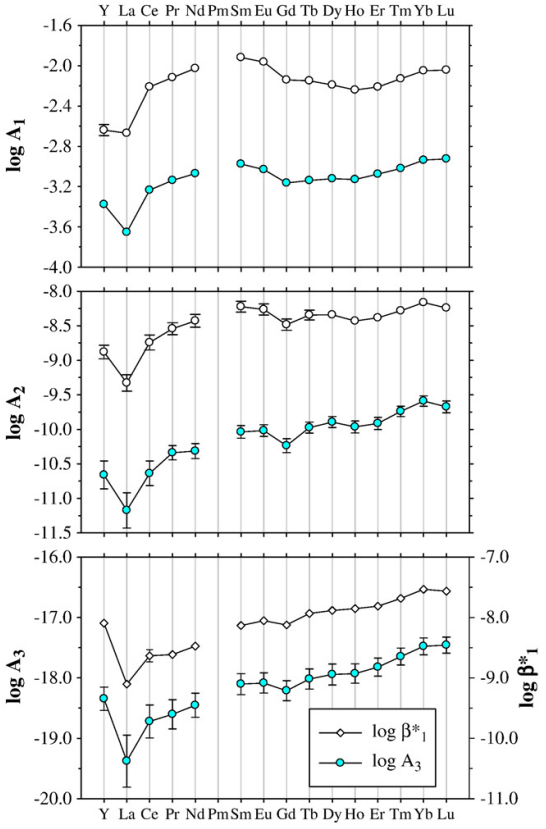

Fig. 3. Comparison of best-fit parameters for regressions of log $_iK_{Fe}$ vs. pH (Eq. (26)) in ~0.025 M NH_4Cl (recalculated with log $_sK_1 = 4.83$; open circles) and in 0.5 M NaCl (Table 2; closed cyan circles). While corresponding constants have different absolute values due to their composite nature as well as to ionic strength effects, their relative values (i.e., shape of the pattern) are very similar. Quinn et al. (2006a) could not determine log A_3, which is compared instead with the first hydrolysis constant, log β_1^* (Klungness and Byrne, 2000). Error bars not shown are within the size of the symbol.

$_iK_{Fe}$ derived from free-ion concentrations i.e., corrected for YREE solution complexation (results not shown). These produced substantially worse fits, markedly underestimating $_iK_{Fe}$ at elevated pH, proof that sorption of YREE–hydroxide complexes (and probably YREE–chloride) is important and must be explicitly incorporated in the model.

Fig. 4 displays the ratio of model-predicted and measured log $_iK_{Fe}$ values for Eu, calculated with the best-fit parameters in Table 2, as a function of pH. The distribution is symmetrical around unity and generally narrow, but more scattered at pH<5, where YREE sorption becomes very weak ($[M]_{diss} \approx [M]_{init}$), leading to error magnification in Eq. (1). Precision was improved by increasing $[Fe]_T$ tenfold in low-pH experiments and the excellent fits in Fig. 2 show that, as expected, log $_iK_{Fe}$ is not altered by the lower load factor. Furthermore, 95% confidence intervals are not discernibly broadened, despite the greater analytical uncertainty.

4.2. Choice of sorption model and interpretation of the best-fit parameters

The deliberate choice of a non-electrostatic model, in which stability constants are not corrected for HFO surface charge and interactions of the functional groups with electrolyte ions are not explicitly included, has distinct benefits as well as certain drawbacks. Although it makes the stability constants conditional, preventing their rigorous thermodynamic interpretation, it also alleviates the need for a detailed characterization of surface properties that may be difficult to quantify for amorphous and/or colloidal substrates like HFO. This approach is helpful when dealing with natural composite materials and was used successfully by Tang and Johannesson (2005) and by Tertre et al. (2008) in their studies of YREE sorption on quartz sand and basalt powder. Non-electrostatic models are especially appropriate for highly polarizing cations such as the YREEs, whose sorption on metal hydroxides is mediated predominantly through stable inner-sphere complexes (Tertre et al., 2008) and weakly dependent on ionic strength (Quinn et al., 2006a). Marmier and Fromage (1999) showed that diffuse-layer and constant-capacitance models of the solid–solution interface were not inherently superior to non-electrostatic models for describing La sorption on hematite in terms of proton release. Sverjensky (2005) pointed out that high dielectric constant solids (e.g., Ti oxide) have the expected greater affinity for smaller alkali ions ($Li^+ \gg Cs^+$), whereas the order is reversed ($Cs^+ \gg Li^+$) for low dielectric constant solids (e.g., Si oxide) which are more sensitive to the energetic cost of ion dehydration. These trends are exactly opposite for the divalent alkaline earth ions (Sverjensky, 2006), yet either way the surface charge of solids with intermediate dielectric constants, including HFO, should be largely independent of electrolyte composition.

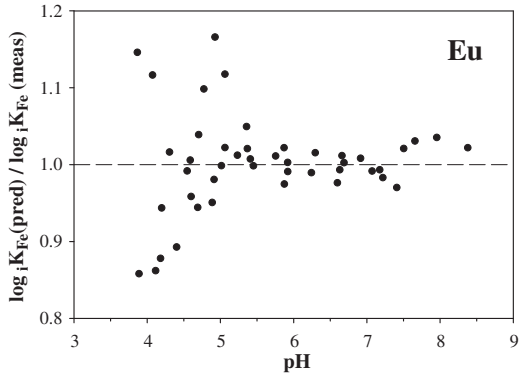

Fig. 4. Ratios of predicted and measured values of log $_iK_{Fe}$ for Eu, shown as a function of pH. Predicted values were calculated using Eq. (26) with the best-fit parameters from Table 2. Ratios are randomly distributed around unity (mean = 1.002), signaling the validity of the model. Increased scatter at low pH is caused by diminished YREE sorption, leading to error magnification as $[M]_{diss}$ approaches $[M]_{init}$ in the numerator of Eq. (1).

Our interpretation of the model results is focused on the mechanism, in other words what YREE solution species are sorbed and what surface complexes they form. The non-electrostatic model tells us much in this regard. First of all, knowledge about the state of the HFO surface may be gleaned from the equilibrium constants $_sK_1$ and $_sK_2$. Quinn et al. (2006a) found that $_sK_2 \sim 0$ at low ionic strength, suggesting that negatively charged groups were absent within their experimental pH window (4–7). The (reoptimized) value of log $_sK_1 = 4.83$ indicates a transition from neutral to positively charged groups near the low end of this range and the assumption that YREE cations do not associate with the latter explains the substantially decreased sorption there. While log $_sK_1$ was not adjusted for surface charge, this correction is minor in dilute solutions and its value is indeed close to the intrinsic value ($\log K_1^0 = 5.1$) reported by Sverjensky (2005). The corresponding value of $\log K_2^0$ (-10.7, when written as a deprotonation reaction) dictates that negatively charged groups will not occur below pH 7 and explains why Quinn et al. (2006a) could not resolve the value of $_sK_2$. In 0.5 M NaCl $_sK_1 \sim 0$, suggesting that no positively charged groups are formed above pH 3.9. This eliminates reaction (20), consistent with the finding that $A_0 = 0$, but it does not preclude sorption of YREE–chloride complexes on neutral or negatively charged groups, through ligand exchange (reaction (19a)) or otherwise (reaction (19b)). The value of log $_sK_2 = -6.16$ is similarly offset from its intrinsic value, reflecting the emergence of negatively charged groups near the high end of our pH range due to proton displacement by Na^+.

Secondly, knowing the state of the HFO surface, some inferences can be made about the types of surface complexes formed by the YREEs. Patterns of A_1 and A_2 are compared in Fig. 3 with those of the reoptimized parameters of Quinn et al. (2006a). In the extended model (Eq. (26)), parameter A_1, besides YREE bonding with neutral groups releasing one proton, represents YREE bonding with negatively charged groups releasing zero protons. Parameter A_2, besides YREE bonding with neutral groups releasing two protons, analogously represents YREE bonding with negatively charged groups releasing one proton. Despite the presence of both neutral and negatively charged groups in 0.5 M NaCl, each interacting with the YREEs, sorption is always weaker than at low ionic strength (Figs. 1 and 2). This can be interpreted as increased competition from Na^+ for the hydroxyl functional groups or its influence on HFO surface charge. Since neither is accounted for in the non-electrostatic model, this has a suppressive effect on values of the conditional stability constants $_3\beta_n$ and $_4\beta_n$, ostensibly lowering the composite stability constants A_1 and A_2 with respect to the low ionic strength solutions without causing additional YREE fractionation (Fig. 3).

Parameter A_3 in the extended model represents YREE bonding with negatively charged groups releasing two protons. As in the case of Quinn et al. (2006a), the model cannot decide whether such bidentate surface complexes are formed with two hydroxyls on a single Fe atom or with two single hydroxyls on adjacent Fe atoms. The coordination of several heavy REEs (HREEs) on HFO was recently investigated using EXAFS by Ohta et al. (2009a,b). These authors found a primary O shell with M–O distances close to those of free YREE ions in aqueous solution (Ohta et al., 2008) and O coordination numbers varying from slightly below 9 for the light REEs (LREEs) to slightly below 8 for the HREEs. In addition they found a secondary Fe shell with a coordination number consistent with 1 for the middle REEs (MREEs) and Y, and with 2 for the HREEs. No distinct Fe shell was found for the LREEs. Ohta et al. (2009a,b) interpret these observations

as the formation of mono- and bidentate Fe–O–M surface complexes, with a possible progression from corner-sharing bidentate complexes for the MREEs to edge-sharing for the HREEs. Dardenne et al. (2001) employed spectroscopic techniques to study Lu sorption on aged HFO over a range of pH and found exclusively monodentate complexes at low pH with a gradual transition to edge-sharing bidentate complexes at pH>5. Manceau et al. (1992) proposed that another trivalent element, Cr^{3+}, also sorbs on HFO via a combination of corner- and edge-sharing bidentate surface complexes.

The non-electrostatic model yields conditional stability constants that apply to a small domain of conditions, but this does not affect YREE fractionation (see also Section 4.3) hence the shape of the ${}_3\beta_1$ and ${}_3\beta_2$ patterns reported by Quinn et al. (2006a) is nearly identical to that of the A_1 and A_2 patterns, respectively (Fig. 3). The A_1 pattern has a single maximum around Sm and relatively little structure for the HREE (Gd–Lu). The A_2 pattern has two additional maxima around Dy and Yb that might be designated 'tetrads' (Ohta and Kawabe, 2000b). The A_3 pattern, which could not be determined by Quinn et al. (2006a) in the absence of negatively charged groups, is different from A_1 and A_2, having both a steeper slope and looking more 'stretched'. Actually, its shape is reminiscent of the first YREE hydrolysis constant, β_1^* (Eq. (16)), a notion supported by linear free-energy relations (LFERs) between β_1^* and each of the parameters A_1–A_3 (Fig. 5). It is not surprising that these are rather poor for A_1 ($r^2 = 0.55$), better for A_2 ($r^2 = 0.83$) and quite good for A_3 ($r^2 = 0.97$); one should expect YREE complexation on a surface dominated by negative hydroxyl groups to resemble complexation with aqueous hydroxide anions (Erel and Morgan, 1991). Quinn et al. (2004), who compared YREE sorption on HFO and on amorphous hydroxides of the Group 13 elements Al, Ga, and In, presented LFERs between β_1^* and ${}_i K_{Fe}$ at a single intermediate pH (~6.1). They found an excellent LFER for Al, slightly worse for In and then Ga, and much worse for Fe. Whereas this trend does not match atomic numbers or ionic radii (Shannon, 1976) it is interesting to note that it is in qualitative agreement with the order of the first hydrolysis constants for these elements: Al (−4.97) < In (−4.0) < Ga (−2.6) < Fe (−2.16) (Baes and Mesmer, 1981).

4.3. Skill of the non-electrostatic model: comparisons with published data

The ability of our non-electrostatic model to reproduce measured data (i.e., its skill) was evaluated two different ways. In Fig. 6, log ${}_i K_{Fe}$ patterns obtained in the present experiments at arbitrary low, intermediate, and high pH values are compared with model predictions derived from Eq. (26), using the best-fit parameters in Table 2 and $\log {}_S K_2 = -6.16$. It can be seen that the model reproduces the data very

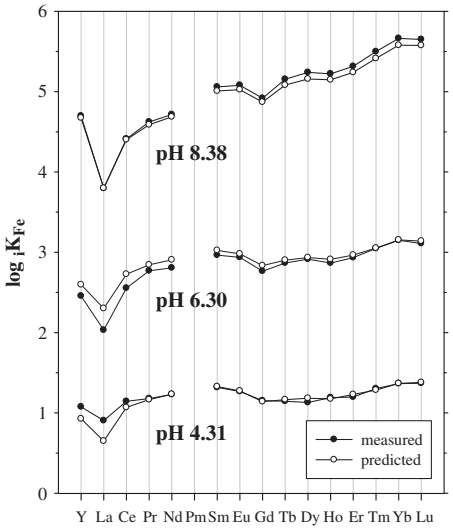

Fig. 6. Comparison of predicted and measured patterns of log ${}_i K_{Fe}$ for three values of pH. Predicted values were calculated using Eq. (26) with the best-fit parameters from Table 2. The model accurately reproduces both relative values (i.e., shape of the pattern) and absolute values of log ${}_i K_{Fe}$.

well in terms of both absolute values and relative behavior (YREE fractionation) manifested by the shape of the patterns. Deviations are largest for Y and the LREEs (La–Nd) at low and intermediate pH, where sorption is weakest and the data more scattered (Figs. 2 and 4). The shape of the log ${}_i K_{Fe}$ patterns clearly changes with increasing pH, illustrating that YREE sorption on HFO at low pH is mediated by reactions associated with parameter A_1, shifting at higher pH to reactions associated with parameter A_2 and ultimately A_3 (*cf.* Fig. 3). The same progression was observed by Quinn et al. (2006b). As the HFO surface becomes negatively charged, reactions with deprotonated hydroxyl groups begin to dominate. Since these release on average one less proton per YREE cation sorbed than the corresponding neutral groups, sorption in 0.5 M NaCl is less pH dependent than at low ionic strength. It may seem odd that the log ${}_i K_{Fe}$ vs. pH curves are so linear (Fig. 1) when the sorption mechanism shifts with increasing pH to reactions that release fewer protons (Eq. (26)); that is because its effect is balanced by concomitant deprotonation of the HFO surface. For example, in Eq. (13), used by Quinn et al. (2006a), the numerator and

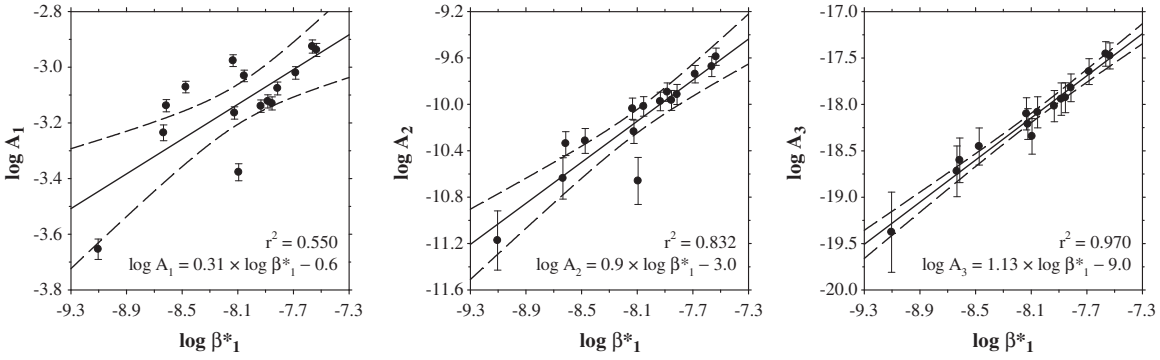

Fig. 5. Linear free-energy relations (LFERs) between the best-fit parameters (Table 2) and the first hydrolysis constant (Klungness and Byrne, 2000). Each point represents a single element. Going from A_1 to A_3 the quality of the LFERs greatly improves, suggesting that YREE complexation with hydroxyl functional groups increasingly resembles YREE hydrolysis in solution as the HFO surface becomes more negatively charged. Dashed curves are 95% confidence intervals.

denominator are both polynomials in $[H^+]$. At low pH, the first term in the numerator is largest and its order is 1. The two terms in the denominator are comparable in size and their mean order is $(-1+0)/2=-0.5$, making the order of the overall equation: $1-(-0.5)=1.5$. At high pH, the first term in the denominator is largest and its order is 0. The two terms in the numerator are comparable in size and their mean order is $(1+2)/2=1.5$, again making the order of the overall equation: $1.5-0=1.5$. The average slope of the curves is thus 1.5 across the experimental pH range, although the transitions occur at slightly different pH in the numerator and denominator, leading to subtle excursions first above and then below the regression lines (Fig. 1). The fact that slopes in 0.5 M NaCl are not a full unit lower than at low ionic strength is probably due to the composite nature of parameters A_1–A_3 and the differential influence of ionic strength on their constituent stability constants, ${}_3\beta_n$ and ${}_4\beta_n$. This may also explain why the slopes at high ionic strength are more variable.

A faithful reproduction of data from the literature constitutes an even better test of model skill. While the conditional nature of our stability constants would render such an exercise rather meaningless for a single element, the unique attributes of the lanthanide series allow examination of whole distribution coefficient patterns, whose shape (i.e., YREE fractionation) is governed by comparative characteristics of the sorbate elements and does not depend on sorbent properties that are linked to its mode of preparation, like crystallinity or specific surface area. A strong case might be made by vetting the model with field experiments, yet extant data are less than ideal because (i) they involve freshwaters; (ii) the data are in a format that does not allow conversion to ${}_iK_{Fe}$ values; or (iii) the mineralogy of the precipitates is very different from HFO. Bozau et al. (2008) studied REE sorption on ferric oxides by exposing Fe(II)-rich anoxic lake water to air for a period of up to 40 weeks. Unfortunately, premature HFO precipitation occurred during sample collection, preventing the authors from measuring total REE concentrations and precluding the calculation of ${}_iK_{Fe}$ values. Gammons et al. (2005b) determined REE distribution coefficients for ferric oxides in an acidic mountain stream, but these were not normalized to particulate Fe concentrations which varied as a result of light- or temperature-driven diel cycles. This system may not have been truly in equilibrium at any time. Verplanck et al. (2004) reported model-dependent YREE distribution coefficients for several acid mine effluents, using an LFER that Quinn et al. (2004) have shown to be invalid at pH<7. Their particles displayed a complex mineralogy involving hydrated Fe(II,III) sulfates e.g., jarosite, schwertmannite, and copiapite.

The next best strategy is to compare the model with laboratory experiments conducted under similar conditions. We are aware of only two such studies: De Carlo et al. (1998) used $NaNO_3$ solutions of 0.1–0.7 M as well as seawater, and Ohta and Kawabe (2001) used 0.5 M NaCl, as we did. Both groups have alternative definitions of the distribution coefficient. The former list the percentage sorbed (i.e., $M_T/[M]_{init}\times 100$), while the others expressed distribution coefficients in terms of mole fractions (i.e., $K=\{M\}/(M_T\times(\{Fe\}+\Sigma\{M\}))$ where the sum is over all YREEs). Their results were converted accordingly to log ${}_iK_{Fe}$. Selected patterns from both datasets are shown in Fig. 7 together with model predictions calculated at corresponding pH values. In order to emphasize the congruence of the patterns, the original model predictions were vertically transposed by an amount that optimizes the overlap with measured patterns for all YREEs simultaneously. The model reproduces the patterns of Ohta and Kawabe (2001) extremely well, nearly perfectly at pH 5.78. The patterns of De Carlo et al. (1998) were chosen near the middle of the sorption edge to avoid insufficient or excessive sorption. Despite the noisier data, probably due to the use of a less sensitive analytical technique (ICP-AES), agreement is very encouraging considering that these experiments were done in different solutions.

The model excels at predicting YREE fractionation caused by sorption on HFO at high ionic strength, yet it is clear that absolute ${}_iK_{Fe}$ values are off the mark. The results of Ohta and Kawabe (2001) are overestimated by about 0.2 log units at pH 5.78, but underestimated by about one log unit at pH 6.58. The $NaNO_3$ pattern of De Carlo et al. (1998) is underestimated by about 0.5 log units and the seawater pattern by about 1.5 log units. These discrepancies are not unexpected and can be attributed to the use of a non-electrostatic model, which does not account for surface charge and other properties of sorbent and electrolyte. Both groups synthesized their HFO particles externally, following dissimilar protocols, whereas our particles were precipitated within the experimental solution. Ohta and Kawabe (2001) made a direct comparison between distribution coefficients derived from externally prepared and 'co-precipitated' particles and found no appreciable difference. The main source of the divergence between measured and modeled values is presumably that we normalized ${}_iK_{Fe}$ to the total dissolved Fe concentration, which may significantly exceed the free hydroxyl site density. However, there are many factors that can contribute to the offset, such as medium effects (YREE speciation) and, for seawater, the presence of competing cations (specifically Ca^{2+} and Mg^{2+}). Regardless, non-electrostatic models can yield fundamental insights about reaction mechanisms, kinetics, and the state of the sorbent surface as a function of pH and ionic strength, even in intricate multi-phase systems (Montavon et al., 2004). They provide a powerful alternative to a thermodynamically rigorous treatment, as long as it is recognized that their utility is restricted to the YREEs and other series of chemical analogs, like the alkaline earths, and generally does not pertain to single elements.

5. Summary and conclusions

Hydrated Fe oxides are a ubiquitous particulate and sedimentary phase in aqueous systems encompassing rivers (Verplanck et al., 2004; Gammons et al., 2005a), lakes (Hamilton-Taylor et al., 2005; Bozau et al., 2008), estuaries (Marmolejo-Rodriguez et al., 2007), aquifers (Charette and Sholkovitz, 2002), and oceans (Olivarez and Owen, 1989; Koschinsky and Hein, 2003). It is established, as exemplified by our observations, that these minerals are quite reactive with regard to dissolved trace metals. Quinn et al. (2006a) studied YREE sorption on HFO under conditions prevalent in freshwaters. They found that the solid/solution distribution coefficients depend strongly on pH, but only modestly on ionic strength and temperature (Quinn et al., 2007). A non-electrostatic sorption model was developed, starting from known chemical properties of the HFO surface and plausible interactions between free YREE ions and hydroxyl functional groups. Model fits to sorption data relevant for freshwaters (pH 4–7) revealed that negatively charged groups are not abundant on the HFO surface and that the YREEs do not associate with positively charged but primarily with neutral groups, forming mono- or bidentate surface complexes via single or double proton exchange. Quinn et al. (2006b) demonstrated that the model can be extended to describe enhanced YREE sorption on HFO in the presence of CO_2 due to the formation of ternary Fe–O–MCO_3 surface complexes. These interactions must be explicitly included in the model if the ligand concentration (P_{CO_2}) is variable.

In the present work, we modified this framework (without carbonate terms) to describe YREE sorption under conditions more relevant for seawater. Our new data imply a transition of the HFO surface from containing mainly neutral to containing more negatively charged groups. These interact with the YREEs by forming the same mono- or bidentate surface complexes as before, yet releasing fewer protons on average. Compounding the effect of ionic strength on stability constants, YREE sorption thus becomes less pH dependent as well as weaker. Consequently, HFO is a more reactive sorbent in freshwaters than in seawater. It also appears that chloride and hydroxide, like carbonate, give rise to ternary YREE surface complexes. No extra terms or constants were required to accommodate these species because the Cl^- concentration remained constant and

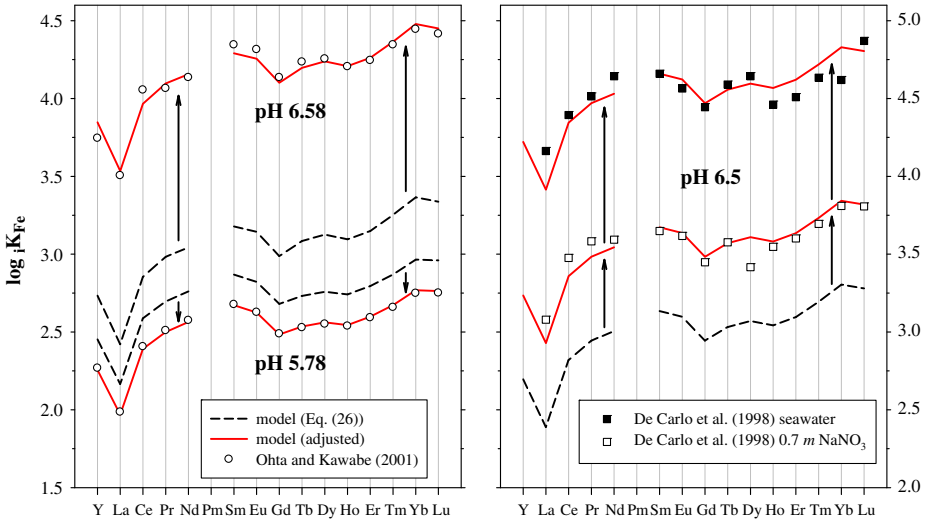

Fig. 7. Comparison of model predictions and selected data from the literature (De Carlo et al., 1998; Ohta and Kawabe, 2001), converted to our definition of log $_iK_{Fe}$. Model predictions were calculated at corresponding pH values, using Eq. (26) with the best-fit parameters from Table 2. The adjusted patterns (solid red curves) were vertically transposed (along the arrows) to optimize overlap with the measured patterns by minimizing the absolute deviation between them, summed over all YREEs. The experiments of De Carlo et al. (1998) were performed in solutions of different composition but equal ionic strength.

OH^- concentration is a direct function of solution pH, which is already the main variable. Ce anomalies never materialized in our prior or present experiments at any pH, either at low or high ionic strength.

The potential of the non-electrostatic model lies in its versatility, enabling it to describe YREE sorption on HFO over wide ranges of pH (3.9–8.4), temperature (10–40 °C), ionic strength (0–0.5 M), and solution speciation (CO_3^{2-}, OH^- and Cl^-), using only two protonation constants for HFO functional groups and three composite stability constants for YREE surface complexes. Although these constants are conditional and have limited thermodynamic meaning, the equation is derived from first principles and can be readily adapted for different conditions, metals, and sorbents. It may therefore be feasible to account for additional processes that play a role in metal sorption, for example competition among metals or among multiple kinds of functional group. The current model does a good job of reproducing YREE fractionation patterns, however its comparatively poor prediction of absolute $_iK_{Fe}$ values in seawater (see Fig. 7 and Quinn et al., 2004) may be due to substantial competition from Ca^{2+} and Mg^{2+}, an hypothesis that we plan to test in future experiments. Notwithstanding its conceptual simplicity and its reliance on a sole variable (pH), the basic algorithm is capable of conveying ample information about the state of the HFO surface and the mechanism whereby various metals bond to it. Some of these results have been verified with advanced spectroscopic techniques (Ohta et al., 2009a, b). Our straightforward approach may lend itself well to the investigation of other environmentally important substrates like Mn oxides, clays, and even organic matter.

Acknowledgments

Acknowledgment is made to the Donors of the American Chemical Society Petroleum Research Fund for support of this research (49028-DNI2). The M.Sc. project of KSM was made possible in part by a CBL Graduate Education Committee fellowship. Additional funding was provided to JS by NSF (OCE-0745881). We thank Kelly Quinn for lively discussions and for sharing her data. Insightful comments from Associate Editor David Turner and two anonymous reviewers are greatly appreciated. This is UMCES publication #4443.

Appendix A. Supplementary data

Supplementary data to this article can be found online at doi:10.1016/j.marchem.2010.09.003.

References

Aagaard, P., 1974. Rare earth elements adsorption on clay minerals. Bull. Gr. Franç. Argil. XXVI, 193–199.
Baes Jr., C.F., Mesmer, R.E., 1981. The thermodynamics of cation hydrolysis. Am. J. Sci. 281, 935–962.
Bau, M., 1999. Scavenging of dissolved yttrium and rare earths by precipitating iron oxyhydroxide: experimental evidence for Ce oxidation, Y–Ho fractionation, and lanthanide tetrad effect. Geochim. Cosmochim. Acta 63, 67–77.
Bau, M., Koschinsky, A., 2009. Oxidative scavenging of cerium on hydrous Fe oxide: evidence from the distribution of rare earth elements and yttrium between Fe oxides and Mn oxides in hydrogenetic ferromanganese crusts. Geochem. J. 43, 37–47.
Bau, M., Dulski, P., Möller, P., 1995. Yttrium and holmium in South Pacific seawater: vertical distribution and possible fractionation mechanisms. Chem. Erde 55, 1–15.
Benjamin, M.M., Leckie, J.O., 1981. Multiple-site adsorption of Cd, Cu, Zn, and Pb on amorphous iron oxyhydroxide. J. Colloid Interf. Sci. 79, 209–221.
Borkowski, M., Siekierski, S., 1992. Factors affecting the position of Y and actinides(III) with respect to lanthanides in the NH_4SCN–Adogen-464SCN extraction system. Radiochim. Acta 56, 31–35.
Bozau, E., Göttlicher, J., Stärk, H.-J., 2008. Rare earth element fractionation during the precipitation and crystallisation of hydrous ferric oxides from anoxic lake water. Appl. Geochem. 23, 3473–3486.
Byrne, R.H., Kim, K.-H., 1990. Rare earth element scavenging in seawater. Geochim. Cosmochim. Acta 54, 2645–2656.
Byrne, R.H., Sholkovitz, E.R., 1996. Marine chemistry and geochemistry of the lanthanides. In: Gschneidner Jr., K.A., Eyring, L. (Eds.), Handbook on the Physics and Chemistry of Rare Earths, vol. 23. Elsevier, Amsterdam, pp. 497–593.
Charette, M.A., Sholkovitz, E.R., 2002. Oxidative precipitation of groundwater-derived ferrous iron in the subterranean estuary of a coastal bay. Geophys. Res. Lett. 29, 1444. doi: 10.1029/2002GL014512.
Chester, R., 1990. Marine Geochemistry. Unwyn Hyman, London, UK, p. 463. Table 13.4.
Coppin, F., Berger, G., Bauer, A., Castet, S., Loubet, M., 2002. Sorption of lanthanides on smectite and kaolinite. Chem. Geol. 182, 57–68.
Dardenne, K., Schäfer, T., Denecke, M.A., Rothe, J., Kim, J.I., 2001. Identification and characterization of sorbed lutetium species on 2-line ferrihydrite by sorption data modeling, TRLFS and EXAFS. Radiochim. Acta 89, 469–479.
Davis, J.A., Leckie, J.O., 1978. Surface ionization and complexation at the oxide/water interface. II. Surface properties of amorphous iron oxyhydroxide and adsorption of metal ions. J. Colloid Interf. Sci. 67, 90–107.
Davranche, M., Pourret, O., Gruau, G., Dia, A., 2004. Impact of humate complexation on the adsorption of REE onto Fe oxyhydroxide. J. Colloid Interf. Sci. 277, 271–279.

Davranche, M., Pourret, O., Gruau, G., Dia, A., Le Coz-Bouhnik, M., 2005. Adsorption of REE(III)–humate complexes onto MnO_2: experimental evidence for cerium anomaly and lanthanide tetrad effect suppression. Geochim. Cosmochim. Acta 69, 4825–4835.
Davranche, M., Pourret, O., Gruau, G., Dia, A., Jin, D., Gaertner, D., 2008. Competitive binding of REE to humic acid and manganese oxide: impact of reaction kinetics on development of cerium anomaly and REE adsorption. Chem. Geol. 247, 154–170.
De Carlo, E.H., Wen, X.-Y., Irving, M., 1998. The influence of redox reactions on the uptake of dissolved Ce by suspended Fe and Mn oxide particles. Aquat. Geochem. 3, 357–389.
Diakonov, I.I., Ragnarsdottir, K.V., Tagirov, B.R., 1998. Standard thermodynamic properties and heat capacity equations of rare earth hydroxides: II. Ce(III)-, Pr-, Sm-, Eu(III)-, Gd-, Tb-, Dy-, Ho-, Er-, Tm-, Yb-, and Y-hydroxides. Comparison of thermochemical and solubility data. Chem. Geol. 151, 327–347.
Dzombak, D.A., Morel, F.M.M., 1990. Surface Complexation Modeling. Hydrous Ferric Oxide. John Wiley & Sons, New York, NY.
Erel, Y., Morgan, J.J., 1991. The effect of surface reactions on the relative abundances of trace metals in deep-ocean water. Geochim. Cosmochim. Acta 55, 1807–1813.
Gammons, C.H., Nimick, D.A., Parker, S.R., Cleasby, T.E., McCleskey, R.B., 2005a. Diel behavior of iron and other heavy metals in a mountain stream with acidic to neutral pH: Fisher Creek, Montana, USA. Geochim. Cosmochim. Acta 69, 2505–2516.
Gammons, C.H., Wood, S.A., Nimick, D.A., 2005b. Diel behavior of rare earth elements in a mountain stream with acidic to neutral pH. Geochim. Cosmochim. Acta 69, 3747–3758.
Ghose, S.K., Waychunas, G.A., Trainor, T.P., Eng, P.J., 2010. Hydrated goethite (α-FeOOH) (1 0 0) interface structure: ordered water and surface functional groups. Geochim. Cosmochim. Acta 74, 1943–1953.
Hamilton-Taylor, J., Smith, E.J., Davison, W., Sugiyama, M., 2005. Resolving and modeling the effects of Fe and Mn redox cycling on trace metal behavior in a seasonally anoxic lake. Geochim. Cosmochim. Acta 69, 1947–1960.
Kawabe, I., Ohta, A., Miura, N., 1999. Distribution coefficients of REE between Fe oxyhydroxide precipitates and NaCl solutions affected by REE-carbonate complexation. Geochem. J. 33, 181–197.
Klungness, G.D., Byrne, R.H., 2000. Comparative hydrolysis behavior of the rare earths and yttrium: the influence of temperature and ionic strength. Polyhedron 19, 99–107.
Koeppenkastrop, D., De Carlo, E.H., 1992. Sorption of rare-earth elements from seawater onto synthetic mineral particles: an experimental approach. Chem. Geol. 95, 251–263.
Koeppenkastrop, D., De Carlo, E.H., 1993. Uptake of rare earth elements from solution by metal oxides. Environ. Sci. Technol. 27, 1796–1802.
Koeppenkastrop, D., De Carlo, E.H., Roth, M., 1991. A method to investigate the interaction of rare earth elements in aqueous solution with metal oxides. J. Radioanal. Nucl. Chem. Art. 152, 337–346.
Koschinsky, A., Hein, J.R., 2003. Uptake of elements from seawater by ferromanganese crusts: solid-phase associations and seawater speciation. Mar. Geol. 198, 331–351.
Krauskopf, K.B., 1986. Thorium and rare-earth metals as analogs for actinide elements. Chem. Geol. 55, 323–335.
Liu, X., Millero, F.J., 1999. The solubility of iron hydroxide in sodium chloride solutions. Geochim. Cosmochim. Acta 63, 3487–3497.
Loder, T.C., Liss, P.S., 1985. Control by organic coatings of the surface charge of estuarine suspended particles. Limnol. Oceanogr. 30, 418–421.
Luo, Y.-R., Byrne, R.H., 2001. Yttrium and rare earth element complexation by chloride ions at 25 °C. J. Solut. Chem. 30, 837–845.
Luo, Y.-R., Byrne, R.H., 2004. Carbonate complexation of yttrium and the rare earth elements in natural waters. Geochim. Cosmochim. Acta 68, 691–699.
Manceau, A., Charlet, L., Boisset, M.C., Didier, B., Spadini, L., 1992. Sorption and speciation of heavy metals on hydrous Fe and Mn oxides. From microscopic to macroscopic. Appl. Clay Sci. 7, 201–223.
Marmier, N., Fromage, F., 1999. Comparing electrostatic and nonelectrostatic surface complexation modeling of the sorption of lanthanum on hematite. J. Colloid Interf. Sci. 212, 252–263.
Marmolejo-Rodriguez, A.J., Prego, R., Meyer-Willerer, A., Shumilin, E., Sapozhnikov, D., 2007. Rare earth elements in oxy-hydroxide rich sediments from the Marabasco River–Estuary System (pacific coast of Mexico). REE affinity with iron and aluminium. J. Geochem. Explor. 94, 43–51.
Montavon, G., Rabung, T., Geckeis, H., Grambow, B., 2004. Interaction of Eu(III)/Cm(III) with alumina-bound poly(acrylic acid): sorption, desorption, and spectroscopic studies. Environ. Sci. Technol. 38, 4312–4318.
Nozaki, Y., Zhang, J., Amakawa, H., 1997. The fractionation between Y and Ho in the marine environment. Earth Planet. Sci. Lett. 148, 329–340.
Ohta, A., Kawabe, I., 2000a. Rare earth element partitioning between Fe oxyhydroxide precipitates and aqueous NaCl solutions doped with $NaHCO_3$: determinations of rare earth element complexation constants with carbonate ions. Geochem. J. 34, 439–454.
Ohta, A., Kawabe, I., 2000b. Theoretical study of tetrad effects observed in REE distribution coefficients between marine Fe–Mn deposit and deep seawater, and in REE(III)–carbonate complexation constants. Geochem. J. 34, 455–473.
Ohta, A., Kawabe, I., 2001. REE(III) adsorption onto Mn dioxide (δ-MnO_2) and Fe oxyhydroxide: Ce(III) oxidation by δ-MnO_2. Geochim. Cosmochim. Acta 65, 695–703.
Ohta, A., Kagi, H., Tsuno, H., Nomura, M., Kawabe, I., 2008. Influence of multi-electron excitation on EXAFS spectroscopy of trivalent rare-earth ions and elucidation of change in hydration number through the series. Am. Mineral. 93, 1384–1392.
Ohta, A., Kagi, H., Nomura, M., Tsuno, H., Kawabe, I., 2009a. Coordination study of rare earth elements on Fe oxyhydroxide and Mn dioxides: part I. Influence of a multi-electron excitation on EXAFS analyses of La, Pr, Nd, and Sm. Am. Mineral. 94, 467–475.
Ohta, A., Kagi, H., Nomura, M., Tsuno, H., Kawabe, I., 2009b. Coordination study of rare earth elements on Fe oxyhydroxide and Mn dioxides: part II. Correspondence of structural change to irregular variations of partitioning coefficients and tetrad effect variations appearing in interatomic distances. Am. Mineral. 94, 476–486.
Olivarez, A.M., Owen, R.M., 1989. REE/Fe variations in hydrothermal sediments: implications for the REE content of seawater. Geochim. Cosmochim. Acta 53, 757–762.
Piasecki, W., Sverjensky, D.A., 2008. Speciation of adsorbed yttrium and rare earth elements on oxide surfaces. Geochim. Cosmochim. Acta 72, 3964–3979.
Pretorius, P.J., Linder, P.W., 1998. Determination of Diffuse Double Layer protonation constants for hydrous ferric oxide (HFO): supporting evidence for the Dzombak and Morel compilation. Chem. Speciat. Bioavail. 10, 115–119.
Quinn, K.A., Byrne, R.H., Schijf, J., 2004. Comparative scavenging of yttrium and the rare earth elements in seawater: competitive influences of solution and surface chemistry. Aquat. Geochem. 10, 59–80.
Quinn, K.A., Byrne, R.H., Schijf, J., 2006a. Sorption of yttrium and rare earth elements by amorphous ferric hydroxide: influence of pH and ionic strength. Mar. Chem. 99, 128–150.
Quinn, K.A., Byrne, R.H., Schijf, J., 2006b. Sorption of yttrium and rare earth elements by amorphous ferric hydroxide: influence of solution complexation with carbonate. Geochim. Cosmochim. Acta 70, 4151–4165.
Quinn, K.A., Byrne, R.H., Schijf, J., 2007. Sorption of yttrium and rare earth elements by amorphous ferric hydroxide: influence of temperature. Environ. Sci. Technol. 41, 541–546.
Schindler, P.W., Stumm, W., 1987. The surface chemistry of oxides, hydroxides, and oxide minerals. In: Stumm, W. (Ed.), Aquatic Surface Chemistry. Chemical Processes at the Particle-Water Interface. John Wiley & Sons, New York, NY, pp. 83–110.
Shannon, R.D., 1976. Revised effective ionic radii and systematic studies of interatomic distances in halides and chalcogenides. Acta Crystallogr. A32, 751–767.
Sverjensky, D.A., 2005. Prediction of surface charge on oxides in salt solutions: revisions for 1:1 (M^+L^-) electrolytes. Geochim. Cosmochim. Acta 69, 225–257.
Sverjensky, D.A., 2006. Prediction of the speciation of alkaline earths adsorbed on mineral surfaces in salt solutions. Geochim. Cosmochim. Acta 70, 2427–2453.
Tang, J., Johannesson, K.H., 2005. Adsorption of rare earth elements onto Carrizo sand: experimental investigations and modeling with surface complexation. Geochim. Cosmochim. Acta 69, 5247–5261.
Tertre, E., Berger, G., Simoni, E., Castet, S., Giffaut, E., Loubet, M., Catalette, H., 2006. Europium retention onto clay minerals from 25 to 150 °C: experimental measurements, spectroscopic features and sorption modelling. Geochim. Cosmochim. Acta 70, 4563–4578.
Tertre, E., Hofmann, A., Berger, G., 2008. Rare earth element sorption by basaltic rock: experimental data and modeling results using the "Generalised Composite approach". Geochim. Cosmochim. Acta 72, 1043–1056.
Verplanck, P.L., Nordstrom, D.K., Taylor, H.E., Kimball, B.A., 2004. Rare earth element partitioning between hydrous ferric oxides and acid mine water during iron oxidation. Appl. Geochem. 19, 1339–1354.
Whitfield, M., Turner, D.R., 1979. Water–rock partition coefficients and the composition of seawater and river water. Nature 278, 132–137.
Wood, S.A., 1990. The aqueous geochemistry of the rare-earth elements and yttrium. 1. Review of available low-temperature data for inorganic complexes and the inorganic REE speciation of natural waters. Chem. Geol. 82, 159–186.

References

Appelo, C. A. J. and Postma, D., 1999. A consistent model for surface complexation on birnessite (-MnO_2) and its application to a column experiment. *Geochimica et Cosmochimica Acta* **63**, 3039-3048.

Arnold, T., Zorn, T., Zänker, H., Bernhard, G., and Nitsche, H., 2001. Sorption behavior of U(VI) on phyllite: Experiments and modeling. *Journal of Contaminant Hydrology* **47**, 219-231.

Balistrieri, L. S. and Murray, J. W., 1984. Marine scavenging: Trace metal adsorption by interfacial sediment from MANOP Site H. *Geochimica et Cosmochimica Acta* **48**, 921-929.

Bau, M., 1999. Scavenging of dissolved yttrium and rare earths by precipitating iron oxyhydroxide: Experimental evidence for Ce oxidation, Y-Ho fractionation, and lanthanide tetrad effect. *Geochimica et Cosmochimica Acta* **63**, 67-77.

Bau, M. and Dulski, P., 1996. Distribution of yttrium and rare-earth elements in the Penge and Kuruman iron-formations, Transvaal Supergroup, South Africa. *Precambrian Research* **79**, 37-55.

Bau, M. and Dulski, P., 1999. Comparing yttrium and rare earths in hydrothermal fluids from the Mid-Atlantic Ridge: implications for Y and REE behaviour during near-vent mixing and for the Y/Ho ratio of Proterozoic seawater. *Chemical Geology* **155**, 77-90.

Bau, M. and Koschinsky, A., 2009. Oxidative scavenging of cerium on hydrous Fe oxide: Evidence from the distribution of rare earth elements and yttrium between Fe oxides and Mn oxides in hydrogenetic ferromanganese crusts. *Geochemical Journal* **43**, 37-47.

Bau, M., Koschinsky, A., Dulski, P., and Hein, J. R., 1996. Comparison of the partitioning behaviours of yttrium, rare earth elements, and titanium between hydrogenetic marine ferromanganese crusts and seawater. *Geochimica et Cosmochimica Acta* **60**, 1709-1725.

Bau, M., Möller, P., and Dulski, P., 1997. Yttrium and lanthanides in eastern Mediterranean seawater and their fractionation during redox-cycling. *Marine Chemistry* **56**, 123-131.

Bayon, G., German, C. R., Burton, K. W., Nesbitt, R. W., and Rogers, N., 2004. Sedimentary Fe-Mn oxyhydroxides as paleoceanographic archives and the role of aeolian flux in regulating oceanic dissolved REE. *Earth and Planetary Science Letters* **224**, 477-492.

Bertram, C. J. and Elderfield, H., 1993. The geochemical balance of the rare earth elements and neodymium isotopes in the oceans. *Geochimica et Cosmochimica Acta* **57**, 1957-1986.

Bonatti, E., Kraemer, T., and Rydell, H., 1972. Classification and genesis of submarine iron-manganese deposits. In: Horn, D. R. (Ed.), *Papers on a conference about ferromanganese deposits on the ocean floor*. National Science Foundation, Washington, D.C.

Borkowski, M. and Siekierski, S., 1992. Factors affecting the position of Y and actinides(III) with respect to lanthanides in the NH_4SCN-Adogen-464SCN extraction system. *Radiochim. Acta* **56**, 31-35.

Bright, C. A., Cruse, A. M., Lyons, T. W., MacLeod, K. G., Glascock, M. D., and Ethington, R. L., 2009. Seawater rare-earth element patterns preserved in apatite of Pennsylvanian conodonts? *Geochimica et Cosmochimica Acta* **73**, 1609-1624.

Byrne, R. H. and Lee, J. H., 1993. Comparative yttrium and rare earth element chemistries in seawater. *Marine Chemistry* **44**, 121-130.

Byrne, R. H. and Sholkovitz, E. R., 1996. Marine chemistry and the geochemistry of the lanthanides. In: Gschneider Jr., K. A. and Eyring, L. Eds.), *Handbook on the Physics and Chemistry of Rare Earths*. Elsevier, New York.

Calvert, S. E. and Price, N. B., 1977. Geochemical variation in ferromanganese nodules and associated sediments from the Pacific Ocean. *Marine Chemistry* **5**, 43-74.

Charette, M. A. and Sholkovitz, E. R., 2006. Trace element cycling in a subterranean estuary: Part 2. Geochemistry of the pore water. *Geochimica et Cosmochimica Acta* **70**, 811-826.

Davis, J. A., Coston, J. A., Kent, D. B., and Fuller, C. C., 1998. Application of the Surface Complexation Concept to Complex Mineral Assemblages. *Environmental Science & Technology* **32**, 2820-2828.

Davranche, M., Pourret, O., Gruau, G., Dia, A., Jin, D., and Gaertner, D., 2008. Competitive binding of REE to humic acid and manganese oxide: Impact of reaction kinetics on development of cerium anomaly and REE adsorption. *Chemical Geology* **247**, 154-170.

Davranche, M., Pourret, O., Gruau, G., Dia, A., and Le Coz-Bouhnik, M., 2005. Adsorption of REE(III)-humate complexes onto MnO_2: Experimental evidence for cerium anomaly and lanthanide tetrad effect suppression. *Geochimica et Cosmochimica Acta* **69**, 4825-4835.

De Baar, H. J. W., Bacon, M. P., Brewer, P. G., and Bruland, K. W., 1985. Rare earth elements in the Pacific and Atlantic Oceans. *Geochimica et Cosmochimica Acta* **49**, 1943-1959.

De Baar, H. J. W., German, C. R., Elderfield, H., and Vangaans, P., 1988. Rare earth element distributions in anoxic waters of the Cariaco Trench. *Geochimica et Cosmochimica Acta* **52**, 1203-1219.

De Carlo, E. H., 1991. Paleoceanographic implications of rare earth element variability within a Fe-Mn crust from the central Pacific Ocean. *Marine Geology* **98**, 449-467.

De Carlo, E. H. and McMurtry, G. M., 1992. Rare earth element geochemistry of ferromanganese crusts from the Hawaiian Archipelago, central Pacific. *Chemical Geology* **95**, 235-250.

De Carlo, E. H., Wen, X.-Y., and Irving, M., 1998. The influence of redox reactions on the uptake of dissolved Ce by suspended Fe and Mn oxide particles. *Aquatic Geochemistry* **3**, 357-389.

De Carlo, E. H., Wen, X. Y., and Cowen, J. P., 2000. Rare earth element fractionation in hydrogenetic Fe-Mn crusts: The influence of carbonate complexation and phosphatization on Sm/Yb ratios. In: Glenn, C. R., Prévôt-Lucas, L., and Lucas, J. Eds.), *Marine Authigenesis: From Global to Microbial*. SEPM (Society for Sedimentary Geology), Tulsa, OK.

Dellwig, O., Leipe, T., Marz, C., Glockzin, M., Pollehne, F., Schnetger, B., Yakushev, E. V., Bottcher, M. E., and Brumsack, H. J., 2010. A new particulate Mn-Fe-P-shuttle at the redoxcline of anoxic basins. *Geochimica et Cosmochimica Acta* **74**, 7100-7115.

Diakonov, I. I., Ragnarsdottir, K. V., and Tagirov, B. R., 1998. Standard thermodynamic properties and heat capacity equations of rare earth hydroxides: II. Ce(III)-, Pr-, Sm-, Eu(III)-, Gd-, Tb-, Dy-, Ho-, Er-, Tm-, Yb-, and Y-hydroxides. Comparison of thermochemical and solubility data. *Chemical Geology* **151**, 327-347.

Duckworth, O. W. and Sposito, G., 2005. Siderophore-Manganese(III) Interactions. I. Air-Oxidation of Manganese(II) Promoted by Desferrioxamine B. *Environmental Science & Technology* **39**, 6037-6044.

Dymond, J., Lyle, M., Finney, B., Piper, D. Z., Murphy, K., Conard, R., and Pisias, N., 1984. Ferromanganese nodules from MANOP Sites H, S, and R--Control of mineralogical and chemical composition by multiple accretionary processes. *Geochimica et Cosmochimica Acta* **48**, 931-949.

Dzombak, D. A. and Morel, F. M. M., 1990. *Surface Complexation Modeling. Hydrous Ferric Oxide*. John Wiley & Sons, New York, NY.

Elderfield, H., Hawkesworth, C. J., Greaves, M. J., and Calvert, S. E., 1981a. Rare earth element geochemistry of oceanic ferromanganese nodules and associated sediments. *Geochimica et Cosmochimica Acta* **45**, 513-528.

Elderfield, H., Hawkesworth, C. J., Greaves, M. J., and Calvert, S. E., 1981b. Rare earth element zonation in Pacific ferromanganese nodules. *Geochimica et Cosmochimica Acta* **45**, 1231-1234.

Fendorf, S. E. and Zasoski, R. J., 1992. Chromium(III) oxidation by δ-MnO_2. 1. Characterization. *Environmental Science & Technology* **26**, 79-85.

Fowler, S. W., Hamilton, T. F., Peinert, R. D., La Rosa, J., and Teyssie, J.-L., 1992. The vertical flux of rare earth elements in the northwestern Mediterranean. *EROS 2000 (European River Ocean System): Proceedings of the Third Workshop on the North-West Mediterranean Sea*, 401-412.

Fox, P. M., Davis, J. A., and Luther Iii, G. W., 2009. The kinetics of iodide oxidation by the manganese oxide mineral birnessite. *Geochimica et Cosmochimica Acta* **73**, 2850-2861.

German, C. R. and Elderfield, H., 1990. Application of the Ce anomaly as a paleoredox indicator: The ground rules. *Paleoceanography* **5**, 823-833.

German, C. R., Holliday, B. P., and Elderfield, H., 1991. Redox cycling of rare earth elements in the suboxic zone of the Black Sea. *Geochimica et Cosmochimica Acta* **55**, 3553-3558.

German, C. R., Masuzawa, T., Greaves, M. J., Elderfield, H., and Edmond, J. M., 1995. Dissolved rare earth elements in the Southern Ocean: Cerium oxidation and the influence of hydrography. *Geochimica et Cosmochimica Acta* **59**, 1551-1558.

Glasby, G. P., 2000. Manganese: Predominant Role of Nodules and Crusts. In: Schulz, H. D. and Zabel, M. Eds.), *Marine Geochemistry*. Springer, New York.

Goldberg, E. D., 1954. Marine Geochemistry 1. Chemical Scavengers of the Sea. *The Journal of Geology* **62**, 249-265.

Haley, B. A., Klinkhammer, G. P., and McManus, J., 2004. Rare earth elements in pore waters of marine sediments. *Geochemica et Cosmochimica Acta* **68**, 1265-1279.

Hayes, S. A., Yu, P., O'Keefe, T. J., O'Keefe, M. J., and Stoffer, J. O., 2002. The phase stability of cerium species in aqueous systems - I. E-pH diagram for the Ce-$HClO_4$-H_2O system. *J. Electrochem. Soc.* **149**, C623-C630.

Heath, G. R., 1981. Ferromanganese nodules of the deep sea. *Econ. Geol.* **75th Anniv. Vol.**, 736-765.

Hem, J. D. and Lind, C. J., 1983. Nonequilibrium models for predicting forms of precipitated manganese oxides. *Geochimica et Cosmochimica Acta* **47**, 2037-2046.

Herd, C. D. K., Borg, L. E., Jones, J. H., and Papike, J. J., 2002. Oxygen fugacity and geochemical variations in the martian basalts: Implications for martian basalt petrogenesis and the oxidation state of the upper mantle of Mars. *Geochimica et Cosmochimica Acta* **66**, 2025-2036.

Holser, W. T., 1997. Evaluation of the application of rare-earth elements to paleoceanography. *Palaeogeography Palaeoclimatology Palaeoecology* **132**, 309-323.

Kakuwa, Y. and Matsumoto, R., 2006. Cerium negative anomaly just before the Permian and Triassic boundary event - The upward expansion of anoxia in the water column. *Palaeogeography Palaeoclimatology Palaeoecology* **229**, 335-344.

Kalhorn, S. and Emerson, S., 1984. The oxidation state of manganese in surface sediments of the deep sea. *Geochimica et Cosmochimica Acta* **48**, 897-902.

Kanungo, S. B., Tripathy, S. S., and Rajeev, 2004. Adsorption of Co, Ni, Cu, and Zn on hydrous manganese dioxide from complex electrolyte solutions resembling sea water in major ion content. *Journal of Colloid and Interface Science* **269**, 1-10.

Kato, Y., Nakao, K., and Isozaki, Y., 2002. Geochemistry of Late Permian to Early Triassic pelagic cherts from southwest Japan: Implications for an oceanic redox change. *Chemical Geology* **182**, 15-34.

Kawabe, I., Kitahara, Y., and Naito, K., 1991. Non-chondritic yttrium/holmium ratio and lanthanide tetrad effect observed in pre-Cenozoic limestones. *Geochemical Journal* **25**, 31-44.

Kawabe, I., Ohta, A., Ishii, S., Tokumura, M., and Miyauchi, K., 1999. REE partitioning between Fe-Mn oxyhydroxide precipitates and weakly acid NaCl solutions: Convex tetrad effect and fractionation of Y and Sc from heavy lanthanides. *Geochemical Journal* **33**, 167-179.

Klungness, G. D. and Byrne, R. H., 2000. Comparative hydrolysis behavior of the rare earths and yttrium: The influence of temperature and ionic strength. *Polyhedron* **19**, 99-107.

Koeppenkastrop, D. and De Carlo, E. H., 1992. Sorption of rare-earth elements from seawater onto synthetic mineral particles: An experimental approach. *Chemical Geology* **95**, 251-263.

Koeppenkastrop, D. and De Carlo, E. H., 1993. Uptake of rare earth elements from solution by metal oxides. *Environmental Science & Technology* **27**, 1796-1802.

Koppi, A. J., Edis, R., Field, D. J., Geering, H. R., Klessa, D. A., and Cockayne, D. J. H., 1996. Rare earth element trends and cerium-uranium-manganese associations in weathered rock from Koongarra, Northern Territory, Australia. *Geochimica et Cosmochimica Acta* **60**, 1695-1707.

Kostka, J. E., Luther, G. W., and Nealson, K. H., 1995. Chemical and biological reduction of Mn (III)-pyrophosphate complexes: Potential importance of dissolved Mn (III) as an environmental oxidant. *Geochimica et Cosmochimica Acta* **59**, 885-894.

Lafferty, B. J., Ginder-Vogel, M., and Sparks, D. L., 2010. Arsenite oxidation by a poorly crystalline manganese oxide 1. Stirred-flow experiments. *Environmental Science & Technology* **44**, 8460-8466.

Li, Y.-H., 1982. Interelement relationship in abyssal Pacific ferromanganese nodules and associated pelagic sediments. *Geochimica et Cosmochimica Acta* **46**, 1053-1060.

MacLeod, K. G. and Irving, A. J., 1996. Correlation of cerium anomalies with indicators of paleoenvironment. *Journal of Sedimentary Research* **66**, 948-955.

Manceau, A. and Charlet, L., 1992. X-ray absorption spectroscopic study of the sorption of Cr(III) at the oxide-water interface : I. Molecular mechanism of Cr(III) oxidation on Mn oxides. *Journal of Colloid and Interface Science* **148**, 425-442.

Manceau, A., Kersten, M., Marcus, M. A., Geoffroy, N., and Granina, L., 2007. Ba and Ni speciation in a nodule of binary Mn oxide phase composition from Lake Baikal. *Geochimica et Cosmochimica Acta* **71**, 1967-1981.

Mascarenhas-Pereira, M. B. L. and Nath, B. N., 2010. Selective leaching studies of sediments from a seamount flank in the Central Indian Basin: Resolving hydrothermal, volcanogenic and terrigenous sources using major, trace and rare-earth elements. *Marine Chemistry* **121**, 49-66.

Masuzawa, T. and Koyama, M., 1989. Settling particles with positive Ce anomalies from the Japan Sea. *Geophys. Res. Lett.* **16**, 503-506.

Mioduski, T., 1993. Covalency of Sc(III), Y(III), and An(III) as manifested in the enthalpies of solution of anhydrous rare earth halides. *J. Radioanal. Nucl. Chem.-Lett.* **176**, 371-382.

Moffett, J. W., 1990. Microbially mediated cerium oxidation in sea water. *Nature* **345**, 421-423.

Moffett, J. W., 1994. A radiotracer study of cerium and manganese uptake onto suspended particles in Chesapeake Bay. *Geochimica et Cosmochimica Acta* **58**, 695-703.

Murray, J. W., 1974. The Surface Chemistry of Hydrous Manganese Dioxide. *Journal of Colloid and Interface Science* **46**, 357-371.

Murray, J. W. and Dillard, J. G., 1979. The oxidation of cobalt(II) adsorbed on manganese dioxide. *Geochimica et Cosmochimica Acta* **43**, 781-787.

Murray, R. W., Buchholtzten Brink, M. R., Brumsack, H. J., Gerlach, D. C., and Russ Iii, G. P., 1991. Rare earth elements in Japan Sea sediments and diagenetic behavior of Ce/Ce*: Results from ODP Leg 127. *Geochimica et Cosmochimica Acta* **55**, 2453-2466.

Nagender Nath, B., Balaram, V., Sudhakar, M., and Plüger, W. L., 1992. Rare earth element geochemistry of ferromanganese deposits from the Indian Ocean. *Marine Chemistry* **38**, 185-208.

Ohnuki, T., Ozaki, T., Kozai, N., Nankawa, T., Sakamoto, F., Sakai, T., Suzuki, Y., and Francis, A. J., 2008. Concurrent transformation of Ce(III) and formation of biogenic manganese oxides. *Chemical Geology* **253**, 23-29.

Ohta, A., Hiroyuki, K., Nomura, M., Tsuno, H., and Kawabe, I., 2009a. Coordination study of rare earth elements on Fe oxyhydroxide and Mn dioxides: Part I. Influence of mulit-electron excitation on EXAFS analyses of La, Pr, Nd, and Sm. *American Mineralogist* **94**, 467-475.

Ohta, A., Ishii, S., Sakakibara, M., Mizuno, A., and Kawabe, I., 1999. Systematic correlation of the Ce anomaly with the Co/(Ni+Cu) ratio and Y fractionation from Ho in distinct types of Pacific deep-sea nodules. *Geochemical Journal* **33**, 399-417.

Ohta, A., Kagi, H., Nomura, M., Tsuno, H., and Kawabe, I., 2009b. Coordination study of rare earth elements on Fe oxyhydroxide and Mn dioxides: Part II. Correspondence of structural change to irregular variations of partitioning coefficients and tetrad effect variations appearing in interatomic distances. *American Mineralogist* **94**, 476.

Ohta, A. and Kawabe, I., 2001. REE(III) adsorption onto Mn dioxide (δ-MnO_2) and Fe oxyhydroxide: Ce(III) oxidation by δ-MnO_2. *Geochimica et Cosmochimica Acta* **65**, 695-703.

Parks, G. A., 1967. Aqueous Surface Chemistry of Oxides and Complex Oxide Minerals; Isoelectric Point and Zero Point of Charge, *Equilibrium Concepts in Natural Water Systems*. American Chemical Society, Washington, D.C.

Pattan, J. N., Pearce, N. J. G., and Mislankar, P. G., 2005. Constraints in using Cerium-anomaly of bulk sediments as an indicator of paleo bottom water redox environment: A case study from the Central Indian Ocean Basin. *Chemical Geology* **221**, 260-278.

Peacock, C. L. and Sherman, D. M., 2007. Crystal-chemistry of Ni in marine ferromanganese crusts and nodules. *American Mineralogist* **92**, 1087-1092.

Piper, D. Z., 1974. Rare earth elements in ferromanganese nodules and other marine phases. *Geochimica et Cosmochimica Acta* **38**, 1007-1022.

Pourret, O., Davranche, M., Gruau, G., and Dia, A., 2008. New insights into cerium anomalies in organic-rich alkaline waters. *Chemical Geology* **251**, 120-127.

Pretorius, P. J. and Linder, P. W., 1998. Determination of Diffuse Double Layer protonation constants for hydrous ferric oxide (HFO): supporting evidence for the Dzombak and Morel compilation. *Chem. Speciation Bioavail.* **10**, 115-119.

Prikryl, J. D., Jain, A., Turner, D. R., and Pabalan, R. T., 2001. Uranium^{VI} sorption behavior on silicate mineral mixtures. *Journal of Contaminant Hydrology* **47**, 241-253.

Quinn, K. A., Byrne, R. H., and Schijf, J., 2004. Comparative scavenging of yttrium and the rare earth elements in seawater: Competitive influences of solution and surface chemistry. *Aquatic Geochemistry* **10**, 59-80.

Quinn, K. A., Byrne, R. H., and Schijf, J., 2006a. Sorption of yttrium and rare earth elements by amorphous ferric hydroxide: Influence of pH and ionic strength *Marine Chemistry* **99**, 128-150.

Quinn, K. A., Byrne, R. H., and Schijf, J., 2006b. Sorption of yttrium and rare earth elements by amorphous ferric hydroxide: Influence of solution complexation with carbonate. *Geochimica et Cosmochimica Acta* **70**, 4151-4165.

Quinn, K. A., Byrne, R. H., and Schijf, J., 2007. Sorption of yttrium and rare earth elements by amorphous ferric hydroxide: Influence of temperature. *Environmental Science & Technology* **41**, 541-546.

Roberts, N. L., Piotrowski, A. M., McManus, J. F., and Keigwin, L. D., 2010. Synchronous Deglacial Overturning and Water Mass Source Changes. *Science* **327**, 75-78.

Sato, Y., Okabe, S., and Takematsu, N., 1989. Major elements in manganese and iron oxides precipitated from seawater. *Geochimica et Cosmochimica Acta* **53**, 1883-1887.

Schijf, J., De Baar, H. J. W., Wijbrans, J. R., and Landing, W. M., 1991. Dissolved rare earth elements in the Black Sea. *Deep-Sea Research Part a-Oceanographic Research Papers* **38**, S805-S823.

Schijf, J. and Marshall, K. S., 2011. YREE sorption on hydrous ferric oxide in 0.5 M NaCl solutions: A model extension. *Marine Chemistry* **123**, 32-43.

Schijf, J. and Zoll, A. M., 2011. When dissolved is not truly dissolved--The importance of colloids in studies of metal sorption on organic matter. *Journal of Colloid and Interface Science* **361**, 137-147.

Scott, M. J. and Morgan, J. J., 1996. Reactions at oxide surfaces. 2. Oxidation of Se(IV) by synthetic birnessite. *Environmental Science & Technology* **30**, 1990-1996.

Shannon, R. D., 1976. Revised effective ionic-radii and systematic studies of interatomic distances in halides and chalcogenides. *Acta Crystallogr. Sect. A* **32**, 751-767.

Shields, G. A. and Webb, G. E., 2004. Has the REE composition of seawater changed over geological time? *Chemical Geology* **204**, 103-107.

Sholkovitz, E. R., 1988. Rare earth elements in the sediments of the North Atlantic Ocean, Amazon Delta and East China Sea: Reinterpretation of terrigenous input patterns to the oceans. *Am. J. Sci.* **288**, 236-281.

Sholkovitz, E. R., Landing, W. M., and Lewis, B. L., 1994. Ocean particle chemistry: The fractionation of rare earth elements between suspended particles and seawater. *Geochimica et Cosmochimica Acta* **58**, 1567-1579.

Sholkovitz, E. R., Shaw, T. J., and Schneider, D. L., 1992. The geochemistry of rare earth elements in the seasonally anoxic water column and porewaters of Chesapeake Bay. *Geochemica et Cosmochimica Acta* **56**, 3389-3402.

Sverjensky, D. A., 2006. Prediction of the speciation of alkaline earths adsorbed on mineral surfaces in salt solutions. *Geochimica et Cosmochimica Acta* **70**, 2427-2453.

Takahashi, Y., Manceau, A., Geoffroy, N., Marcus, M. A., and Usui, A., 2007. Chemical and structural control of the partitioning of Co, Ce, and Pb in marine ferromanganese oxides. *Geochimica et Cosmochimica Acta* **71**, 984-1008.

Takahashi, Y., Sakami, H., and Nomura, M., 2002. Determination of the oxidation state of cerium in rocks by Ce L_{III}-edge X-ray absorption near-edge structure spectroscopy. *Analytica Chimica Acta* **468**, 345-354.

Tan, W. F., Lu, S. J., Liu, F., Feng, X. H., He, J. Z., and Koopall, L. K., 2008. Determination of the point-of-zero charge of manganese oxides with different methods including an improved salt titration method. *Soil Sci.* **173**, 277-286.

Tanaka, K., Tani, Y., Takahashi, Y., Tanimizu, M., Suzuki, Y., Kozai, N., and Ohnuki, T., 2010. A specific Ce oxidation process during sorption of rare earth elements on biogenic Mn oxide produced by Acremonium sp. strain KR21-2. *Geochimica et Cosmochimica Acta* **74**, 5463-5477.

Tebo, B. M., Johnson, H. A., McCarthy, J. K., and Templeton, A. S., 2005. Geomicrobiology of manganese(II) oxidation. *Trends in Microbiology* **13**, 421-428.

Tonkin, J. W., Balistrieri, L. S., and Murray, J. W., 2004. Modeling sorption of divalent metal cations on hydrous manganese oxide using the diffuse double layer model. *Appl. Geochem.* **19**, 29-53.

Tripathy, S. S. and Kanungo, S. B., 2005. Adsorption of Co^{2+}, Ni^{2+}, Cu^{2+} and Zn^{2+} from 0.5 M NaCl and major ion sea water on a mixture of δ-MnO2 and amorphous FeOOH. *Journal of Colloid and Interface Science* **284**, 30-38.

Turner, A., Le Roux, S. M., and Millward, G. E., 2008. Adsorption of cadmium to iron and manganese oxides during estuarine mixing. *Marine Chemistry* **108**, 77-84.

Turner, D. R., Whitfield, M., and Dickson, A. G., 1981. The equilibrium speciation of dissolved components in freshwater and seawater at 25°C and 1 atm pressure. *Geochemica et Cosmochimica Acta* **45**, 855-881.

Turner, G. D., Zachara, J. M., McKinley, J. P., and Smith, S. C., 1996. Surface-charge properties and UO_2^{2+} adsorption of a subsurface smectite. *Geochimica et Cosmochimica Acta* **60**, 3399-3414.

Usui, A., Bau, M., and Toshitsugu, Y., 1997. Manganese microchimneys buried in the Central Pacific pelagic sediments: Evidence of intraplate water circulation? *Marine Geology* **141**, 269-285.

Valley, P. M., Fisher, C. M., Hanchar, J. M., Lam, R., and Tubrett, M., 2010. Hafnium isotopes in zircon: A tracer of fluid-rock interaction during magnetite-apatite ("Kiruna-type") mineralization. *Chemical Geology* **275**, 208-220.

van Cappellen, P., Viollier, E., Roychoudhury, A., Clark, L., Ingall, E., Lowe, K., and Dichristina, T., 1998. Biogeochemical cycles of manganese and iron at the oxic-

anoxic transition of a stratified marine basin (Orca Basin, Gulf of Mexico). *Environmental Science & Technology* **32**, 2931-2939.

Villalobos, M., Toner, B., Bargar, J., and Sposito, G., 2003. Characterization of the manganese oxide produced by pseudomonas putida strain MnB1. *Geochimica et Cosmochimica Acta* **67**, 2649-2662.

Wang, K., Chatterton, B. D. E., Attrep, M., and Orth, C. J., 1993. Late Ordovician mass extinction in the Selwyn Basin, northwestern Canada: geochemical, sedimentological, and paleontological evidence. *Can. J. Earth Sci.* **30**, 1870-1880.

Webb, G. E. and Kamber, B. S., 2000. Rare earth elements in Holocene reefal microbialites: a new shallow seawater proxy. *Geochimica et Cosmochimica Acta* **64**, 1557-1565.

Westerlund, S. and Öhman, P., 1992. Rare earth elements in the Arctic Ocean. *Deep-Sea Research Part a-Oceanographic Research Papers* **39**, 1613-1626.

Wright, J., Schrader, H., and Holser, W. T., 1987. Paleoredox variations in ancient oceans recorded by rare earth elements in fossil apatite. *Geochimica et Cosmochimica Acta* **51**, 631-644.

Yakushev, E., Pakhomova, S., Sorenson, K., and Skei, J., 2009. Importance of the different manganese species in the formation of water column redox zones: Observations and modeling. *Marine Chemistry* **117**, 59-70.

Yoshida, T., Ozaki, T., Ohnuki, T., and Francis, A. J., 2004. Adsorption of rare earth elements by γ-Al_2O_3 and Pseudomonas fluorescens cells in the presence of desferrioxamine B: Implication of siderophores for the Ce anomaly. *Chemical Geology* **212**, 239-246.

Yu, P., Hayes, S. A., O'Keefe, T. J., O'Keefe, M. J., and Stoffer, J. O., 2006. The phase stability of cerium species in aqueous systems II. The Ce(III/IV)-H_2O-H_2O_2/O_2 systems. Equilibrium considerations and Pourbaix diagram calculations. *J. Electrochem. Soc.* **153**, C74-C79.

Zhang, G. S., Qu, J. H., Liu, H. J., Liu, R. P., and Li, G. T., 2007. Removal mechanism of As(III) by a novel Fe-Mn binary oxide adsorbent: Oxidation and sorption. *Environmental Science & Technology* **41**, 4613-4619.

Zhang, J., Amakawa, H., and Nozaki, Y., 1994. The comparative behaviors of yttrium and lanthanides in the seawater of the North Pacific. *Geophys. Res. Lett.* **21**, 2677-2680.

Zoll, A. M. and Schijf, J., in prep. A surface complexation model of YREE sorption on *Ulva lactuca* in 0.05-5.0 M NaCl. *Geochemica et Cosmochimica Acta*.